N71-75025

A Reproduced Copy

OF

Reproduced for NASA

by the

NASA Scientific and Technical Information Facility

FFNo 672 Aug 65

TRANSMISSION OF FAR INFRARED RADIATION THROUGH THIN FILMS OF SUPERCONDUCTING ..

R. E. Harris, 1969

Published on demand by
UNIVERSITY MICROFILMS
University Microfilms Limited, High Wycomb, England
A Xerox Company, Ann Arbor, Michigan, U.S.A.

LIBRARY COPY
APR 13 1971

FACILITY FORM 602

N71-75025
(ACCESSION NUMBER)

137
(PAGES)

CR-121883
(NASA CR OR TMX OR AD NUMBER)

(THRU)

None
(CODE)

(CATEGORY)

* * *

This is an authorized facsimile and was produced by microfilm-xerography in 1971 by University Microfilms, A Xerox Company, Ann Arbor, Michigan, U.S.A.

* * *

70-13,342

HARRIS, Richard Elgin, 1941-
TRANSMISSION OF FAR INFRARED RADIATION THROUGH THIN FILMS OF SUPERCONDUCTING AMORPHOUS BISMUTH AND GALLIUM.

University of Illinois, Ph.D., 1969
Physics, solid state

University Microfilms, Inc., Ann Arbor, Michigan

THIS DISSERTATION HAS BEEN MICROFILMED EXACTLY AS RECEIVED

10.00

TRANSMISSION OF FAR INFRARED RADIATION THROUGH THIN FILMS OF SUPERCONDUCTING AMORPHOUS BISMUTH AND GALLIUM

BY

RICHARD ELGIN HARRIS
B.S., University of Rochester, 1963
M.S., University of Illinois, 1965

THESIS

Submitted in partial fulfillment of the requirements
for the degree of Doctor of Philosophy in Physics
in the Graduate College of the
University of Illinois, 1969

Urbana, Illinois

C-97116-B

UNIVERSITY OF ILLINOIS

THE GRADUATE COLLEGE

June, 1969

I HEREBY RECOMMEND THAT THE THESIS PREPARED UNDER MY SUPERVISION BY RICHARD ELGIN HARRIS

ENTITLED TRANSMISSION OF FAR INFRARED RADIATION THROUGH THIN FILMS OF SUPERCONDUCTING AMORPHOUS BISMUTH AND GALLIUM

BE ACCEPTED IN PARTIAL FULFILLMENT OF THE REQUIREMENTS FOR THE DEGREE OF DOCTOR OF PHILOSOPHY

D. M. Ginsberg
In Charge of Thesis

GM Almy
Head of Department

Recommendation concurred in†

D. M. Ginsberg
Leo Kadanoff
Emily V. Klein
R. E. Thompson
E. J. Witt

Committee on Final Examination†

† Required for doctor's degree but not for master's.

D517

ACKNOWLEDGMENTS

The author is delighted to express his sincere appreciation to Professor D. M. Ginsberg for his excellent guidance, thoughtful encouragement, and great patience during the course of this work.

He is grateful for financial support from the Advanced Research Projects Agency under grant number SD-131 and from the National Science Foundation. He is also grateful for fellowship support from the National Aeronautics and Space Administration.

For unpublished results which made possible the interpretation of his data, he thanks Professor C. V. Briscoe, Professor J. D. Leslie, and Professor S. B. Nam.

Finally he thanks his parents and his wife Catharine for their encouragement.

TABLE OF CONTENTS

		Page
I.	BACKGROUND AND MOTIVATION FOR THE EXPERIMENT	1
	BACKGROUND	1
	PLAN FOR THIS EXPERIMENT	7
II.	EXPERIMENTAL METHOD	10
	EXPERIMENTAL APPARATUS	10
	Requirements for the Cryostat	10
	Cryostat	10
	Movable Slide	13
	Substrates	14
	Thermometers and Heater	15
	Mask	15
	Evaporator	16
	Light Pipe	16
	Light Cone and Detector Can	18
	Monochrometer	18
	Dry Box	21
	Detector	24
	Detector Mount	25
	Precautions Against Spurious Reflections	26
	Measurement of the Bolometer Signal	27
	Current Supply for Driving the Film Normal	32
	Infrared Errors	33
	Temperature Regulation	34
	Resistance Measurement	35
	Optical Thickness Measurement	36
	PROCEDURE FOR TAKING AND ANALYZING THE DATA	36
	Far Infrared Measurements	37
	Analyzing the Far Infrared Data	38
	Transition Temperature Measurement and Analysis	39

Page

III. THEORY AND NUMERICAL CALCULATIONS 40

RESPONSE OF A NORMAL CONDUCTOR TO AN ELECTROMAGNETIC FIELD 40

RESPONSE OF A SUPERCONDUCTOR TO AN ELECTROMAGNETIC FIELD 42

Weak-Coupling Result 43

Strong-Coupling Result 45

Transmission Ratio 47

OPTICAL THEOREMS 48

Kramers-Kronig Relations 48

Sum Rule 50

NUMERICAL CALCULATION OF THE CONDUCTIVITY 51

From the Weak-Coupling Formula 51

From the Strong-Coupling Formula 52

Numerical Results 54

IV. RESULTS AND DISCUSSION 70

RESULTS 70

Lead Film 73

Bulk Lead and Lead Alloy Samples--Comparison with the Theory 74

Amorphous Bismuth Films 84

Amorphous Gallium Films 97

Annealed Gallium Films 104

DISCUSSION 115

Fluctuations 116

Far Infrared Radiation and Strongly-Coupled Superconductors 116

LIST OF REFERENCES 119

APPENDIX

THE NORMAL STATE DATA 125

VITA 130

LIST OF TABLES

Table		Page
1.	Ideal Filter Characteristics	21
2.	Main Grating Settings and Filters	22
3.	Summary of Results	71
4.	Results of Other Experiments	94

Figure		Page
16.	Data and theory for Bi-1. Data were taken with KBr filter.....	88
17.	Data and theory for Bi-2.....	90
18.	Data and theory for Bi-3.....	92
19.	$2\omega_g$ and T_c versus resistance for amorphous bismuth films.....	96
20.	Data and theory for Ga-1.....	99
21.	Data and theory for Ga-2.....	101
22.	Data and theory for Ga-3.....	103
23.	$2\omega_g$ and T_c versus resistance for amorphous gallium films.....	106
24.	Data and theory for Ga-1 annealed at 77 K.....	108
25.	Data and theory for Ga-1 annealed at 200 K.....	110
26.	Data and theory for Ga-2 annealed at 77 K.....	112
27.	Normal state data for lead film.....	125
28.	Normal state data for Bi-1.....	126
29.	Normal state data for Bi-2.....	126
30.	Normal state data for Bi-3.....	127
31.	Normal state data for Ga-1.....	127
32.	Normal state data for Ga-2.....	128
33.	Normal state data for Ga-3.....	128
34.	Normal state data for Ga-1 annealed at 77 K.....	129
35.	Normal state data for Ga-2 annealed at 77 K.....	129

I. BACKGROUND AND MOTIVATION FOR THE EXPERIMENT

BACKGROUND

Almost a quarter of a century elapsed between the discovery of superconductivity by Kamerlingh Onnes [1] in 1911 and the first suggestion by Fritz London in 1935 [2] that a gap in the energy spectrum of electrons in superconductors might be responsible for the phenomenon. Quantitative results did not arrive until 1953 when measurement of electronic thermal conductivity [3] by Goodman and of specific heat by Brown, Zemansky, and Boorse [4] showed exponential behavior characteristic of an energy gap. In 1955 Bardeen showed that the Meissner effect, or complete exclusion of magnetic flux from the interior of a superconductor, followed from the existence of an energy gap. [5] The currently accepted basic theory of superconductivity by Bardeen, Cooper, and Schrieffer [6] (BCS), published in 1957, forty-six years after Onnes' discovery, did indeed predict an energy gap having a value $\hbar\omega_g = 3.53\ k_B T_c$, where T_c is the superconducting transition temperature in zero magnetic field, and provided an explanation of most of the experimental results available at that time.

Why was the energy gap not measured directly and accurately by this time? It might seem simple to have made spectroscopic measurements: electrons could be excited above the gap only by those photons whose energies were greater than the gap; a sharp break should occur at the gap. We now know from the BCS theory that the photons would have to have twice the gap energy because they are all paired at zero temperature and must therefore be excited in pairs. Using the BCS prediction and assuming a transition temperature of between 1 and 7 K, the wavelength of radiation

at the gap edge would be between 2000 and 300 microns, a range in which radiation was, and still is, difficult to generate. Optical techniques produce radiation with sufficient intensity to be easily and accurately detected only for wavelengths shorter than a few hundred microns; microwave technology becomes very difficult with wavelengths shorter than 2000 microns (2 mm).

Hence it was not until 1957 that the first of many experiments, on superconductors with relatively large energy gaps appeared. The initial work by Glover and Tinkham[7] used far infrared radiation transmitted through thin films of lead and tin and produced results consistent with zero absorption below $3k_BT_c$ to $4k_BT_c$ and gradually rising to the normal state value above that. Microwave experiments were performed by them also. These experiments were of limited accuracy because of the limitations of the Golay cell detector which was used, and because of the low intensity of radiation available.

More accurate results were possible after the advent of the carbon bolometer[8] detector. This device was employed in subsequent experiments by Ginsberg and Tinkham[9] on thin films of lead, tin, mercury, and indium, and by Richards and Tinkham[10] on bulk samples of indium, tin, mercury, tantalum, vanadium, lead, and niobium.

By this time Mattis and Bardeen[11] (MB) had applied the BCS theory, which is valid for superconductors in which the coupling between electrons and phonons is relatively weak, to the problem of the interaction between photons and superconducting electrons. The new experiments showed qualitative agreement with the theory, but some nagging difficulties

remained: in lead, which is strongly-coupled and to which the MB theory does not necessarily apply, the onset of absorption beyond the gap edge was more rapid than predicted, and structure, with magnitude near the expected experimental error and at frequencies below the gap, was unexplained. Within experimental error, other materials probably gave adequate agreement with the theory.

In the experiments on thin films, measurements were made of one quantity, the ratio T_s/T_n of radiation transmitted through a film in the superconducting state to that transmitted through it in the normal state. The fundamental quantity determining the response of the superconductor to electromagnetic radiation, however, is the conductivity $\sigma_s(\omega) \equiv \sigma_1(\omega) - i\sigma_2(\omega)$ where $\sigma_1(\omega)$ and $\sigma_2(\omega)$ are real. Since $\sigma_1(\omega)$ and $\sigma_2(\omega)$ are related by the very generally derived Kramers-Kronig relations, these measurements of one quantity, the transmission ratio, could be analyzed to produce the two quantities σ_1 and σ_2. The difficulty in applying these relations is that they require, in effect, that the data be integrated from zero frequency to infinity. Since data are available over a finite range only, they must be extrapolated to the required limits, a process possibly leading to error. The "precursor" absorption observed was close to the estimated experimental error, particularly if errors associated with the transformation are included.

In the experiments on bulk samples, a temperature dependence of the precursor was observed. This is thought to show that the structure was not due to impurity radiation, a common problem in far infrared experiments.

Two other techniques which provided measurements of the energy gap were developed. First, measurements using microwaves were carried out for aluminum by Biondi and Garfunkel.[12]. Aluminum, which has weak electron-phonon coupling, has a small enough energy gap to be spanned by microwave frequencies. The data obtained for the surface resistance of these samples was subsequently interpreted by Miller[13] within the BCS framework. Second, the accuracy of energy gap measurements was dramatically advanced in 1960 with the discovery of electron tunneling through a thin, insulating layer separating two superconductors.[14] Simply by measuring the conductance of such a device, the gap could be measured. Although both of these techniques, especially tunneling did make possible improved understanding of superconductivity, neither applies sufficiently to this work to warrant further discussion in this brief introduction.

The early far infrared experiments by Ginsberg, Richards, and Tinkham had shown absorption peaks somewhat below the main gap edge in lead. It was thought for some time that these might be associated with effects of anisotropy, but experiments on alloys of lead by Ginsberg and Leslie[15] ruled out this explanation. According to the Anderson theory of "dirty" superconductors,[16] in which $\ell \ll \xi_o$, ℓ being the electronic mean free path length and ξ_o, the superconducting coherence length for a pure metal, these alloys should have had an isotropic energy gap because of their short mean free paths. However, the small precursors to the gap persisted. Another possible explanation was the existence of some kind of collective effect. Theorists have never been able, however, to show that such an effect would have the proper magnitude and dependence on mean free

path to explain the observations. This experiment, like the earlier ones on lead, also showed an onset of absorption above the gap, which was more rapid than predicted by MB.

At this point, a great improvement in far infrared technique occurred. The standard detector, a bolometer made from an ordinary carbon resistor, was replaced by one made from a single-crystal of semiconductor, generally germanium,[17] but occasionally gallium arsenide.[18,19] These detectors produced a signal-to-noise ratio several times higher than the earlier ones had[20] and subsequent experiments generally produced better data.

In 1966 Palmer and Tinkham[21] revealed a remarkable experiment in which both transmission of far infrared radiation through a thin film of lead and that reflected from it were measured simultaneously. Thus the complex conductivity could be obtained from the data without the use of Kramers-Kronig transforms, and the necessity of extrapolating the data beyond the region of the measurements did not occur. For frequencies above about two-thirds of the gap frequency, these data showed no precursor in σ_1/σ_n larger than about 0.1, a factor of two smaller than that previously thought might exist. However, even in this experiment which had the advantage of a germanium bolometer and modern, low-noise lock-in amplifier, either a low signal-to-noise ratio or systematic error made it impossible to rule out the existence of a precursor. The question remains open.

A new theory had also become available: Nam[22] had calculated the frequency-dependent complex conductivity of a superconductor, accurately including the effects of strong-coupling between electrons and phonons, as

occurs in lead and mercury for example. The agreement of this theory with the results of Palmer and Tinkham was vastly superior to that with the MB theory. Although the real part of Nam's conductivity was very similar to the MB result, it showed small structure due to structure in the phonon density of states. The imaginary part of the conductivity, however, was decreased markedly below that of MB. With only a small scaling of the gap, the data of Palmer and Tinkham could be described within a few percent, for frequencies above the gap and slightly below it.

Experiments on bulk samples of lead all had shown structure on the gap edge, at least until the results of Norman and Douglass[23,24] became known. These experiments were designed to search for a precursor by measuring directly the absorption of a foil or thick film. The lowest upper limit to date on the magnitude of a possible precursor was set by this experiment. From the experimental point of view, the same authors reported slightly later the first time that far infrared radiation had been frequency modulated, at an audio rate, to enable the direct measurement of the derivative of the absorption.[25] Sharp breaks occurred at the energy gaps giving measurements of them with accuracy rivalling those possible in tunneling experiments.

It is possible that the precursor exists for some samples, but not for others. The effect of strains in the sample may be significant. Surface preparation is also important as radiation does not penetrate deeply into a metal. As in the case of thin films the question of the precursor in bulk samples is not yet resolved.

One mark of the maturity of the field of superconductivity is the large number of excellent review articles available. Those most useful in this work are by Douglass and Falicov,[25] Tinkham,[26,27] and Ginsberg and Hebel.[28]

PLAN FOR THIS EXPERIMENT

The two recent experiments and one theory described above show an increasing understanding of the interaction of far infrared radiation with strongly-coupled superconductors. The theory, however, has been applied to only one metal: lead. Moreover, the question of a precursor has not been resolved. Thus further experimental studies of strongly-coupled superconductors would provide a further check on the theory.

The choice of materials for such work is rather straightforward. Only two metals are available which are strongly-coupled and superconducting in bulk form: lead and mercury. Lead has been examined already. Mercury has an energy gap of about 13 cm^{-1}, below which frequency little radiation is available, making accurate measurements below the gap impossible at the present time.

Fortunately three other strongly-coupled examples are available. When gallium, bismuth, and beryllium are evaporated onto a liquid helium temperature substrate they condense into an amorphous form in which they are superconducting.[29,30] In this form gallium and beryllium have transition temperatures dramatically increased from their values in the bulk. Bismuth is not now known to be superconducting in the bulk at atmospheric pressure. Beryllium can be excluded, however, because when

inhaled in finely divided form, as might be likely to result from evaporation, it is exceedingly poisonous. Thus the choice of bismuth and gallium was made for this experiment.

The remarkable properties of amorphous superconductors are interesting in themselves. A review of the properties of amorphous bismuth and gallium films is given by Buckel.[31] Recently theoretical work has been done in an attempt to explain their enhanced transition temperatures in terms of a phonon density of states enhanced at low frequencies.[32,33,34] Furthermore, if the films are made very thin, interesting shifts in the transition temperatures have been observed.[35] None of these observations has included the energy gap, which an infrared experiment can measure.

Next a choice must be made amongst the optical properties to measure: reflection, absorption, or transmission. Reflection experiments using non-focusing, far infrared light pipes are rather difficult because spurious reflections cannot easily be eliminated. An absorption experiment would have been difficult with very thin films. Thus a transmission experiment was deemed most useful. As all information pertinent to superconductivity is contained in the ratio of transmitted intensities T_s/T_n, an absolute measurement was unnecessary. Since only one quantity was measured, the conductivity could not be calculated without recourse to the Kramers-Kronig transformation. However, the theoretical values of conductivity can be used to calculate the measured transmission ratio, enabling a comparison with theory.

In Section II, the experimental apparatus and method of taking the measurements are described. The theory and numerical calculations from it are discussed in Section III; experimental results and a discussion of them are presented in Section IV.

II. EXPERIMENTAL METHOD

EXPERIMENTAL APPARATUS

Requirements for the Cryostat

A cryostat adequate for making the desired measurements had to meet several criteria. First, the film had to be evaporated onto a liquid helium temperature substrate, and be kept below 9 K and in high vacuum until the experiment was completed. Second, the far infrared radiation had to be transmitted into the cryostat, through the film, and to a detector which had to be maintained at a constant temperature near 1 K. Third, it had to be possible to cause the radiation to pass alternately through the substrate with the film evaporated on it and through a clean, but otherwise identical, substrate so that the intensity of the radiation passing through the film could be normalized. Finally, the film would have to be maintained at a constant temperature in the range 5 to 9 K so that its transition temperature could be measured.

Cryostat

An all-metal cryostat previously used in this laboratory [37] was modified to meet these requirements. It is shown in Figure 1. The bulk of the room temperature radiation was shielded from the experimental region of the cryostat by a cylindrical copper heat shield thermally connected to a liquid nitrogen tank. Inside this was another concentric heat shield cooled by a tank filled with up to 2.5 liters of liquid helium. Innermost was a 0.5 liter liquid helium tank which could be pumped on to reduce the temperature of the liquid helium to about 1 K. When the liquid

Figure 1. Cryostat

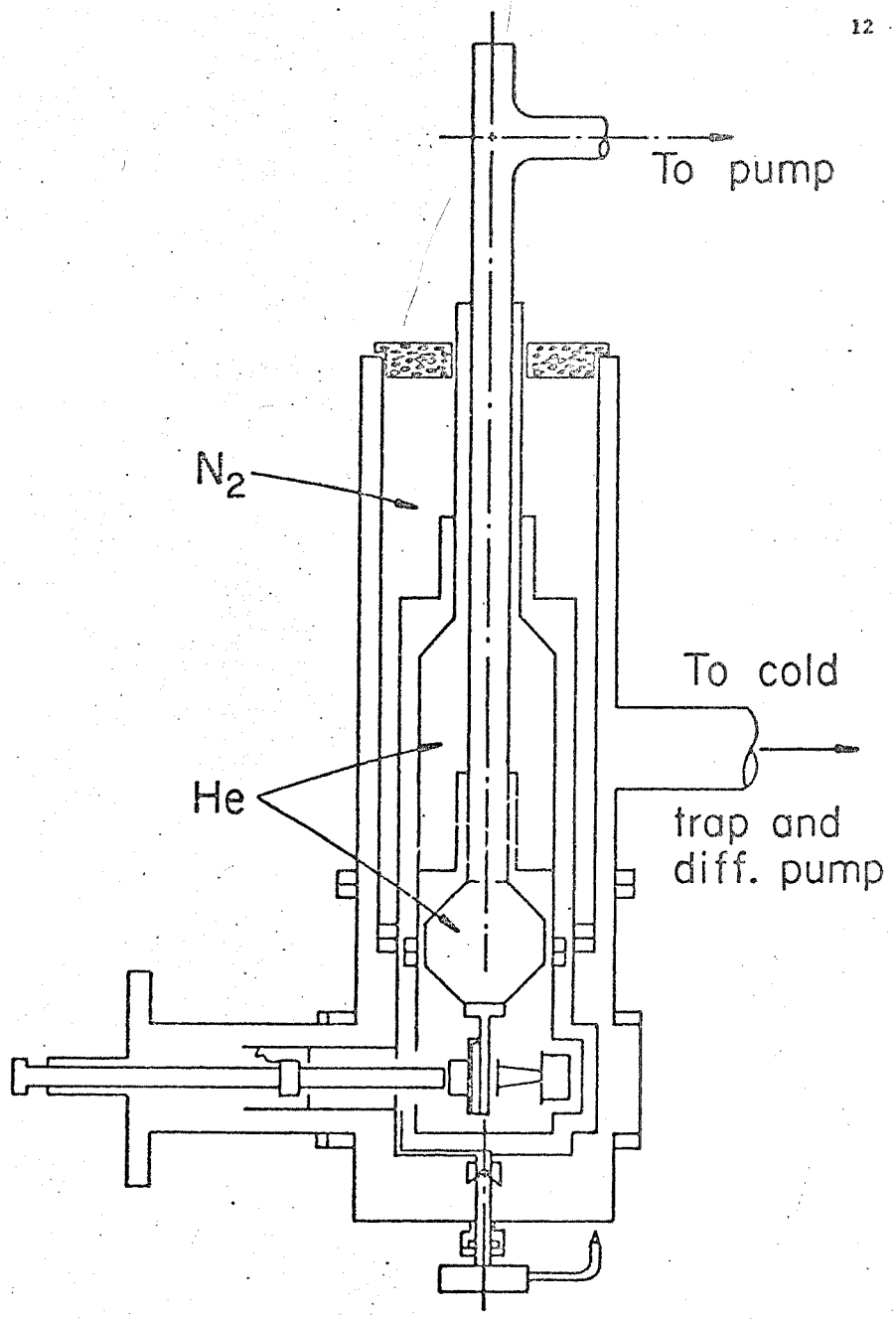
To pump
N_2
To cold
He
trap and
diff. pump

helium was boiled out of the inner tank, leaving helium gas at atmospheric pressure, the gas provided sufficient thermal contact through the pumping line with the outer helium tank that the temperature of the inner tank remained at about 5.3 K. A heater could then be used to increase the temperature of the inner tank to as high as 77 K while liquid helium remained in the outer tank.

Movable Slide

To the bottom of the inner tank was attached a vertical copper plate machined to look like the letter "H" turned on its side. In the crossbar of the H was a 0.500 in. diameter hole to permit the radiation to pass through. Two teflon tracks were attached to the sides of the H. A gap at the center of each track prevented differential contraction between the copper and teflon from breaking the tracks. In addition the tracks were attached to the copper with small spring-loaded bolts passing through slotted holes in the tracks. Sliding in the tracks was a copper slide containing two recessed areas 1.010 in. by 1.010 in. into which the substrates were placed. A hole 0.500 in. in diameter at the center of each recessed area lined up exactly with the hole in the H-shaped copper plate when the slide was moved to the proper end of the track. Thus radiation arriving at the front surface of the slide could be made to pass through either substrate and the copper H by moving the slide to the appropriate end of its track. A bundle of about 200 number 36 copper wires, 4 in. long, thermally connected to the slide with the copper H, but still permitted the slide to be moved. A 0.010 in. diameter stainless steel wire attached to each end of the slide permitted it to be pulled to either end of the tracks. These wires passed through the head shields

and were attached to springs, which were in turn connected to stranded nylon fishing line which could be wound onto pulleys which were at room temperature. Each of the wires was thermally anchored to the 4 K heat shield by a bundle of about 25 number 36 copper wires. Each pulley was attached to a shaft which passed through a double o-ring seal and could be turned by a knob outside the cryostat. At each end of the track an electrically insulated contact was grounded when the slide reached that end of the track. This completed a circuit, lighting either of two neon bulbs outside the cryostat to indicate the position of the slide.

Substrates

The substrates were optically-polished, z-cut, single-crystal quartz plates 1.000 in. by 1.000 in.[37] To reduce interference from multiple reflections within the substrates, they were wedge-shaped, varying in thickness from 0.070 in. to 0.090 in. On the substrate onto which the films were evaporated were four evaporated gold electrodes to enable a four-terminal measurement of the film resistance. Electrical connection to these electrodes was achieved by pressure contact to phosphor bronze tabs covered with gold foil. Thermal contact between the substrates and copper slide was enhanced by a thin layer of Apiezon N-grease[38] between them. Care was necessary to keep the layer of grease sufficiently thin that it did not squeeze out into the 1/2 in. diameter hole in the slide and thus possibly interfere with the radiation passing through. During the evaporations the helium bath was cooled to about 1.2 K. The bismuth films were found to be in the normal state during the evaporations, but the gallium ones were superconducting. Thus the surface temperature of the

substrates during the evaporations is estimated from the transition temperatures of the films to be less than about 8 K.

Thermometers and Heater

On the face of the copper H away from the slide, and below the hole in the crossbar, a 56 ohm Ohmite carbon resistor was mounted to be used for regulating the temperature.

Above this thermometer and the hole was a heater wound by Shier[39] from 0.002 in. diameter manganin wire and potted with GE 7031 varnish. With a resistance of about 2300 ohms it was used to boil away helium in the inner tank, heat the inner tank to temperatures as high as 77 K, and, as part of a feedback circuit whose sensory element was the carbon resistor, to regulate the temperature of the cryostat.

For accurate thermometry a germanium thermometer[40] was mounted in a hole in a short extension at the end of the slide near the film. Thermal contact was achieved by Apiezon N-grease. This thermometer was calibrated against a similar thermometer which had been calibrated commercially.[41]

Mask

In front of the slide was a mask which defined the area onto which the film was to be evaporated. It was attached at the bottom of the H-shaped plate in such a way that it did not interfere with the movement of the slide. The area defined by the mask was 1.000 in. by 0.625 in.

Evaporator

The evaporator consisted of a molybdenum filament supported between the outer wall of the cryostat and the nitrogen temperature heat shield on two copper posts which were attached to, but electrically insulated from, the bottom of the cryostat. The filament was at the same height as the center of the mask, but was horizontally displaced from that center by six degrees to avoid interference with the light pipe. The filament was a strip 1/8 in. wide cut from a sheet of 0.002 in. thick molybdenum. It was folded to make a V-shaped depression to contain the metal to be evaporated. A tab on the strip was folded to form a back and a top for the depression. A teflon gasket between each copper post and the bottom of the cryostat provided a vacuum seal and electrical isolation. The maximum current necessary to evaporate any of the metals used was about 25 A for gallium.

Between the filament and mask, holes were cut in the heat shields to permit the evaporated metal to reach the substrate. The holes were made as small as possible to minimize the heating effects of radiation and evaporated metal arriving in the experimental region. A shutter normally covered the hole in the 77 K heat shield and was opened only for the evaporations.

Light Pipe

Far infrared radiation was transmitted into the cryostat through a 1/2 in. o.d. by 0.008 in. wall monel light pipe.[42] The light pipe was thermally grounded to an extension of the nitrogen temperature heat shield and to the helium temperature heat shield. The extension was

necessary to decrease the heat flow into the 4 K bath. To permit the cryostat to be disassembled, the extension was removable. At the 4 K end of the light pipe was a wedged, sooted-quartz filter[37] 0.625 in. in diameter and varying in thickness from 0.080 in. to 0.086 in. The filter and soot removed some of the radiation above the frequency range of interest. The wedged shape averaged out multiple reflections within the filter. During the experiments on bismuth and gallium the filter was removed from the light pipe and attached to the 1 K mask. This left a gap between the pipe and the 1 K region with the pipe thermally anchored only to the 77 K heat shield. This reduced the heat flow into the 4 K bath and increased from 8 hours to about 14 hours the time it took the helium in the outer helium tank to boil away. When this change was made the lowest attainable temperature of the helium bath increased from about 1.02 K to about 1.08 K, presumably from the radiation from the 77 K pipe.

For some of the measurements a potassium bromide filter was placed in the light pipe at about its mid-point and thermally connected to the 77 K bath. This filter was 0.625 in. in diameter and was also wedged, varying in thickness from 0.232 in. to 0.240 in. It, combined with the sooted quartz, removed frequencies above about 30 cm^{-1}, thus providing a check for the presence of high frequency contamination in data at frequencies between about 15 cm^{-1} and 30 cm^{-1}. As it was not possible to make infrared measurements on a given sample both with and without the filter, a direct comparison to determine its effect was not possible. None of the data taken suggested that it was necessary so that for most samples it was not used as it prevented measurements above 30 cm^{-1}. An indication of those

samples for which data was taken with this filter will be given in Section IV with the data.

Light Cone and Detector Can

In back of the copper H and slide were a brass light cone and a can containing the detector. The light cone was designed to reduce the diameter of the 1/2 in. beam as much as possible while transmitting the most divergent rays (18°) from our f/1.5 monochrometer. The cone was 1 5/8 in. long, 0.500 in. in diameter at the entrance, and 0.188 in. in diameter at the exit. A 3/8 in. gap between the cone and back of the copper H reduced the intensity of radiation not absorbed by the detector, reflected back to the back of the substrate, and then reflected back to the cone. The can completely shielded the detector from all external radiation except that coming through the cone. The mounting of the detector will be described later.

Monochrometer

A far infrared monochrometer, shown in Fig. 2, the same as that used by Cappelletti,[43] provided radiation having wave numbers between 9 cm^{-1} and 90 cm^{-1} with a bandwidth of between 6 and 9 percent full-width at half-maximum, depending on the wave number. The filters used to remove high frequency multiples of the fundamental were chosen differently from before, however.

The original choice of filters was made by Leslie[44] before the construction of the dry box discussed below. Cappelletti selected filters after the dry box was put into use. However, these were chosen

Figure 2. Far infrared monochrometer.

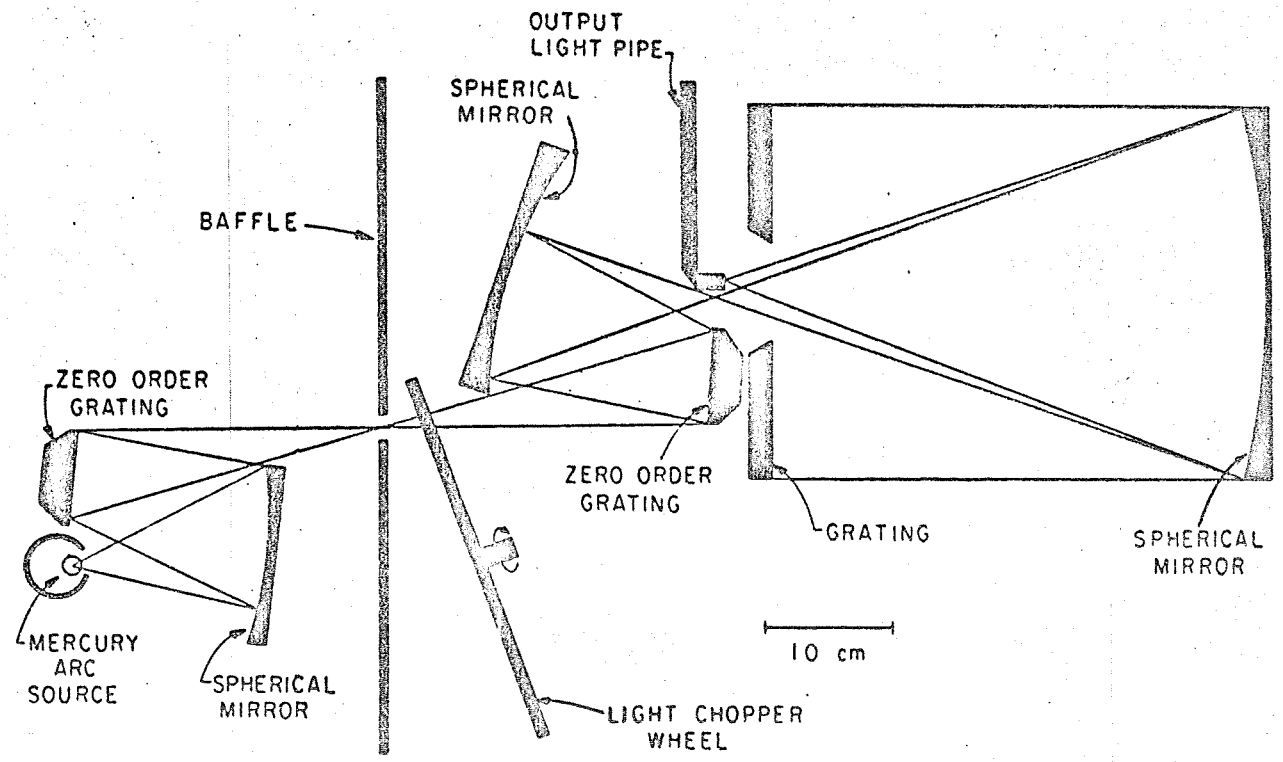
OUTPUT
LIGHT PIPE
SPHERICAL
MIRROR
BAFFLE
ZERO ORDER
GRATING
ZERO ORDER
GRATING
GRATING
SPHERICAL
MIRROR
MERCURY
ARC
SOURCE
SPHERICAL
MIRROR
10 cm
LIGHT CHOPPER
WHEEL

so that the intensity of the second harmonic was reduced only one hundred times more than the fundamental. Those selected for this work provide a reduction by a factor of two hundred. Furthermore most of the filtering by this new choice of filters is done after the chopper. Thus radiation emitted from the surfaces of the optical components cannot contaminate unchopped radiation which is yet to be filtered. Table 1 shows the ideal which was approximately matched by the filters at each frequency. (I_f is the fraction of radiation at frequency f which is passed.)

Table 1

IDEAL FILTER CHARACTERISTICS

	Filter Grating Near Source	Filter Grating After Chopper	Transmission Filter
I_{2f}/I_f	1.33	50.0	3.0
I_f	0.9	0.47	0.47

Thus the second harmonic was reduced 200 times more than the fundamental, while the fundamental itself was reduced by a factor of 5. Table 2 lists the actual filters used. Leslie[44] gives a complete description of the filters, denoted by small letters and numbers, and main gratings, denoted by capital letters.

Dry Box

Water vapor has many absorption lines in the far infrared which interfere with the operation of a monochrometer in the atmosphere. This monochrometer was therefore enclosed in a dry box made of 3/8 in. thick

Table 2

MAIN GRATING SETTINGS AND FILTERS

Wave No. (cm^{-1})	Bandwidth (Percent)	Wavelength (Microns)	Main Grating Angle (Divisions) and Filters†
8.89	5.2	1125.	E247 i h 5
9.41	5.5	1063.	E233 i h 4
10.00	5.9	1000.0	E219 i d'4
10.58	6.2	945.6	E207 i d'4
11.22	6.6	891.2	E195 h d 4
11.95	7.1	836.8	E183 g'd 4
12.78	7.6	782.2	E171 g'd 4
13.74	8.1	727.6	E159 g c'4
14.85	6.1	673.6	D212 g c'3
15.73	6.4	635.7	D200 f'c 3
16.73	6.9	597.9	D188 f'c 3
17.86	7.3	560.0	D176 f b'3
19.16	7.9	522.0	D164 f b'3
19.91	8.2	502.3	D158 e'b'3
20.66	8.5	484.0	D152 e'b 3
21.59	8.9	463.2	D146 e'b 3
22.40	5.7	446.5	C225 e a'3
23.02	5.8	434.4	C219 e a'3
23.64	6.0	422.9	C213 e a'3
25.04	6.4	399.3	C201 d'a'3
26.62	6.8	375.7	C189 d'a 2
28.41	7.3	352.0	C177 d'a 2
30.47	7.8	328.2	C165 d a 2
32.84	8.5	304.5	C153 d a 2
35.62	9.2	280.7	C141 c'a 1
38.86	6.0	257.3	B216 c'a 1
41.13	6.3	243.1	B204 c a 1
43.68	6.7	228.9	B192 c a 1

Table 2 (continued)

Wave No. (cm^{-1})	Bandwidth (Percent)	Wavelength (Microns)	Main Grating Angle (Divisions) and Filters†
46.57	7.2	214.7	B180 b'a 1
49.87	7.7	200.5	B168 b'- 1
53.69	8.3	186.3	B156 b - 1
58.14	9.0	172.0	B144 b a'1
63.23	6.5	158.1	A199 a'a -
67.26	6.9	148.7	A187 a'a -
71.84	7.4	139.2	A175 a a'-
77.09	7.9	129.7	A163 a a'-
83.19	8.6	120.2	A151 a a'-

†In this list the main grating is specified by the capital letter. The main grating angle is given in divisions marked on the main grating vernier. (20 divisions = 0.9 degrees.) The two filter gratings are specified by the two lower case letters, the first letter corresponding to the filter nearer the main grating. The final number denotes the transmission filter.

The dimensions of the main gratings, unprimed filter gratings, and transmission filters are given in Reference 44. The groove spacing of a primed filter is half-way between that of the unprimed filter and that of the filter next in the alphabet; e.g., b' has groove spacing half-way between b and c.

Lucite. Neoprene gloves [45] at five ports permitted easy access to the monochrometer for changing gratings and filters, aligning the instrument, and changing the lamp. To dry the gas, the box was first flushed with several times its volume of dry nitrogen gas. Then a fan was used to continuously circulate the gas through a U-shaped tube of drying agent[46] at one end of the box. Vibrations from the fan were decoupled from the monochrometer by mounting the fan on springs. The gas was blown through a tube to the other end of the box to provide circulation within the box.

Vibration from the chopper was also reduced by mounting it on a support which rested directly on the concrete floor of the laboratory. The only mechanical coupling between the chopper and monochrometer was through the concrete floor, the electrical leads to the chopper motor, the atmosphere in the box, and a flexible polyethylene seal which prevented water vapor from entering the dry box around the chopper support. All of these types of coupling were very small indeed.

Detector

The detector was a bolometer made from a semiconducting gallium arsenide single crystal,[47] doped with 1 to 2×10^{17} atoms/cm^3 of zinc. Its electron mobility at room temperature was 200 to 300 $cm^2 V^{-1} sec^{-1}$. Leads were attached to the gallium arsenide by soldering in a hydrogen atmosphere as described by Cappelletti.[43] The leads used were 0.005 in. diameter copper wire, in contrast to the constantan leads used previously. When using the special solder previously used to produce ohmic contacts, the copper leads melted before the solder became hot enough to wet the gallium arsenide. Thus, as suggested by Wheeler and Hill,[18] copper was

evaporated onto each end of the blank which was then heated in a vacuum to 400°C for several hours. The copper leads were finally attached with indium solder to the evaporated copper.

Cappelletti was able to use low thermal conductance constantan leads by admitting helium exchange gas into the space around his bolometer in order to produce any desired thermal conductance between his bolometer and the helium bath. This procedure was attempted and found inadequate with this experimental arrangement. The substrate with the film on it shielded the detector from unchopped radiation unavoidably present in the beam. When the clean substrate was removed into place, the bolometer was no longer shielded from this radiation and its temperature increased. This could be corrected for as described below, but the helium exchange gas also became warmer, changing its pressure and thus the thermal contact between the bolometer and bath. Although conceivably this could also have been corrected for, difficulties in measuring pressure made the stable, reproduceable thermal link provided by copper leads preferable.

A number of germanium bolometers were also manufactured from samples doped with antimony[48] and gallium.[49] Ohmic contacts were easily made, and the resulting detectors had about the same sensitivity as the gallium arsenide devices. However, since the best germanium detector produced twice as much noise, they were all rejected in favor of the gallium arsenide one.

Detector Mount

The detector was mounted on a copper plate inside the previously-mentioned can. The plate was supported by three threaded studs and

thermally grounded to the can by a copper braid. Two 0.005 in. thick copper sheets were epoxied[50] to separate halves of one face of the plate using 0.0005 in. thick Mylar for electrical insulation. Each bolometer lead was soldered to a tab on each copper sheet. The relatively large area of the copper sheets provided good thermal contact to the copper plate. The resulting thermal conductance between the gallium arsenide and bath, including all thermal impedances, was about 7×10^{-6} W/K at the operating temperature and the device had a time constant of about two milliseconds.

Precautions Against Spurious Reflections

A major difficulty in far infrared work is the high reflectance in the far infrared of the metals necessarily used in the cryogenic apparatus. This high reflectance was reduced by two commercial products. The first was 3M Nextel Velvet Point[51] which was applied in eight thin coats producing a total thickness of about one mm. The second was Eccosorb LS - 22,[52] a flexible black foam sheet 1/8 in. thick. It could be cut with sissors into convenient forms and attached to a metal surface with rubber cement. To test the efficacy of these absorbers, as well as that of felt, the filter grating after the chopper was replaced by an aluminum mirror or a second mirror which was coated with the paint. In the case of the paint, measurements were made of the ratio r of the signal detected when the painted mirror was in place to that detected when the bare mirror was in place. For the felt and foam, measurements were made of the ratio r of the signal detected when the bare mirror had a sample of felt or foam placed in front of it to that detected with the sample removed. It can be

seen from Figure 3 that the foam was far superior to the other two absorbers, giving a ratio of less than about one percent reflection for all frequencies at which it was examined. After outgassing, neither the foam nor the paint adversely affected the pressure in our cryostat: about 5×10^{-5} torr at room temperature and about 10^{-7} torr when the cryostat was cooled.

The black paint was used on the entire inner surface of the 4 K heat shield and on the inside of the bolometer can. The foam sheet was used in the gap between the H and light cone, but outside the 1/2 in. hole, and in the region around the end of the light pipe. Small pieces were also attached around the bolometer.

Measurement of the Bolometer Signal

As the radiation is chopped, or turned on and off, it alternately heats and cools the bolometer, whose resistance thus falls and rises. Thus if a constant current is passed through the bolometer a voltage varying at the frequency of the chopping appears across it. This is then detected by a lock-in amplifier.

The circuit used is shown in Figure 4. The ac component of the voltage across the bolometer is detected by a Princeton Applied Research HR-8 lock-in amplifier,[53] using a high impedance, Type A preamplifier. The bolometer is one arm of a Wheatstone bridge.[54] A helipot forms one of the other arms so that a balance may be achieved and detected with a dc null detector.[55] The setting of the helipot at null can be converted to the resistance of the bolometer, which is used to correct for changes in sensitivity due to changes in resistance caused by moving the film out of place. A second helipot can be inserted into the circuit in place of the

Figure 3.. Efficacy of various far infrared absorbers. For these measurements the filter grating nearer the main grating was replaced by a mirror. The ordinate r is defined as the ratio of the signal detected with the absorber in front of that mirror to the signal detected with the absorber removed.

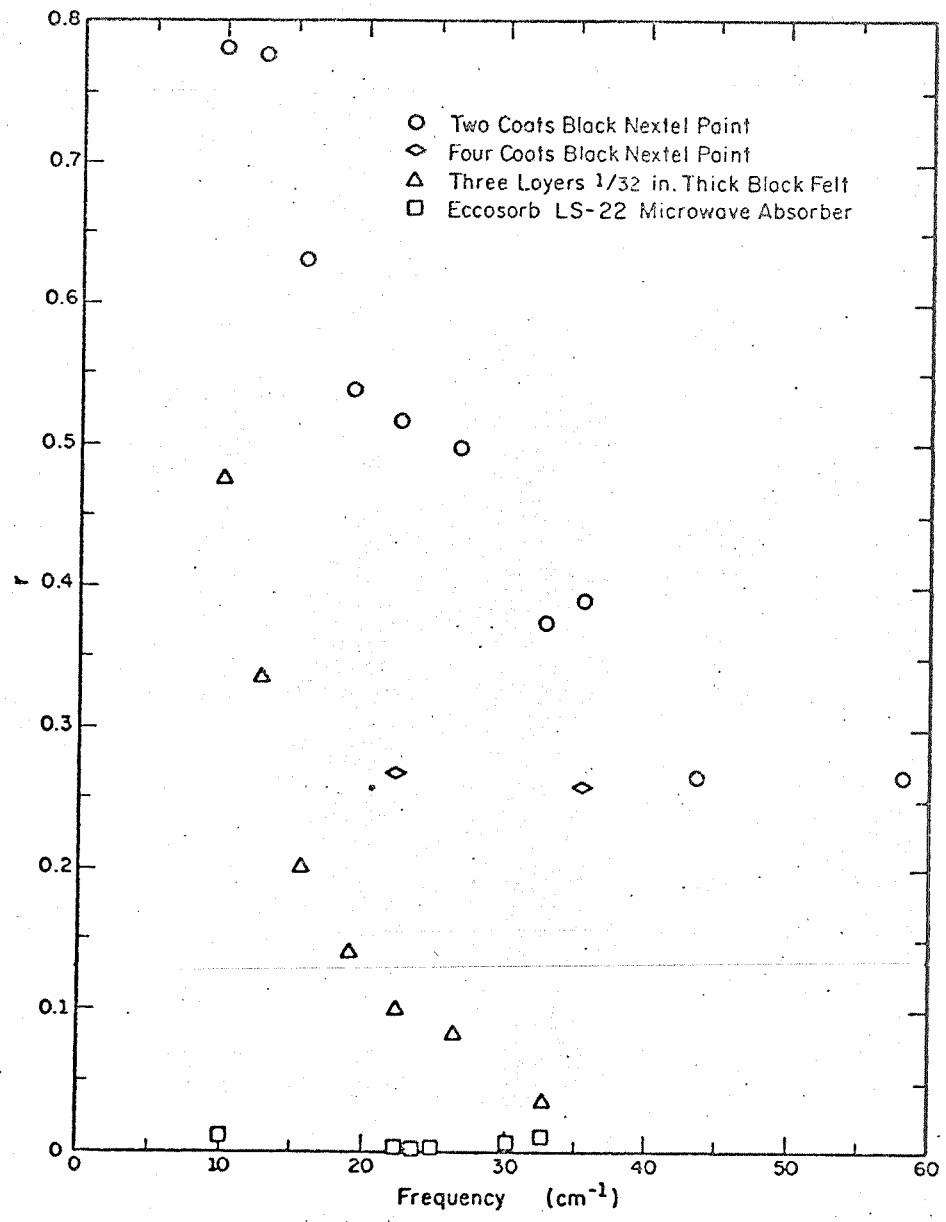
Two Coats Black Nextel Paint
Four Coats Black Nextel Paint
Three Layers 1/32 in. Thick Black Felt
Eccosorb LS-22 Microwave Absorber
r
0.8
0.7
0.6
0.5
0.4
0.3
0.2
0.1
0
0
10
20
30
40
50
60
Frequency (cm^{-1})

Figure 4. Bolometer circuit.

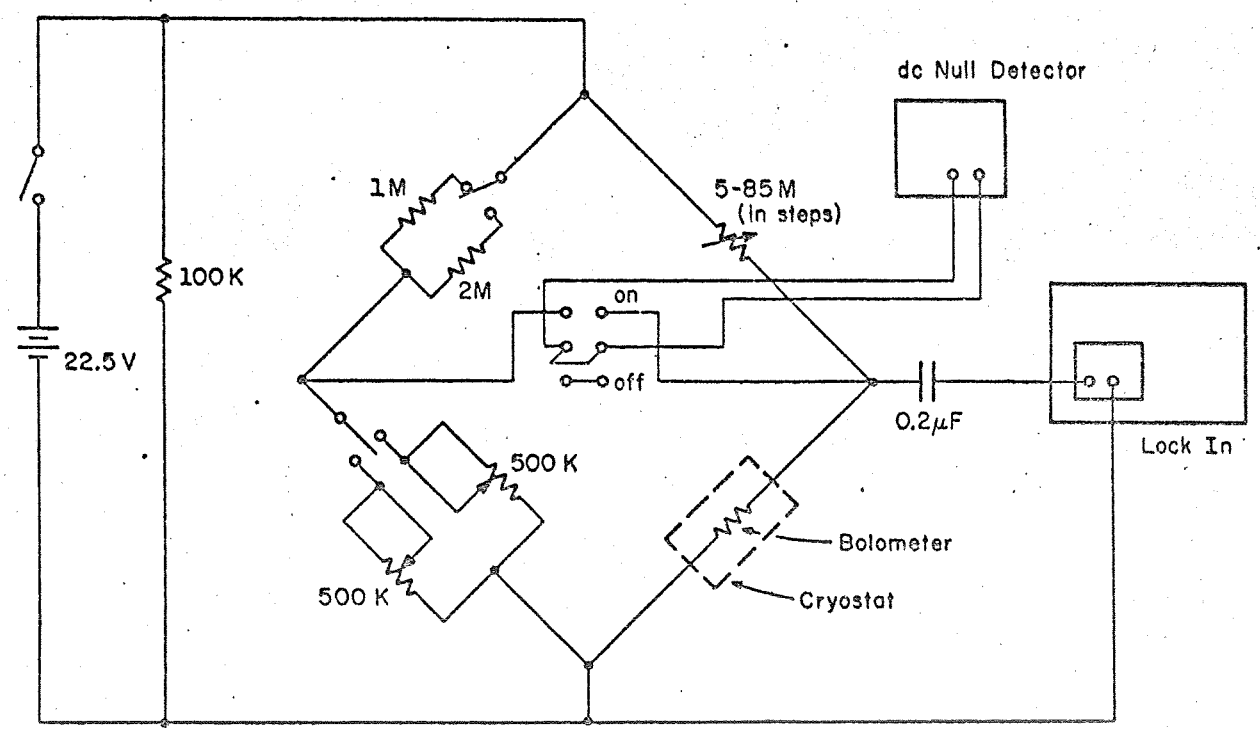
dc Null Detector
1M
2M
5-85 M
(in steps)
100 K
22.5 V
on
off
0.2μF
Lock In
500 K
500 K
Bolometer
Cryostat

first by a switch. One was used when the film was in front of the detector and the other when the clean substrate was there. This reduced the necessary adjustments for each data point.

Current Supply for Driving the Film Normal

For normal state measurements the films were driven normal by passing a current through them. Joule heating resulted after the transition into the normal state had occurred. Thus the current had to be reduced well below the critical current before the film could become superconducting again. Since the joule heating produced by a current as large as the critical current might have annealed an amorphous sample, a special precaution was taken to electronically reduce the current as the film went normal.

A regulated power supply,[56] programmed to supply a constant voltage at its output terminals, was used to supply the current to the film. The voltage drop across a one ohm resistor, in series with the film, enabled the current to be measured. Thus the voltage at the output of the power supply was equal to the sum of the voltages across the film, the one ohm resistor, and the leads to the film. The voltage across the film was zero in the superconducting state. To drive the film normal, the voltage at the power supply was increased slowly until the current reached the critical current of the film. Voltage appeared across the film, and the regulated power supply then decreased the current to maintain the same voltage at its output. The resulting current through the film was slightly more than necessary to keep it in the normal state. The reduction in current was by a factor of between three and five.

Infrared Errors

Both random and systematic errors may arise in the far infrared data. First random errors must be considered. These might be due to electronic noise or to temperature fluctuations which affect the bolometer sensitivity. A good estimate of the magnitude of these errors can be obtained by examining the scatter in the normal state data, plotted in Figures 27 through 35 in the Appendix. Each normal state data point in each of these figures has been divided by the average of all the points in that figure.

It can be seen that these data usually lie within three percent of their average. Random errors in the superconducting data are probably smaller since, as will be mentioned later, the bolometer temperature was lower for those measurements and the signal-to-noise ratio higher.

Systematic errors might be of several types also. Ginsberg[57] has calculated that the effect of the non-normal incidence of some of the radiation from the f/1.5 monochrometer is less than 0.2 percent. He also found that the radiation from a monochrometer essentially identical to the one used in this experiment was free of harmonics of the fundamental to better than 99.5 percent.

Ironically, during these experiments it was not contamination by higher frequencies, but rather lower ones, which was of concern. The measured transmission curves contained bumps at the frequencies at which main gratings were changed. These bumps, never larger than about five percent, could be explained by assuming that the grating used at the frequency below the bump, with the larger groove spacing and smaller angle,

allowed more low frequency contamination to pass. Low frequency contamination is enhanced by the low-pass filters used to remove the high frequency contamination. An extensive experimental search was made for stray, low frequency radiation by covering various surfaces within the monochrometer with the previously-mentioned lossy foam sheet. No improvement was obtained. Two attempts were made to develop a model for the contamination. The first considered the finite number of grooves in the main grating; the second, the shift in phase of radiation impinging upon two adjacent grooves of the main grating because of the spherical, rather than parabolic, mirror in the monochrometer. Neither calculation showed an effect of sufficient magnitude. It is difficult to assess the source of this problem as no instruments are available to measure the frequency spectrum from the monochrometer. It may be that with gratings such as these, made with standard machine shop tools, errors in groove spacing are sufficiently large to produce this effect. Similar bumps in the data of Palmer and Tinkham[21,52] may derive from the same origin.

Temperature Regulation

In order to measure the transition temperature of the films, it was necessary to be able to adjust the temperature of the film and have it remain stable for at least a few minutes. To achieve this the carbon resistor was inserted into one arm of an ac Wheatstone bridge, the error signal from the bridge amplified by a narrow band amplifier, and used to control a dc current to the heater. The method and circuitry were developed by Blake, Chase, and Maxwell[58] and Blake and Chase,[59] and the use of

the apparatus was described by Smith.[60] In this cryostat, short term regulation of 1 mK at about 7 K was achieved.

During the far infrared measurements all valves in the pumping lines were completely opened to provide maximum pumping speed and the lowest possible temperature. The temperature was sufficiently stable that no regulation was necessary.

Resistance Measurement

The resistance of the film was measured with both an ac and a dc technique. When making an ac measurement, an ac constant current at 975 Hz was passed through the film and the resulting ac voltage, which was proportional to the resistance, detected by a lock-in amplifier. As adequate sensitivity was available when using only very small currents, joule heating was sufficiently small to permit this method to be used to determine the resistive transition temperature of the film. The maximum current used was 120 nA. Just above the transition temperature, determined by measuring the ac resistance, the dc resistance was measured in order to calibrate the ac measurement. By placing the film in series with a 1.5 V battery, a current-limiting resistor, and a calibrated carbon resistor, a potentiometer[61] could be used to measure the voltage across the film and the calibrated resistor, enabling the resistance of the film to be calculated.

A nearly identical dc technique was used to measure the resistance of the calibrated germanium thermometer. A 6 V storage cell and a standard resistance[62] having a low temperature coefficient permitted a more accurate measurement of the current than used for measurement of the film

resistance. The voltage across the thermometer was kept below 15 mV. according to the manufacturers' instructions.

Optical Thickness Measurement

Film thicknesses were measured optically for most of the films by the method of Tolansky.[63] The films of bismuth and gallium were warmed to room temperature in the vacuum of the cryostat, exposed to the atmosphere for up to six hours, and then inserted into another evaporator where a reflective coating of silver was evaporated onto them. Optical interferrometric measurements were made at the edges of the films which were over one of the gold electrodes. Thus the difference between the thickness of both the gold electrode and the film and the gold electrode alone was measured. The method is further discussed by Smith[59] and Jacobs.[64]

PROCEDURE FOR TAKING AND ANALYZING THE DATA

Now that the various pieces of experimental equipment have been described, it is possible to explain how they were used in a typical experimental run. Also discussed are the methods used to convert the measured quantities into a form which can be compared with theory.

Two essentially different experiments were performed: measurement of the far infrared properties of a thin film sample and of its transition temperature. As the former was more involved, the approach used there is presented first.

Far Infrared Measurements

Measurements of the far infrared radiation transmitted through the film were first made as a function of frequency for the superconducting state. Then the measurements were repeated with the film in the normal state.

In the superconducting state, the slide was first moved so that the substrate with the film on it was between the light pipe and detector. After the output of the lock-in amplifier had come to equilibrium, the output was recorded on a strip chart recorder for a minimum of twenty times the time constant of the lock-in amplifier. Then the null detector was switched into the circuit, the Wheatstone bridge balanced and the setting of the helipot recorded. Next the slide was moved to position the clean substrate between the light pipe and detector and the above measurements repeated. Finally a new frequency was selected by adjusting the setting of the main grating of the monochrometer and changing filters. This procedure was repeated until the desired frequency range had been spanned; it usually took nearly twenty-four working hours, spread over two days.

Normal state measurements were taken in the same manner as the superconducting ones except that a current sufficiently large to drive the film normal was passed through it. A current-voltage plot was produced on an x-y plotter, enabling the minimum current for which the film was ohmic to be selected. The current passing through the normal film produced joule heating. Thermal equilibrium obtained in several minutes, after which far infrared measurements were made.

These normal state results were found, by extensive preliminary measurements, to be independent of frequency within a few percent. Thus for the bismuth and gallium films, normal state data were taken at only about one-third as many frequencies as superconducting data.

Analyzing the Far Infrared Data

Joule heating resulted in a bolometer temperature about 0.3 K higher for the normal state measurements than those for the superconducting state. The bolometer sensitivity was thus different. A procedure for correcting for this difference was devised by Ginsberg[57] and was employed with these data. Since superconducting data were all taken at very nearly the same temperature and all normal state data taken very close to another temperature, this correction reduced approximately to multiplying all values of the transmission ratio by a constant, which was about 0.8 to 0.9, with variations of order 0.1 percent.

The normal state data were taken to be constant after the previously-discussed correction. The average value of the corrected data was used in calculating the transmission ratio.

To ensure that the transmission ratio T_s/T_n had been accurately determined, an additional procedure was used to determine it experimentally at one frequency. After normal state measurements were completed, the resistance of the bolometer was noted for each position of the slide. Then with the film in the superconducting state, i.e., with no current passing through the film, the heater was used to simulate the joule heating in the film. The heater current was adjusted to produce the same bolometer resistance as that which obtained in the normal state measurements; thus

in this superconducting state measurement, the bolometer had the same sensitivity as it had in the normal state measurement. Thus an accurate measurement of T_s/T_n was possible. Because the heat applied increased the bolometer temperature and therefore reduced its signal-to-noise ratio, and boiled away the liquid helium in the inner tank an an inconvenient rate as well, only a limited number of superconducting data were taken in this fashion. The remaining data were multiplied by a constant ratio, of about 0.95, determined by these measurements, to account for the difference in sensitivity.

Transition Temperature Measurement and Analysis

The transition temperature was measured by controlling the film temperature at successively higher temperatures, passing through the transition. At each temperature the resistance of the film was measured, using the ac technique described above, with the output of the lock-in amplifier recorded on a strip chart recorder. Simultaneously the resistance of the germanium thermometer was determined. From these measurements a plot of film resistance versus temperature could be obtained. T_c was chosen to be the temperature at which the resistance was one-half of its normal state value.

About 0.2 K above the transition temperature, a temperature high enough so that the full normal state resistance of the film had been restored, the resistance of the film was measured accurately using the dc technique.

III. THEORY AND NUMERICAL CALCULATIONS

In order to interpret the transmission ratio T_s/T_n which was experimentally measured by the apparatus discussed in Section II, it is necessary to consider the predictions made possible by rather sophisticated theoretical techniques developed by solid state theorists. To begin, the current in a conductor is written as an integral of the field. In the integral is a kernel which can be derived for superconductors. In two limiting cases it is shown that the integral expression produces a relatively simple ratio of the conductivity in the superconducting state to that in the normal state. Two general theorems from optics are stated. Then the conductivity derived for weak-coupling superconductors is given. The limitations of this result are discussed, prior to stating the more complicated expression for strong-coupling superconductors. Finally to be discussed are the numerical calculations necessary to describe the results of this experiment on strongly-coupled superconductors. By using the two theorems from optics, the general features of the differences in behavior between the two types of superconductors are explained.

RESPONSE OF A NORMAL CONDUCTOR TO AN ELECTROMAGNETIC FIELD

The response of a conductor to an electromagnetic field can generally be described by a complex conductivity which is the constant of proportionality between the Fourier transforms of the electric field and the current:

$$\vec{J}(\vec{q},\omega) = \sigma(\vec{q},\omega)\ \vec{E}(\vec{q},\omega). \qquad (1)$$

In general σ should be a tensor, but for this discussion it will be treated as a scalar. As stated in Section I, $\mathrm{Re}(\sigma) \equiv \sigma_1$ and $\mathrm{Im}(\sigma) \equiv -\sigma_2$.

For a metal in the normal state, the response can be simply written in time and space by using the well-known Chambers formula[65]:

$$\vec{J}(\vec{r},t) = \frac{3\sigma_o}{4\pi\ell} \int \frac{\vec{R}[\vec{R}\cdot\vec{E}(\vec{r}\,',t-R/v_o)]e^{-R/\ell}}{R^4}\, d^3r' \tag{2}$$

where $\vec{R} = \vec{r} - \vec{r}\,'$, $\sigma_o = ne^2\ell/mv_o$ is the long wavelength or dc conductivity, ℓ is the electronic mean free path, n is the concentration of free electrons, e is the electronic charge, and v_o is the Fermi velocity. The Fourier transform of this expression is useful for evaluating limiting forms of the conductivity[27,66]:

$$\sigma_n(q,\omega) = \frac{3\sigma_o}{4iq\ell}\left[(z^2-1)\ln\frac{z-1}{z+1} + 2z\right] \tag{3}$$

where $z = \frac{\omega}{qv_o} - \frac{i}{q\ell}$.

These equivalent expressions are simply statements that when the electric field varies rapidly over a mean free path, the electrons remember these variations since they were last scattered: thus the electric field is evaluated at time $t - R/v_o$. A non-local relation is described: $\vec{J}(\vec{r},t)$ depends not on $\vec{E}(\vec{r},t)$, but on an average about $\vec{r}$ of $\vec{E}(\vec{r}\,',t)$. Using $\vec{E} = -\frac{1}{c}\frac{\partial\vec{A}}{\partial t}$ and explicitly indicating a Fourier transform over frequency, (2) can be written

$$\vec{J}(\vec{r},t) = \frac{3\sigma_o}{4\pi^2\ell hc}\sum_\omega(-i\pi\hbar\omega)e^{i\omega t}\int\frac{[\vec{R}(\vec{R}\cdot\vec{A}_\omega(\vec{r}\,')]e^{-R/\ell}e^{-iR\omega/v_o}\, d^3r'}{R^4}\,. \tag{4}$$

This form, in terms of the vector potential $\vec{A}$, will later be useful for comparison with the corresponding relation for superconductors.

RESPONSE OF A SUPERCONDUCTOR TO AN ELECTROMAGNETIC FIELD

In the superconducting state a result similar to the Chambers expression is found:

$$\vec{J}(\vec{r},t) = \frac{3\sigma_o}{4\pi^2 \ell \hbar c} \sum_{\omega} e^{i\omega t} \int \frac{\vec{R}[\vec{R}\cdot\vec{A}_{\omega}(\vec{r}')]\ I(\omega,R,T)\, e^{-R/\ell}}{R^4} d^3r' . \qquad (5)$$

The kernel $I(\omega,R,T)$ is quite complicated and in general must be evaluated numerically. The expression (5) can be shown to contain (4) as a limiting case.

Fortunately, in the case of very thin films, such as the ones studied in this experiment, a great simplification occurs. In the theory of superconductivity there is a minimum length ξ, called the coherence length, for the variation of the superconducting wave function in space. If ξ_o is the coherence length in the absence of impurity scattering, ℓ is the mean free path, and α is a constant of order unity, then $\xi = (\xi_o^{-1} + \alpha^{-1}\ell^{-1})^{-1}$. When the electromagnetic field penetrates into the superconductor only slightly, $\lambda \ll \xi$ (where λ is the penetration depth), or in our case, when the thickness d of the film is small compared to ξ, then $I(\omega,R,T)$ can be taken to be a constant over the region of integration, evaluating it at $R = 0$. In this case (5) is much more tractible because the remaining integral is of the same form as that for the normal state. Thus the wave vector independent ratio σ_s/σ_n can be formed:

$$\frac{\sigma_s}{\sigma_n}(\omega) = \frac{I(\omega,0,T)}{-i\pi\hbar\omega} . \tag{6}$$

This is the non-local limit of (5), called the Pippard, or extreme anomalous, limit.

Another useful limiting form is for the London, or extreme local limit, in which $\ell \ll \xi_o$. Here a factor exp $(-R/\ell)$ in the integrand causes the integral to be dominated by $I(\omega,0,T)$. Thus again the kernel can be brought outside the integral, once more obtaining the result (6).

Weak-Coupling Result

Mattis and Bardeen[11] have evaluated (6) according to the BCS description of superconductivity, as was done independently by Abrikosov, Gor'kov, and Khalatnikov.[67] For finite temperature their result must be evaluated numerically, but for zero temperature there is a simple form:

$$\frac{\sigma_1}{\sigma_n} = \left[1 + \frac{2\omega_g}{\omega}\right] E(k) - 2\left(\frac{2\omega_g}{\omega}\right) K(k), \quad \omega > 2\omega_g, \tag{7a}$$

$$\frac{\sigma_2}{\sigma_n} = \frac{1}{2}\left[\left(\frac{2\omega_g}{\omega} + 1\right) E(k') + \left(\frac{2\omega_g}{\omega} - 1\right) K(k')\right], \tag{7b}$$

where $k = |2\omega_g - \omega|/|2\omega_g + \omega|$, $k' = (1 - k^2)^{\frac{1}{2}}$, and $E(k)$ and $K(k)$ are the complete elliptic integrals. Of course, $\sigma_1/\sigma_n = 0$ for $\omega < 2\omega_g$.

If the limitations on the MB result are to be clearly understood it is necessary to examine the assumptions they have made. To begin, MB based their calculation on the BCS theory of superconductivity. In turn BCS postulated a pairing interaction between electrons of opposite spin and momentum. Bardeen and Pines[68] had shown that the matrix element governing

the scattering of electrons with momentum $\vec{k}$ and $\vec{k}'$ into $\vec{k}+\vec{X}$ and $\vec{k}'-\vec{X}$, by exchange of a phonon $\vec{X}$, is

$$\frac{2\hbar\omega_{\vec{X}}\left|M_{\vec{X}}\right|^2}{\left(\epsilon_{\vec{k}}-\epsilon_{\vec{k}+\vec{X}}\right)^2-\left(\hbar\omega_{\vec{X}}\right)^2}, \tag{8}$$

where $M_{\vec{X}}$ is the matrix element for single electron scattering by the electron-phonon coupling, $\epsilon_{\vec{k}}$ is the Bloch electron energy measured from the Fermi surface and $\hbar\omega_{\vec{X}}$ is the phonon energy. This matrix element is negative for $\left|\epsilon_{\vec{k}}-\epsilon_{\vec{k}+\vec{X}}\right| < \left|\hbar\omega_{\vec{X}}\right|$. BCS made the further assumption that for $\left|\epsilon_{\vec{k}}\right| \leq k_B\,\theta_D$ (where θ_D is the Debye temperature), the matrix element is nearly constant with a value

$$-\frac{2\left|M_{\vec{X}}\right|^2}{\hbar\omega_{\vec{X}}}. \tag{9}$$

To this BCS added the Coulomb repulsion $4\pi e^2/X^2_{eff}$. Then for frequencies below $\omega_c \sim \omega_D$ they approximated the matrix element by -V, a constant attractive potential. For higher frequencies the matrix element was assumed to be zero. Thus it can be seen that BCS removed all details of the phonons except two: the cutoff frequency ω_c and the average interaction -V between electrons.

The greatest contribution to the attractive interaction between electrons, described by the matrix element (8), comes from virtual excitations with energy of the order of the Debye energy $\hbar\omega_D$. It is possible, however, for such a real excitation with this energy to decay by emission of a

phonon, producing a finite lifetime and non-vanishing level width for that state. The BCS theory is valid when the level widths are small enough, compared to the energies, for the states to be reasonably well-defined. This is the case for superconductors in which there is weak electron-phonon coupling.

There do exist superconductors, however, such as lead and mercury, which have low Debye temperature and high transition temperature, in which the electron-phonon coupling is sufficiently large that the lifetimes become so short that the widths of states near the Debye frequency are comparable to their energies. Hence an approach other than that of BCS is needed.

Strong-Coupling Result

Using a Green's function technique, Migdal[69] showed how to avoid this problem in describing the electron-phonon interaction in the normal state. Eliashberg[70] and Nambu[71] gave the application to superconductors and Schrieffer, Scalapino, and Wilkins[72] added the Coulomb repulsion and showed that the technique could be used to accurately describe tunneling into strongly-coupled superconductors.

The virtue of the Green's function approach is that it is not an expansion in a small electron-phonon coupling constant, but rather is accurate to order $(m/M)^{\frac{1}{2}}$, the square root of the electron-ion mass ratio; that is, it is good to about a tenth of a percent.

The theory produces the so-called Eliashberg gap equations which define a complex frequency-dependent gap parameter $\Delta(\omega)$ and a renormalization parameter $Z(\omega)$. The gap parameter $\Delta(\omega)$ corresponds closely to the constant BCS energy gap. Its imaginary part arises because of the lifetime effects

and its real part falls below zero for high frequencies at which the Bardeen-Pines interaction becomes repulsive. The gap parameter has the property that $\Delta(\omega_g) = \omega_g$.

By applying these results, Nam[22] was able to derive the frequency-dependent conductivity of a strongly-coupled superconductor. This result appears in the same form as that for weakly-coupled superconductors, although actually Nam's kernel was defined so that it encompassed the factor $\exp(-R/\ell)$ in (2), (4), and (5). Again in the extreme anomalous limit one can evaluate the kernel at $R = 0$, move it outside the integral, and divide by the normal state result to obtain a wave vector independent conductivity. Similarly this ratio obtains also in the local limit. The results are more complicated than those of MB: in the $T = 0$ limit, where the weakly-coupled result is stated in terms of complete elliptic integrals, for strongly-coupled materials the proper expression is the following:

$$\frac{\sigma_1}{\sigma_n}(\omega) = \frac{1}{\omega}\int_{\omega_g-\omega}^{-\omega_g} d\omega' \; g_1(\omega',\omega+\omega'), \quad \omega > 2\omega_g \tag{10a}$$

and

$$\frac{\sigma_2}{\sigma_n}(\omega) = \frac{1}{\omega}\int_{[\omega_g-\omega,-\omega_g]}^{\omega_g} d\omega' \, g_2(\omega',\omega+\omega') + \frac{1}{\omega}\int_{\omega_g}^{\infty} d\omega' [g_2(\omega',\omega'+\omega) + g_2(\omega+\omega',\omega')], \tag{10b}$$

where

$$g_1(\omega',\omega+\omega') = n(\omega')\; n(\omega+\omega') + p(\omega')\; p(\omega+\omega'),$$

$$g_2(\omega',\omega+\omega') = \tilde{n}(\omega')\; n(\omega+\omega') + \tilde{p}(\omega')\; p(\omega+\omega'),$$

and $$n(\omega) + i\tilde{n}(\omega) = \omega/[\omega^2 - \Delta^2(\omega)]^{\frac{1}{2}},$$

$$p(\omega) + i\tilde{p}(\omega) = \Delta(\omega)/[\omega^2 - \Delta^2(\omega)]^{\frac{1}{2}}.$$

Here $\hbar = 1$, and $[a,b]$ denotes the algebraically larger of the quantities a and b. Using $\Delta(\omega) = \Delta(\omega_g) = \omega_g$, the first equation and the second term of the second equation reduce to the MB result. The first term of the equation for σ_2/σ_n is strictly a strong-coupling result.

Transmission Ratio

The conductivity ratio can be used to simply evaluate the ratio T_s/T_n of the intensity of radiation transmitted through a superconducting film and substrate to the intensity transmitted in the normal state.[57] What is actually measured is the ratio $\overline{T}$ of the intensity of radiation transmitted through the film and substrate to that transmitted through an identical substrate with no film on it. If the film is much thinner than the penetration depth and the effects of multiple reflections are assumed averaged out by the wedged shape of the substrate, then in the superconducting state

$$\overline{T}_s = \left| 1 + \left[\frac{Z_o}{(n+1)R}\right] \left(\frac{\sigma_1}{\sigma_n} - i\,\frac{\sigma_2}{\sigma_n}\right) \right|^{-2}, \tag{11a}$$

where Z_o is the impedance of free space (377 ohms), n is the index of refraction of the substrate, and R is the far infrared resistance per square of the film. Since σ_n is a real constant in the normal state in the far infrared,

$$\overline{T}_n = \left\{1 + \left[\frac{z_o}{(n+1)R}\right]^2\right\}^{-1}. \tag{11b}$$

The ratio T_s/T_n is then equal to $\overline{T}_s/\overline{T}_n$.

If the theory correctly predicts that $\sigma_1/\sigma_n = 0$ for frequencies below the gap $2\omega_g$, then in this region (11) shows that T_s/T_n is determined by σ_2/σ_n and R. With increasing ω below the gap, the ratio T_s/T_n thus increases because σ_2/σ_n decreases there. At the gap is a discontinuous change in the slope of T_s/T_n, reflecting the onset of absorption and described by a non-zero σ_1/σ_n. Above the gap, however, the transmission ratio for small R may continue to increase, as σ_2/σ_n is decreasing so rapidly that it more than compensates for the absorption. Eventually σ_2/σ_n levels off and the transmission ratio goes through a maximum and decreases to unity at very high frequencies.

Since the peak does not necessarily occur at the gap frequency, it is obviously not possible to assign a measured frequency of the peak to the gap frequency. Neither can the discontinuity in slope at the gap be experimentally observed with present technology. In fact, even in a theoretical plot of the transmission curve the discontinuity is difficult to see if R is small. Thus the gap must be determined by fitting a theoretical curve to the data over a range of frequencies about the gap.

OPTICAL THEOREMS

Kramers-Kronig Relations

Leaving aside, for the moment, the detailed microscopic equations, much can be learned from very general arguments alone. First a very general

relationship exists between the real and imaginary parts of a response function which describes a linear relation between two variables, which represents a causal process, and which is bounded. Actually it is sufficient for the function to be analytic in the upper half plane: linearity, causality, and boundedness imply this, however. Applied to conductivity these Kramers-Kronig[73] relations are

$$\sigma_1(\omega_o) = \frac{2}{\pi} P \int_0^\infty \frac{\omega\sigma_2(\omega)\, d\omega}{\omega^2 - \omega_o^2} + \text{constant} \tag{12a}$$

$$\sigma_2(\omega_o) = \frac{2\omega_o}{\pi} P \int_0^\infty \frac{\sigma_1(\omega)\, d\omega}{\omega_o^2 - \omega^2} \tag{12b}$$

where P denotes the principal value of the integral. This form of these equations is useful in theoretical considerations.

Experiments, however, measure transmission, reflection, or absorption. In particular, a complex transmission coefficient $t = |t|\exp(i\theta)$ can be defined which relates the amplitude and phase of a transmitted wave to that of an incident wave. A Kramers-Kronig relation also exists for this function[74]:

$$\theta_s(\omega_o) - \theta_n(\omega_o) = \frac{2\omega_o}{\pi} P \int_0^\infty \frac{\ln|t_s/t_n|\, d\omega}{\omega_o^2 - \omega^2} . \tag{13}$$

The inverse transform also exists, but is not usually needed. The virtue of this equation is that if one wishes to perform a transform on some transmission data he can simply perform an integral over the measured transmission amplitude to obtain the phase shift. The conductivity can then be calculated algebraically from these two quantities. If the transform is

computed with relations for conductivity, an iterative procedure will have to be used, and problems of convergence may arise.[21]

The difficulty in applying (13) is that the transmission ratio is not known for all frequencies. Thus an extrapolation of the measurements to other frequencies must be made. In the case of superconductors, T_s/T_n is not known for low frequencies where it is expected to change with frequency almost as fast as near the gap. Neither is it known for high frequencies where theoretically it is expected to deviate slightly from unity over a wide frequency range, thus contributing significantly to the integral in (13). Extrapolation of the measurements into these regions with the aid of a theory is possible, but it may lead to erroneous results. A reliable comparison between theory and experiment may instead be made by calculating the experimentally determined parameter from the theory. This is the type of comparison which is made in this work.

Sum Rule

A second theorem can be derived from the general sum rule for oscillator strengths:

$$\int_0^\infty \sigma_1(q,\omega)\,d\omega = \frac{\pi}{2} \sum_i \frac{n_i e_i^2}{m_i} \tag{14}$$

where n_i is the number density of particles with charge e_i and mass m_i. The electrons dominate the sum since their e/m is larger than that for the ions. No change occurs in this sum with the transition into the superconducting state, so that

$$\int_0^\infty \sigma_{1n}(q,\omega)\,d\omega = \int_0^\infty \sigma_{1s}(q,\omega)\,d\omega \tag{15}$$

a statement that the area under the real part of the conductivity curve must be a constant.[75]

Examination of the MB result shows that σ_1 is less than σ_n for all frequencies. Thus the area removed in the superconducting transition must be replaced: this is done by adding a delta function $A(q)\delta(\omega)$ at the origin which corresponds to energy stored in the form of persistent currents. $A(q)$ is given by

$$A(q) = \int_{0+}^{\infty} [\sigma_{1n}(q,\omega) - \sigma_{1s}(q,\omega)]d\omega. \tag{16}$$

The delta function term in the real part of the conductivity leads, by the Kramers-Kronig relations, to a term $2A/\pi\omega$ in the imaginary part. This term dominates σ_2 at low frequencies. In the MB theory[76] $A(q) = \sigma_n(q,0)\pi^2\,\omega_g/2$. As we shall see later this sum rule may also be used to help understand the difference between the weak- and strong-coupling results.

NUMERICAL CALCULATION OF THE CONDUCTIVITY

Obtaining numerical values from the expressions (7) and (10) for the conductivity is a difficult process, especially in the strong-coupling case. Following is a discussion of the evaluation of the conductivity from these formulas[77]:

From the Weak-Coupling Formula

The conductivity of Mattis and Bardeen can be evaluated at $T = 0$ with a slide rule and table of complete elliptic integrals. For $T \neq 0$ it has been calculated for several temperatures by Miller[13] and Waldram.[78] A computer program was prepared by the author to do calculations at any

temperature. Agreement with Miller's results was good except for several small errors which Waldram had noted also. The program was used by Palmer and Tinkham[21] to provide a theoretical comparison with their data on lead films. Ginsberg[79] also used the program to check his more general calculations in a limiting case. It was noted that, for temperatures at which $\exp(-\omega_g/k_BT)$ was small, the difference between the finite and zero temperature conductivities was very small.

From the Strong-Coupling Formula

Another computer program was prepared by the author to calculate the conductivity from the strong-coupling formulas. The calculations were done at $T = 0$ since negligible differences were expected at the low reduced temperatures used in this experiment. While the calculations will not be discussed in detail, the general approach used to avoid the singularities in the integrands will be mentioned.[80] Near the several singularities the integrand can be written in a form

$$f[\omega,\Delta(\omega)]/[\omega^2 - \Delta^2(\omega)]^{\frac{1}{2}},$$

where f is a well-behaved function and ω is near ω_g. At ω_g, the denominator goes to zero since $\omega_g = \Delta(\omega_g)$. This can be rewritten

$$\left[\frac{\omega^2 - \omega_g^{\,2}}{\omega^2 - \Delta^2(\omega)}\right]^{\frac{1}{2}} \frac{f[\omega,\Delta(\omega)]}{[\omega^2 - \omega_g^{\,2}]^{\frac{1}{2}}} .$$

The ratio in square brackets assumes a well-defined limit at ω_g. If we assume $\Delta(\omega) = \omega_g + B(\omega - \omega_g)$ near ω_g then

$$\lim_{\omega \to \omega_g} \left[\frac{\omega^2 - \omega_g^{\,2}}{\omega^2 - \Delta^2(\omega)} \right]^{\frac{1}{2}} = \left[\frac{1}{1-B} \right]^{\frac{1}{2}} .$$

The remaining singularity was handled by a transformation of coordinates, $y = (\omega^2 - \omega_g^{\,2})^{\frac{1}{2}}$. Hence

$$\frac{d\omega}{(\omega^2 - \omega_g^{\,2})^{\frac{1}{2}}} = \frac{dy}{(y^2 + \omega_g^{\,2})^{\frac{1}{2}}} ,$$

which is free of the singularity. While variations on these ideas were necessary for several of the singularities, this short discussion does illustrate the transformations which were made.

Two checks were performed to verify that the program was operating correctly. First a constant gap parameter was used. In this case, the conductivity should have reduced numerically to the MB result: it did. Secondly, Shaw and Swihart[81] independently evaluated σ_s/σ_n for lead using a $\Delta(\omega)$ calculated from $\alpha^2F(\omega)$, in turn calculated by McMillan and Rowell[82] from their experimental data; σ_2/σ_n was obtained by Kramers-Kronig transforming σ_1/σ_n. Our calculations compared favorably with theirs: σ_1/σ_n agreed to better than one part in 10^4, as good as could be expected considering the limitations on our numerical integration technique; σ_2/σ_n agreed to about a few parts in 10^3 which, while not as good agreement as for σ_1/σ_n, was judged adequate because in their Kramers-Kronig transform, they had integrated σ_1/σ_n which itself must have contained small numerical errors. It was not significant that one of the integrals in this direct evaluation of σ_2/σ_n must be carried to infinity. This integration was simply carried to the highest frequency for which $\Delta(\omega)$ was available and then terminated.

For lead, the maximum error in this frequency range from this cutoff was estimated to be less than 0.003 percent, only a small portion of the difference between the two calculations of σ_2/σ_n. Additional errors, due to errors in the values of $\Delta(\omega)$ with which we were supplied, are of unknown magnitude.

Numerical Results

The conductivity of lead as calculated by Shaw and Swihart, with the evaluation of the imaginary part extended to higher frequencies in this work, differs from that calculated by Nam.[22] In Figures 5 and 6 are shown the real and imaginary parts of each calculation as well as that of MB. The discrepancy between the two strong-coupling results probably originates in the difference in the phonon spectrum assumed in the two calculations. Nam used a gap parameter calculated by Schrieffer, Scalapino, and Wilkins[72] from an approximate phonon density of states consisting of two Lorentzian peaks. This was shown to closely approximate tunneling data on lead. Shaw and Swihart, however, calculated a gap parameter from a phonon density of states which was derived from experimental data by McMillan and Rowell. Since the latter is more accurate, calculations of conductivity which are based on it should be more accurate than those of Nam. In Section IV, it will be shown experimentally for our thin films that the opposite is true.

Use of the program to calculate the conductivity of amorphous bismuth and gallium was possible because others had performed tunneling experiments which they had analyzed to obtain $\Delta(\omega)$. In fact they were basically interested in $\sum_\lambda \alpha_\lambda^2 f_\lambda(\omega)$, the electron-phonon coupling constant times the phonon density of states, but $\Delta(\omega)$ was, for this work, a useful

Figure 5. Real part of the conductivity ratio for lead. For clarity the Nam result has been omitted since it is very close to the result of Shaw and Swihart.

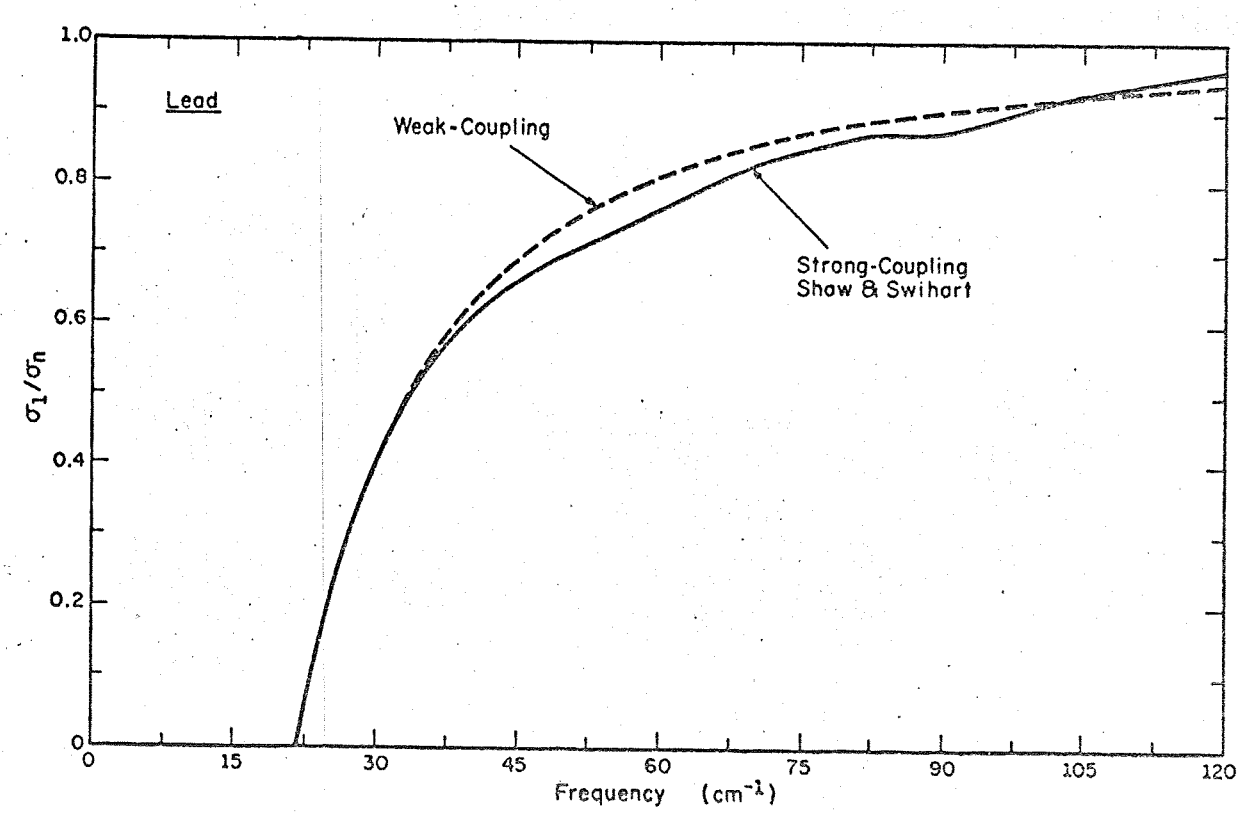
Lead
Weak-Coupling
Strong-Coupling
Shaw & Swihart
σ_1/σ_n
1.0
0.8
0.6
0.4
0.2
0
0
15
30
45
60
75
90
105
120
Frequency (cm^{-1})

Figure 6. Imaginary part of the conductivity ratio for lead.

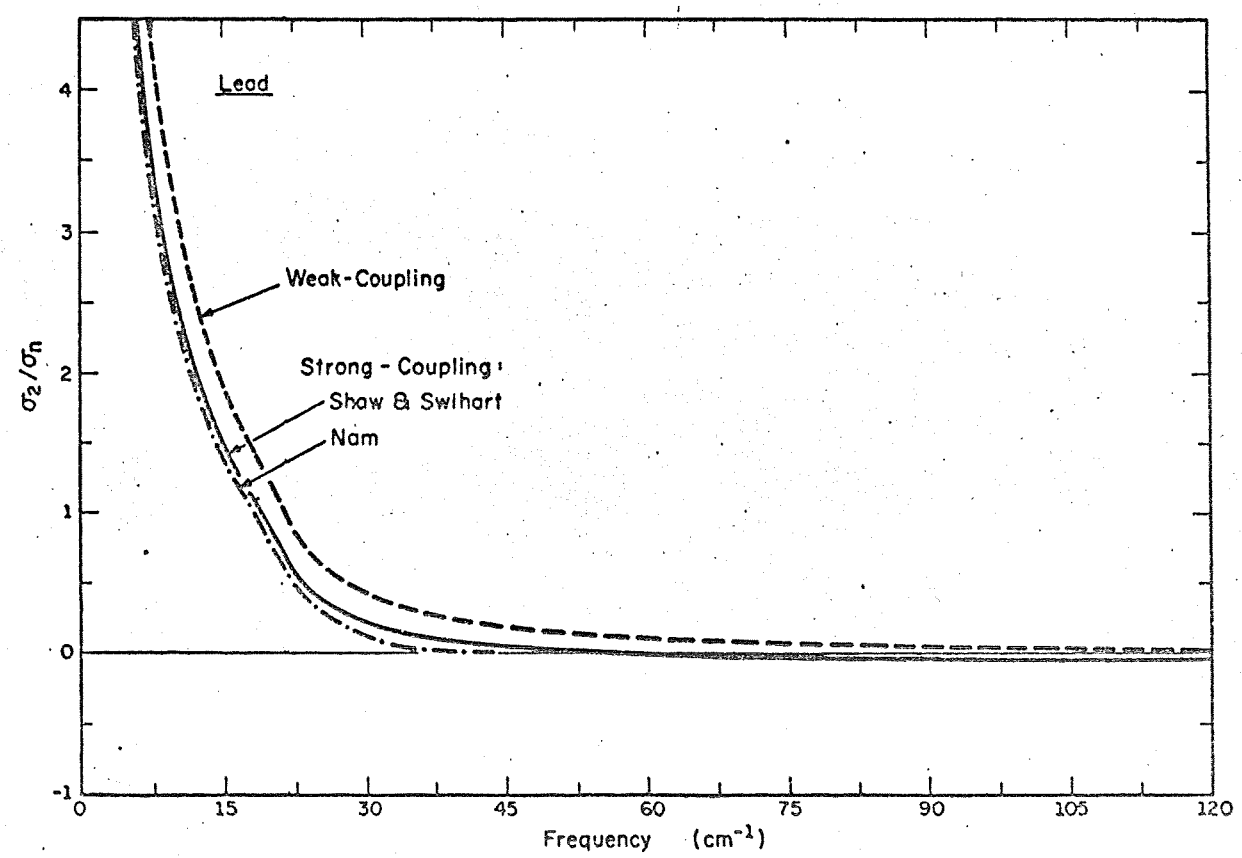
Lead
Weak-Coupling
Strong - Coupling :
Shaw & Swihart
Nam
σ_2/σ_n
4
3
2
1
0
-1
0
15
30
45
60
75
90
105
120
Frequency (cm^{-1})

byproduct. The conductivity of amorphous bismuth was calculated from a gap parameter derived by Chen et al[83] from their tunneling data. Used for amorphous and β-phase gallium were preliminary calculations of those gap parameters, derived by Wühl, Jackson, and Briscoe[84,85] from their experimental work.

The values of the gap parameter as a function of frequency which were supplied extended only down to the energy gap $\Delta(\omega_g)$. Other values were of no interest in the analysis of tunneling data since the quantity involving $\Delta(\omega)$ which multiplies the kernels in the Eliashberg gap equations vanishes for $0 \leq \omega \leq \omega_g$. These missing values of $\Delta(\omega)$ are important in calculating conductivity, however, since one of the integrals contributing to σ_2/σ_n is over the range $0 \leq \omega \leq \omega_g$. The missing values of the gap parameter could be calculated from those supplied by using two useful properties.[86] First, $\Delta(\omega)$ is an analytic function[87] and its real and imaginary parts therefore satisfy the Kramers-Kronig relations in (12). Secondly, the imaginary part of $\Delta(\omega)$ vanishes for $0 \leq \omega \leq \omega_g$. Thus $\mathrm{Im}\,\Delta(\omega) \equiv \Delta_2(\omega)$ was extrapolated trivially to zero frequency and $\mathrm{Re}\,\Delta(\omega) \equiv \Delta_1(\omega)$ was calculated as the KK transform of $\Delta_2(\omega)$. Obviously, the numerical integration could not be carried out to infinity. The remaining portion of the integral was treated as a constant and incorporated into the constant to be added to the transform of $\Delta_2(\omega)$. The constant was determined by fitting $\Delta_1(\omega)$ for $\omega < \omega_g$ smoothly to $\Delta_1(\omega)$ for $\omega > \omega_g$. The accuracy of this calculation of σ_2/σ_n does depend upon the accuracy of this transformation of Δ_2, as the calculation by Shaw and Swihart depended upon the direct transformation

of σ_1/σ_n. As a check, $\Delta_1(\omega)$ was then Kramers-Kronig transformed into $\Delta_2(\omega)$ and good agreement was found.

The conductivity ratios for amorphous bismuth and gallium are shown in Figures 7 through 10. In each case the MB result is shown also. It is immediately apparent that the strong-coupling formalism makes little difference in σ_1/σ_n. However, σ_2/σ_n is greatly reduced in both cases. This can be understood using the sum rule. Although at a given frequency σ_1/σ_n changes only slightly with strong-coupling, integrating the small difference over all frequencies produces a change in the coefficient A of the delta function term of σ_1/σ_n. The change is a sizeable fraction of A itself, and thus A for strong-coupling is reduced noticeably from its MB value. This reduction is reflected in σ_2/σ_n as a smaller ω^{-1} term. Since this term provides a relatively large portion of σ_2/σ_n at frequencies below the gap, a significant decrease in A should produce a corresponding decrease in σ_2/σ_n, which in fact is what happens.

Shaw and Swihart noted for lead that all but about one percent of the change in σ_2/σ_n at frequencies below $2\omega_g$ results from a change in A. The same is true for bismuth and gallium, and is in fact true for frequencies up to 2.5 times the gap $2\omega_g$ for those materials.

Since strong coupling changes σ_1/σ_n only slightly at a given frequency, and since a good approximation to the strong-coupling σ_2/σ_n can be obtained by subtracting an ω^{-1} term from the MB value, it seems that a good estimate of the strong-coupling conductivity can be simply obtained in this way from the MB results, without doing complicated computer calculations.[88] The real and imaginary parts of this approximate conductivity

Figure 7. Real part of the conductivity ratio for amorphous bismuth.

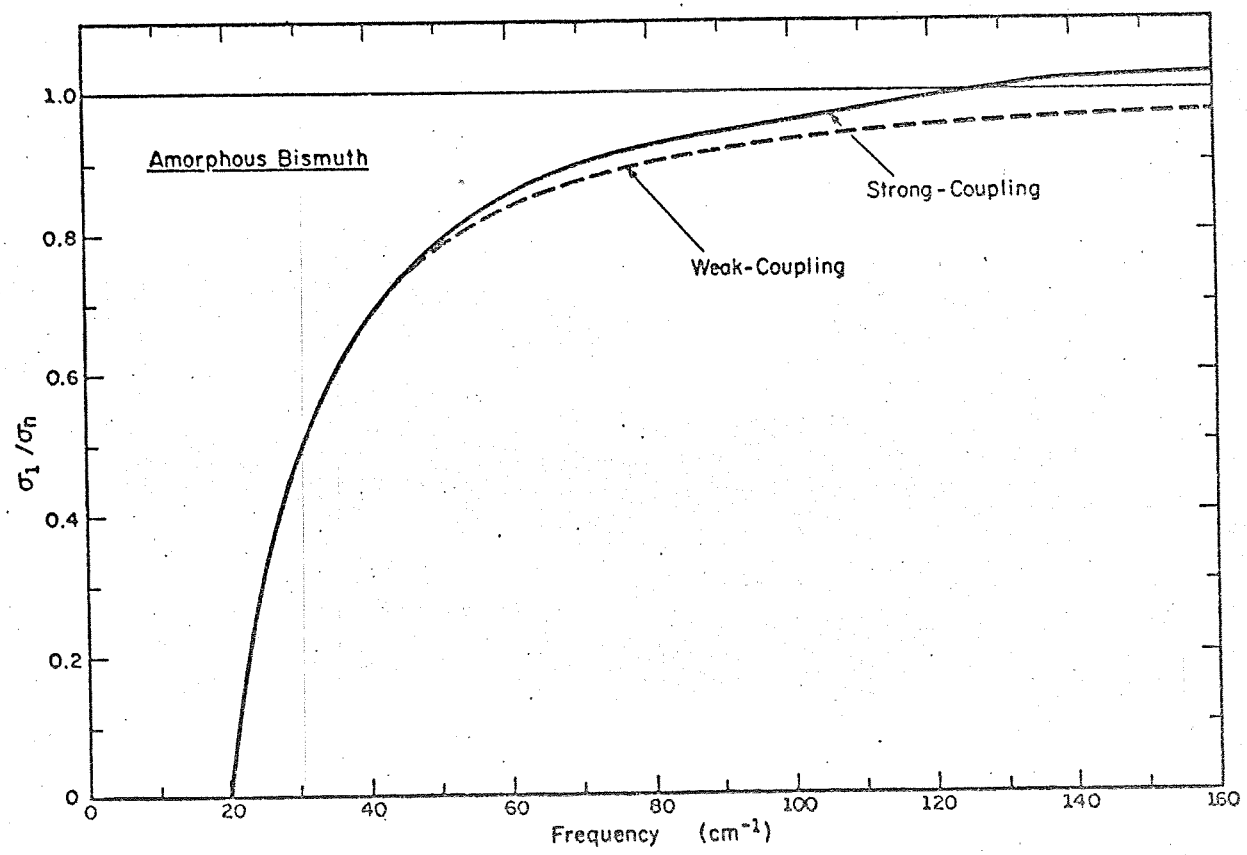
Amorphous Bismuth
Strong-Coupling
Weak-Coupling
σ_1/σ_n
1.0
0.8
0.6
0.4
0.2
0
0
20
40
60
80
100
120
140
160
Frequency (cm^{-1})

Figure 8. Imaginary part of the conductivity ratio for amorphous bismuth.

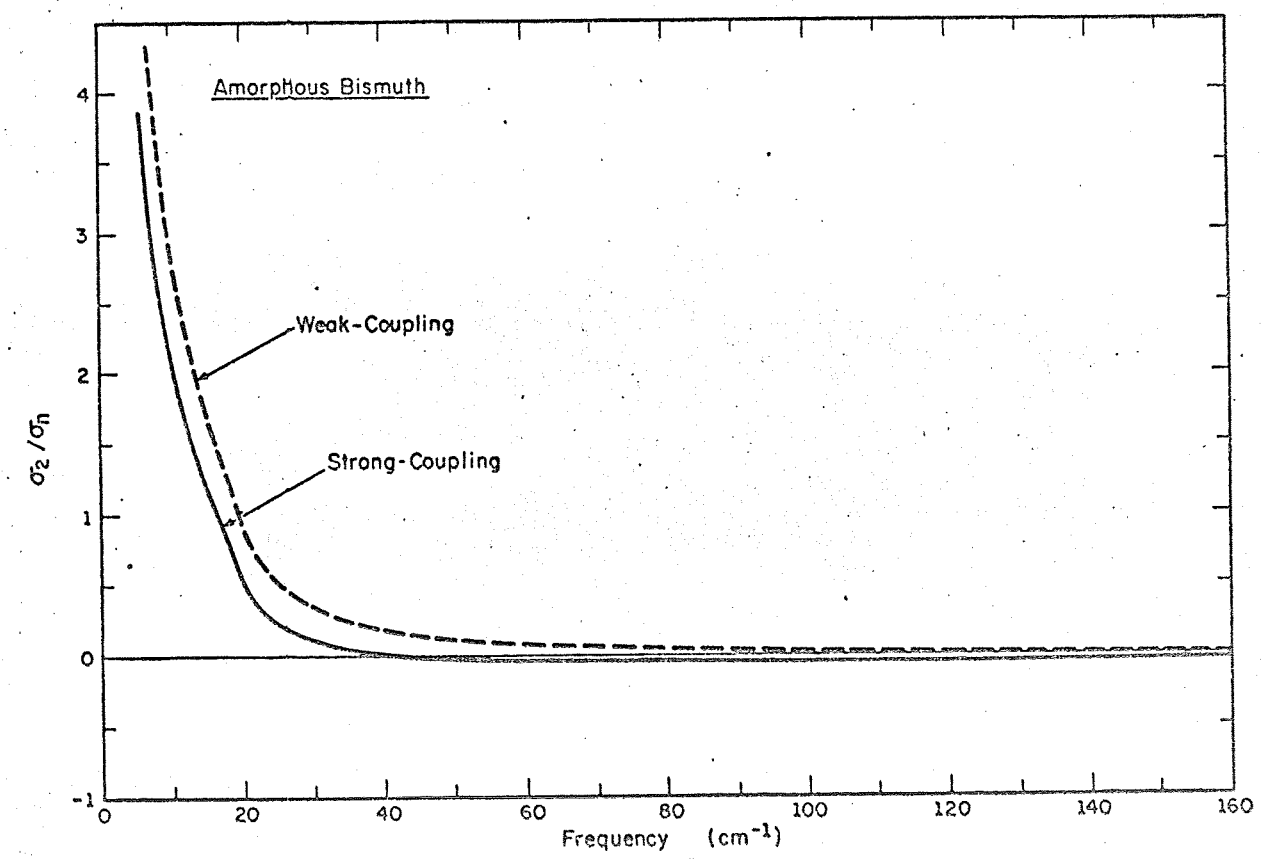
Amorphous Bismuth
Weak-Coupling
Strong-Coupling
σ_2/σ_n
4
3
2
1
0
-1
0
20
40
60
80
100
120
140
160
Frequency (cm^{-1})

Figure 9. Real part of the conductivity ratio for amorphous gallium.

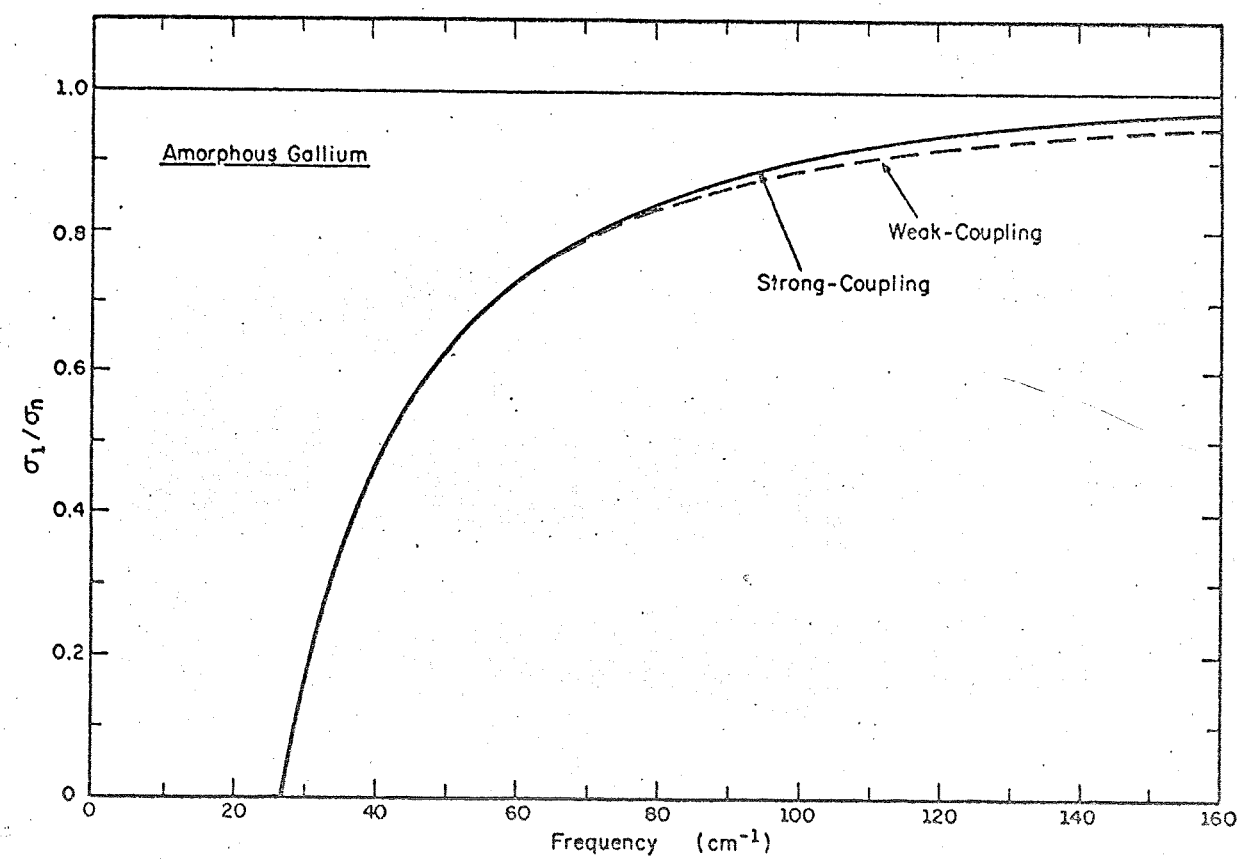
Amorphous Gallium
Weak-Coupling
Strong-Coupling
σ_1/σ_n
1.0
0.8
0.6
0.4
0.2
0
0
20
40
60
80
100
120
140
160
Frequency (cm^{-1})

Figure 10. Imaginary part of the conductivity ratio for amorphous gallium.

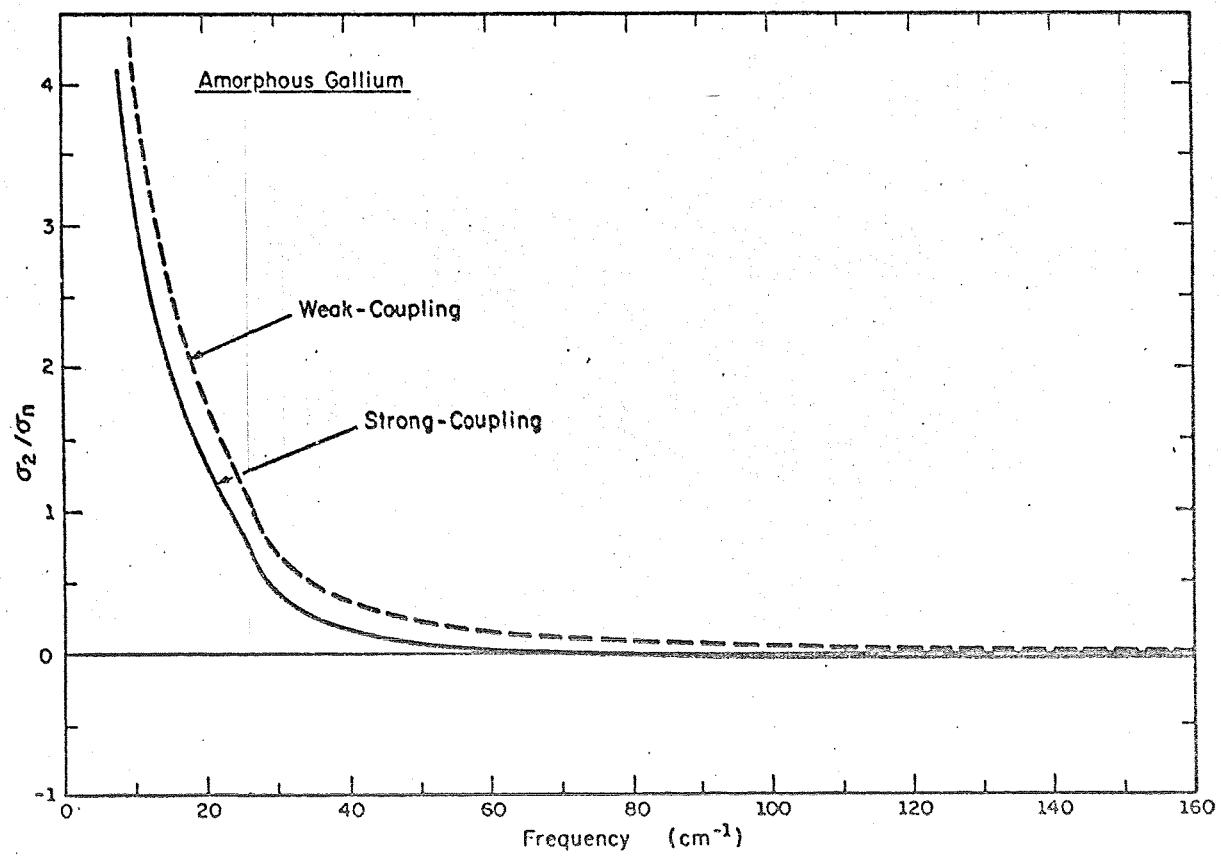
Amorphous Gallium
Weak-Coupling
Strong-Coupling
σ_2/σ_n
4
3
2
1
0
-1
0
20
40
60
80
100
120
140
160
Frequency (cm^{-1})

would not be Kramers-Kronig transforms of each other, and this would have to be kept in mind as it might affect some types of calculations.

IV. RESULTS AND DISCUSSION

The experimental results obtained by using the equipment discussed in Section II are presented in this section. In a table, the data are summarized. For each material the comparison of the far infrared data with the numerical calculations is given. Comparisons with results of other investigators are also presented.

RESULTS

The summary of the results is given in Table 3. Some explanation of the table is necessary. First, not all the columns are applicable for every sample, as can be noted by the absence of some entries. The transition temperatures are presented with estimated uncertainties. The range of uncertainty for the gallium samples is higher than for the other samples because of difficulties with the thermometer during those measurements. The energy gap $2\omega_g$ determined by fitting the far infrared data is given with its estimated uncertainty from the fitting. The next column contains $2\omega_g/k_BT_c$ with the uncertainty being due almost entirely to that in $2\omega_g$. The dc resistance R in ohms per square of the films is obtained by multiplying the actual resistance of the films by the ratio of their width to length, giving the resistance they would have if they were square. If a value of resistance other than R was used in fitting the infrared data to the numerical results it is enclosed in parentheses next to the dc resistance. The thickness t determined by the optical thickness measurements is given. The resistivity ρ was calculated from R and t. Finally given is the temperature $T_{annealing}$ at which the resistance of the film indicated the onset of crystallinity. In

Table 3

SUMMARY OF RESULTS†

Film	T_c (K)	$2\omega_g$ (cm^{-1})	$2\omega_g/k_BT_c$	R (Ω/□) (± 0.5%)	t (Å) (± 20Å)	ρ (μΩ-cm)	$T_{annealing}$ (K)
Pb (77 K)	7.00 ± .03	$21.60^{+0.6}_{-1.0}$	$4.44^{+.12}_{-.21}$	163			
Bi-1	5.82 ± .03	$18.75^{+0.8}_{-0.3}$	$4.63^{+0.20}_{-0.08}$	87.5	143	125 ± 18	
Bi-2	5.68 ± .03	$18.63^{+0.5}_{-0.3}$	$4.72^{+.13}_{-.08}$	132.7	112	149 ± 27	26 ± 3
Bi-3	5.35 ± .03	17.7 ± 0.6	4.76 ± .16	246			
Bi-4	5.97 ± .03			51.8			21 ± 2
Bi-5	5.87 ± .03			90.1	200	180 ± 18	> 29
Bi-6	6.11 ± .03			1.3 ± 0.1			19 ± 2
Ga-1	8.05 ± .07	24.33 ± 0.8	4.35 ± .16	51	210	107 ± 11	48 - 82
Ga-2	7.87 ± .07	$24.00^{+1.5}_{-0.8}$	$4.39^{+.28}_{-.16}$	103(110)	48	49 ± 21	38 ± 5
Ga-3	7.09 ± .07	21.67 ± 1.0	4.40 ± .21	469(240)			> 31
Ga-4	8.45 ± .07			0.18 ± .01			19 ± 2

Table 3 (continued)

Film	T_c (K)	$2\omega_g$ (cm^{-1})	$2\omega_g/k_BT_c$	R (Ω/□) (± 0.5%)	t (Å) (± 20 Å)	ρ (μΩ-cm)	$T_{annealing}$ (K)
Ga-1 (77 K)	7.74 ± .07	20.8 ± 1.0	3.87 ± .19	29.9	210	63 ± 6	200 ± 15
Ga-1 (200 K)	6.55 ± .07	17.95 ± 0.7	3.94 ± .16	24.0	210	50 ± 5	
Ga-2 (77 K)	6.31 ± .07	17.1 ± 0.6	3.90 ± .23	52.1	48	25 ± 11	110 - 240
Ga-4 (20 K)	6.26 ± .07			0.6 ± 0.1			

†Uncertainties shown are estimated maximum values.

some cases the resistance was not followed up to the phase change so it can only be stated that $T_{annealing}$ is greater than (>) the temperature shown. In some other cases the change occurred while the cryostat was unattended so it is possible only to say that the change occurred in a given temperature interval. For films which were annealed before the measurements were made, the temperatures at which the annealing was done are shown in parentheses next to the film numbers.

In the plots of far infrared data to be presented in this section, no error bars are shown. As stated in Section II, under "Infrared Errors," however, the random error in T_s/T_n is estimated to be less than about three percent and the known systematic error to be less than about five percent. The systematic error has an estimated maximum this large only near the points where the main gratings were changed. As $\overline{T}_n$ was assumed to be constant with frequency it does not contribute to the random error. It is estimated, however, that the uncertainty in the determination of $\overline{T}_n$ is less than about one percent. The normal state data are given in the Appendix.

The discussion of the results is begun with lead, the only strongly-coupled material previously studied in detail. Data on one sample studied in this work is presented and some of the results of earlier measurements will also be compared with the numerical calculations done in this work.

Lead Film

During the development of the cryostat and far infrared techniques, lead films were examined because they were much easier to make and it was not necessary to keep them cooled to helium temperatures at all times, as

with the amorphous films of other materials. One was made after the cryostat had evolved to the form used in the later measurements. This film was evaporated onto a 77 K substrate and annealed at this temperature for about one day. The experimental far infrared transmission ratio T_s/T_n is shown in Figure 11, along with two theoretical curves. The lower theoretical curve was calculated from the gap parameter supplied by Shaw and Swihart which was derived from the tunneling measurements of McMillan and Rowell. The upper theoretical curve resulted from Nam's values of σ_s/σ_n.

It can be seen that the experimental data agree better with the Nam result than the Swihart one, the opposite of what should have occurred since the Nam result is based on a good, but necessarily incomplete, theoretical model of the phonon spectrum while Shaw and Swihart's is derived from experimental data. The Shaw and Swihart result for the peak height is 11 percent below the data, and the Nam result is 7 percent below the data.

Palmer and Tinkham[21] also compare the data for one of their samples with the Nam result and find excellent agreement. Had they used the Shaw and Swihart result the agreement would not have been as good, but would still have been within their estimated uncertainty of five percent.

Bulk Lead and Lead Alloy Samples--Comparison with the Theory

The calculated values of σ_s/σ_n were also used to evaluate the surface impedance ratio R_s/R_n for comparison with the experimental data of Leslie and Ginsberg.[15] Using formulas discussed elsewhere,[25,27] this ratio was evaluated in both the extreme anomalous limit and the extreme local limit using the Shaw and Swihart conductivity. For comparison with

Figure 11. Data and theory for lead film.

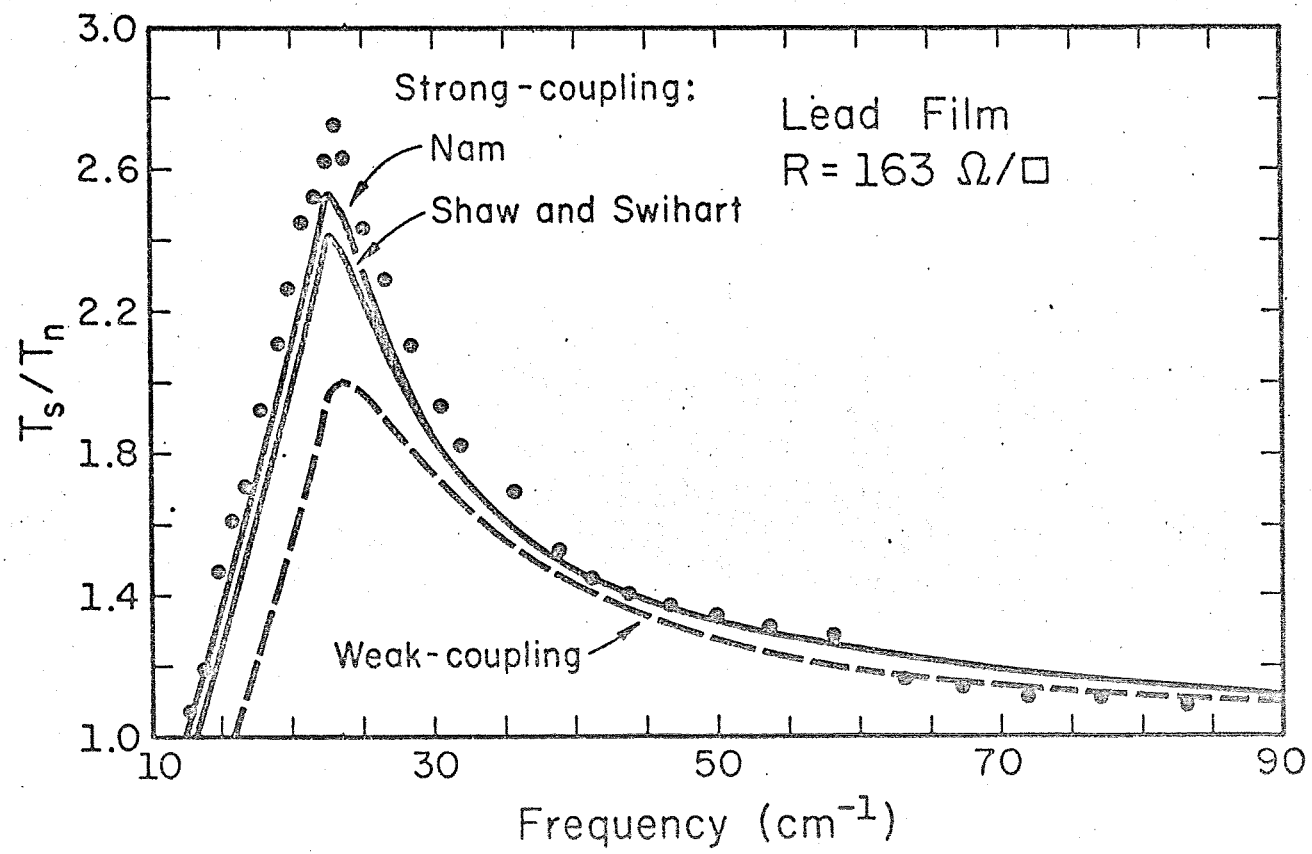
Strong-coupling:
Nam
Shaw and Swihart
Lead Film
R = 163 Ω/□
Weak-coupling
T_s/T_n
3.0
2.6
2.2
1.8
1.4
1.0
10
30
50
70
90
Frequency (cm^{-1})

the data the experimentally determined quantity $P(\omega)$ was evaluated from the surface resistance ratio:

$$P(\omega) = \frac{R_n(\omega) - R_s(\omega)}{R_n(\omega_g) - \frac{1}{k} R_s(\omega)} ,$$

where k is an experimentally determined parameter. Figure 12 shows data for the sample closest to the extreme anomalous limit where $\lambda \ll \xi$; it nevertheless does not well satisfy this condition as $\lambda/\xi = 0.51$. Plotted with the data are the results of the numerical calculation in the extreme anomalous and local limits. The experimental onset of absorption near the gap appears more rapid than either of the theoretical curves, but at high frequencies, the experimental decrease in $P(\omega)$ is less rapid than that of the theory.

Figures 13 and 14 show data and theory for the two samples closest to the local limit, where $\ell \ll \xi_o$. As shown on the figures these conditions are not met by the samples. In both cases, however, remarkably good agreement occurs with the theoretical curve for the extreme anomalous limit, rather than that for the local limit. In Figure 13 is also shown the weak-coupling numerical calculation done by Ginsberg.[87] Here the latter result lies above both the strong-coupling results for all frequencies above the gap.

Detailed conclusions cannot be drawn without performing strong-coupling calculations which do not resort to a limiting form. It can be observed, however, that the strong-coupling theory does provide about the experimentally determined steepening of the curves beyond the MB prediction.

Figure 12. Theory compared with data on sample 7 of Reference 15. $\lambda/\xi = 0.51$ and $\ell/\xi_o = 120$.

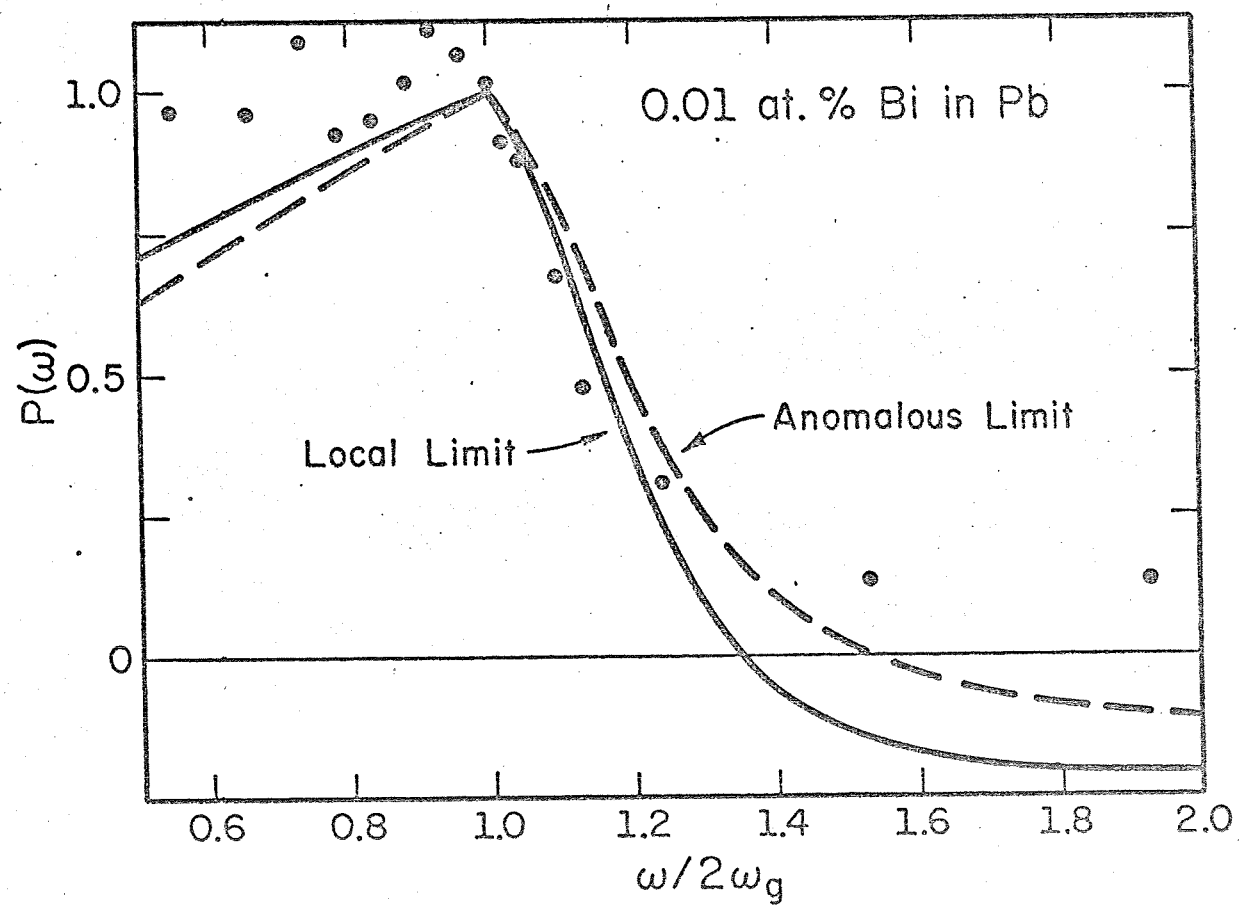
0.01 at. % Bi in Pb
Local Limit
Anomalous Limit
P(ω)
1.0
0.5
0
0.6
0.8
1.0
1.2
1.4
1.6
1.8
2.0
ω/2ω_g

Figure 13. Theory compared with data on sample 9 of Reference 15. $\lambda/\xi = 0.20$ and $\ell/\xi_o = 4.0$.

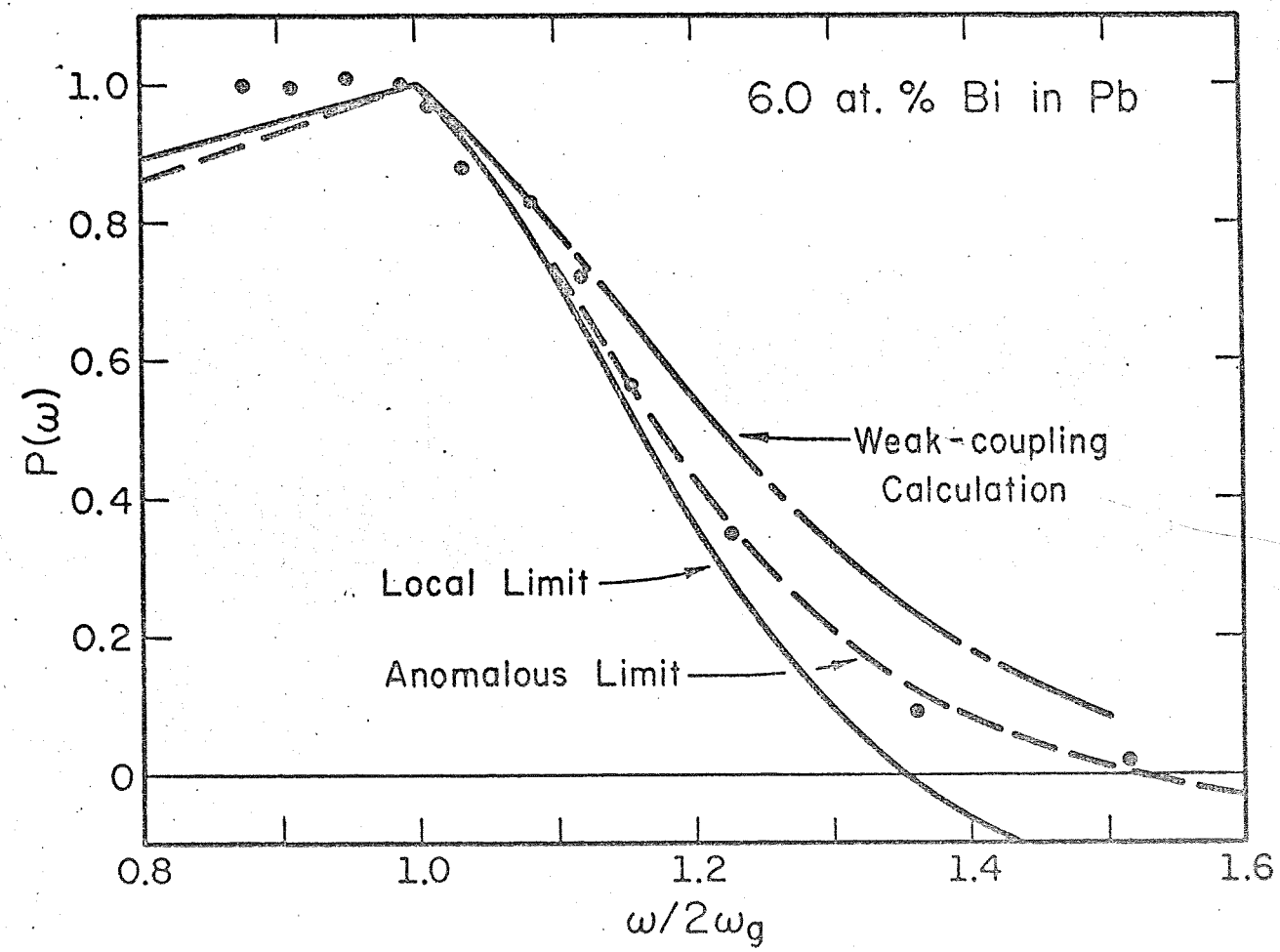
6.0 at. % Bi in Pb
Weak-coupling Calculation
Local Limit
Anomalous Limit
P(ω)
1.0
0.8
0.6
0.4
0.2
0
0.8
1.0
1.2
1.4
1.6
ω/2ω_g

Figure 14. Theory compared with data on sample 5 of Reference 15. $\lambda/\xi = 0.23$ and $\ell/\xi_o = 3.5$.

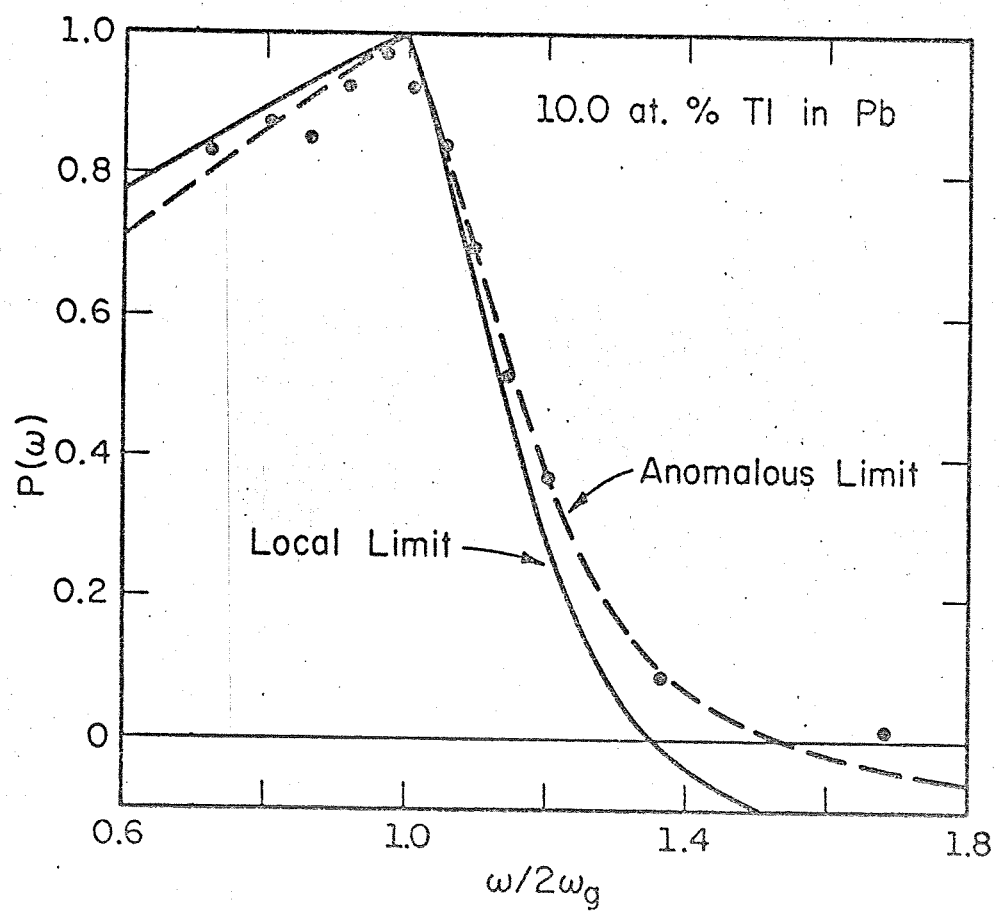
10.0 at. % Tl in Pb
Anomalous Limit
Local Limit
P(ω)
1.0
0.8
0.6
0.4
0.2
0
0.6
1.0
1.4
1.8
ω/2ω_g

If the correction to the limiting forms derived by Ginsberg were to apply directly to the strong-coupling result and were as large as for the weak-coupling case, then indeed the predicted steepening would be too great.

The data of Norman and Douglass[25] can also be compared with the results of the numerical calculation. Their data for lead films are presented in terms of the surface resistance ratio R_s/R_n. These films are considered to be bulk samples as their thicknesses are greater than the coherence length for lead. Here again the samples are not in either of the limits where a simple form of the conductivity describes them. The data, shown in Figure 15, lie above the theory for frequencies near the gap edge. That is, the onset of absorption is even more rapid than predicted by the strong-coupling theory in either of the limits. The calculations of Ginsberg suggest, however, that the agreement might be improved if the surface resistance were evaluated without resort to one of the limiting forms.

Amorphous Bismuth Films

The far infrared data for the bismuth samples are shown in Figures 16 through 18 and the parameters characterizing these films in Table 3. Plotted along with the far infrared data are theoretical curves giving the predictions of the MB and strong-coupling theories, with their frequencies scaled to the $2\omega_g$ given in Table 3. In each case the strong-coupling theory is a distinct improvement over the weak-coupling result. For bismuth films Bi-1, Bi-2, and Bi-3 the agreement is good. Moreover, to obtain this fit, the only adjustable parameter was the scaling of the frequency. The resistance used was the measured dc resistance. For two other films,

Figure 15. Theory compared with data on samples Pb-II and Pb-III of Reference 25. For Pb-II $\lambda/\xi = 0.5$, $\ell/\xi_o = 12.1$, and two gaps were observed. For Pb-III $\lambda/\xi = 1.0$ and $\ell/\xi_o = 1.45$.

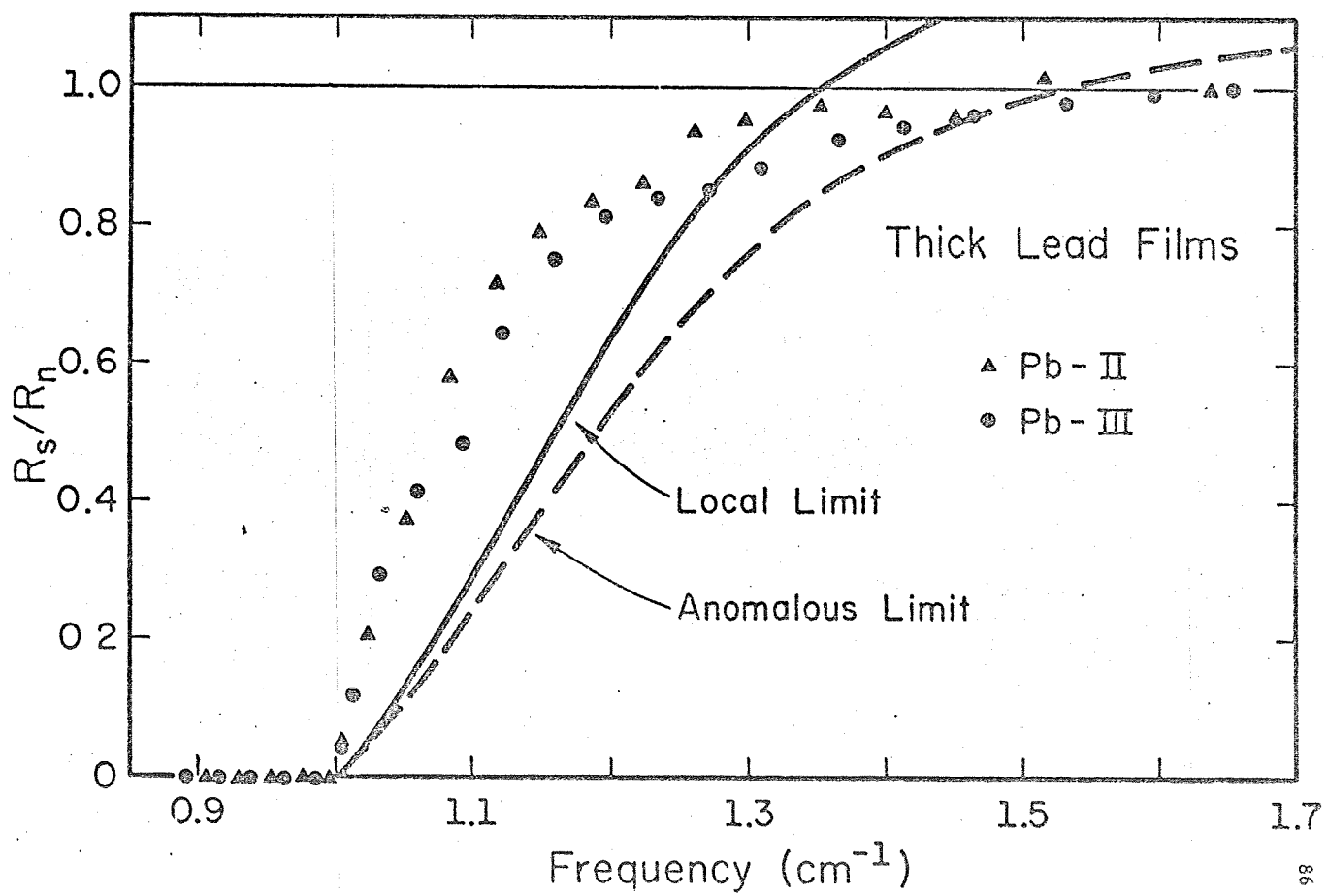
Thick Lead Films
Pb - II
Pb - III
Local Limit
Anomalous Limit
R_s/R_n
1.0
0.8
0.6
0.4
0.2
0
0.9
1.1
1.3
1.5
1.7
Frequency (cm^{-1})

Figure 16. Data and theory for Bi-1. Data were taken with KBr filter.

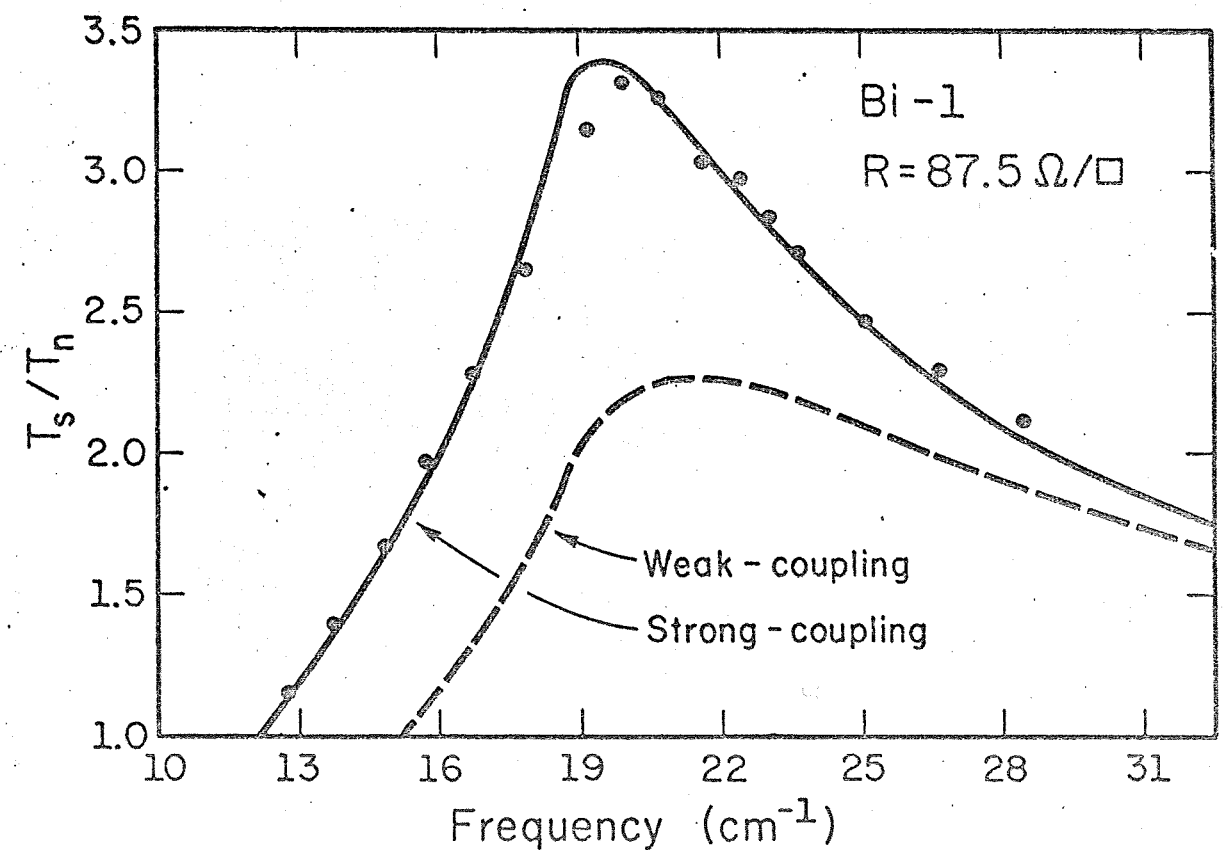
Bi -1
R = 87.5 Ω/□
Weak - coupling
Strong - coupling
T_s/T_n
3.5
3.0
2.5
2.0
1.5
1.0
10
13
16
19
22
25
28
31
Frequency (cm^{-1})

Figure 17. Data and theory for Bi-2.

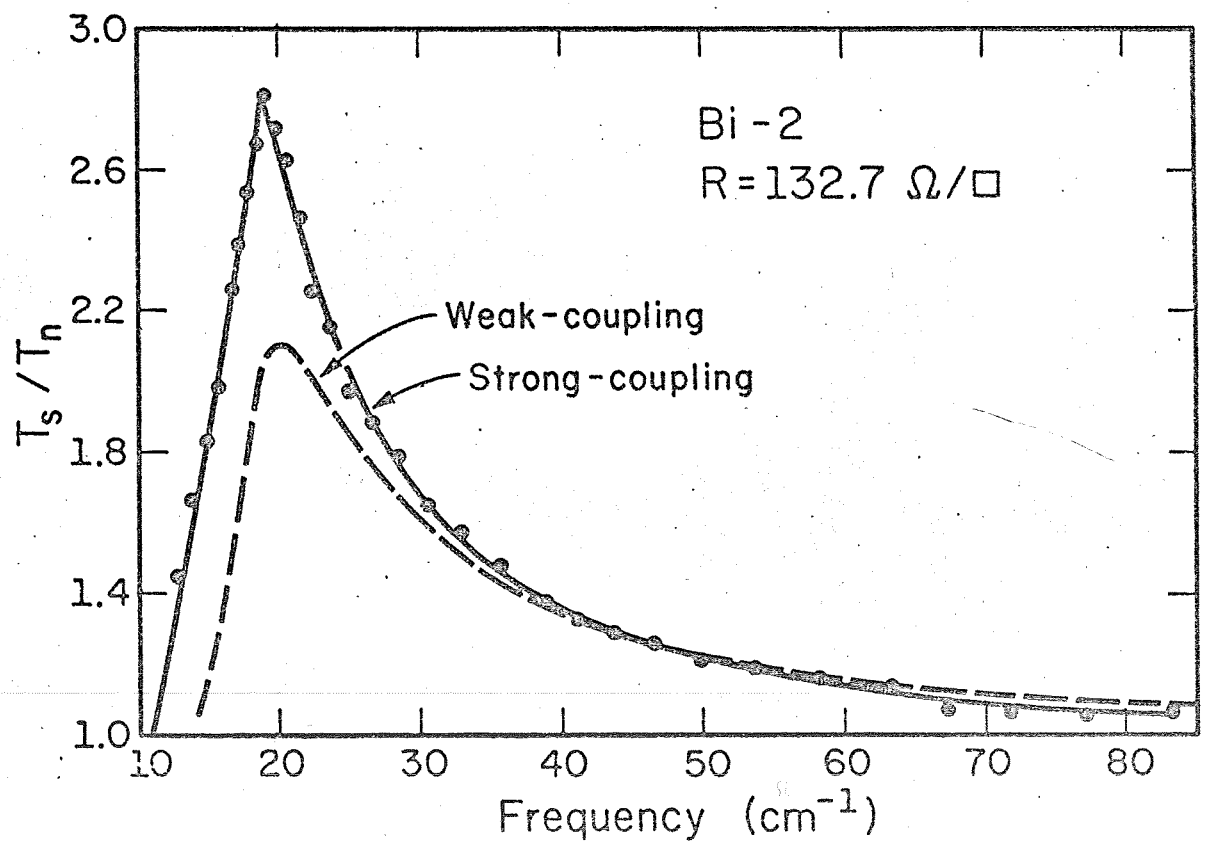
Bi-2
R=132.7 Ω/□
Weak-coupling
Strong-coupling
T_s/T_n
3.0
2.6
2.2
1.8
1.4
1.0
10
20
30
40
50
60
70
80
Frequency (cm^{-1})

Figure 18. Data and theory for Bi-3.

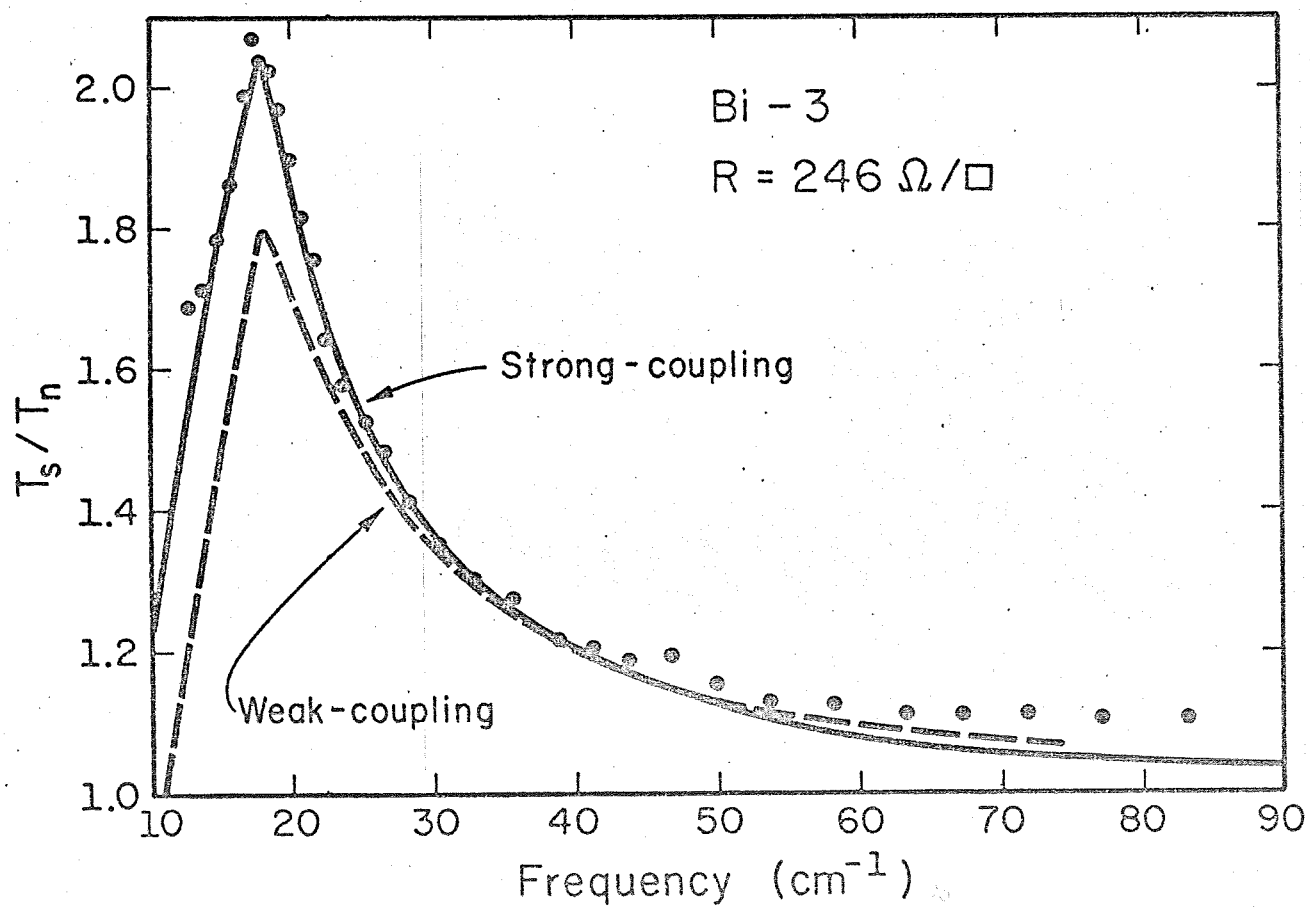
Bi - 3
R = 246 Ω/□
Strong - coupling
Weak - coupling
T_s / T_n
2.0
1.8
1.6
1.4
1.2
1.0
10
20
30
40
50
60
70
80
90
Frequency (cm^{-1})

which were accidentally annealed before measurements were completed, no normal state data were available so that an accurate determination of the energy gap $2\omega_g$ was not possible. A final sample, much thicker than the others, was made to check agreement of transition temperature with those reported for tuneling and other measurements. The comparison is shown in Table 4.

The differences in the transition temperatures listed are probably due to a combination of differing crystallinity, thickness, purity, and thermometry for various samples. Naugle and Glover[35] have reported that for films thicker than 150 Å, there is a downward shift in T_c which is nearly linear in reisstance, a drop of about 10 mK occurring for a 1000 Å film. This may account for some of the differences observed.

In Figure 19 are plotted the energy gaps $2\omega_g$ and transition temperatures versus resistance for the bismuth films. They have each been normalized to the thick film results of Chen et at.[83] A decrease in both, with increasing resistance, is apparent. Also included in this figure is a dashed line indicating the nearly linear decrease in T_c found by Naugle and Glover: it lies below our data, as might be expected from their observation that for the films less than 150 Å thick T_c is depressed less than the linear dependence. Our thickest film was only 200 Å thick.

As indicated in Table 3, the temperatures at which the bismuth films annealed into the crystalline state were all above the thick film result of 19 K and the commonly reported value of about 15 K, for thick films. The onset of crystallinity is associated with an irreversible and

Table 4

RESULTS OF OTHER EXPERIMENTS

Reference	T_c (K)	$2\omega_g$ (meV)	$2\omega_g/k_BT_c$
Amorphous Bismuth			
Shier and Ginsberg[36]	6.17 ± .03		
Zavarittski[89]	6	2.370	4.6
Minnegerode and Rothenberg[90]	5.93 ± .12	2.33	4.56 ± .09
Chen *et al*[83]	6.11 ± .03	2.42 ± .02	4.59 ± .06
This work†	6.11 ± .03	$2.19^{+.06}_{-.09}$	$4.63^{+.20}_{-.08}$
		$-2.32^{+.10}_{-.04}$	- 4.76 ± .16
Amorphous Gallium			
Minnegerode and Rothenberg[90]	8.47 ± .17	3.29 - 3.30	4.50 ± .08
			- 4.52 ± .08
Wühl, Jackson, and Briscoe[84]	8.4 ± .1	3.30 ± .06	4.5
Chen *et al*[83]	8.56 ± .02	3.32 ± .02	4.51 ± .04
This work†	8.45 ± .07	3.02 ± .10	4.35 ± .16
		- 2.69 ± .13	- 4.40 ± .21
β-Phase Gallium			
Minnegerode and Rothenberg[90]	6.21 ± .12	2.11 - 2.15	3.95 ± .08
			- 4.02 ± .08
Wühl, Jackson, and Briscoe[84]	6.2 ± .1	2.08 ± .04	3.9
This work†	6.26 ± .07	2.58 ± .13	3.79 ± .19
		- 2.12 ± .08	- 3.94 ± .16

†The values of T_c are for thick films and should be directly comparable with the values obtained from other experiments. The values of $2\omega_g$ and $2\omega_g/k_BT_c$ are for the thin films studied. Uncertainties shown are estimated maximum values.

Figure 19. $2\omega_g$ and T_c versus resistance for amorphous bismuth films.

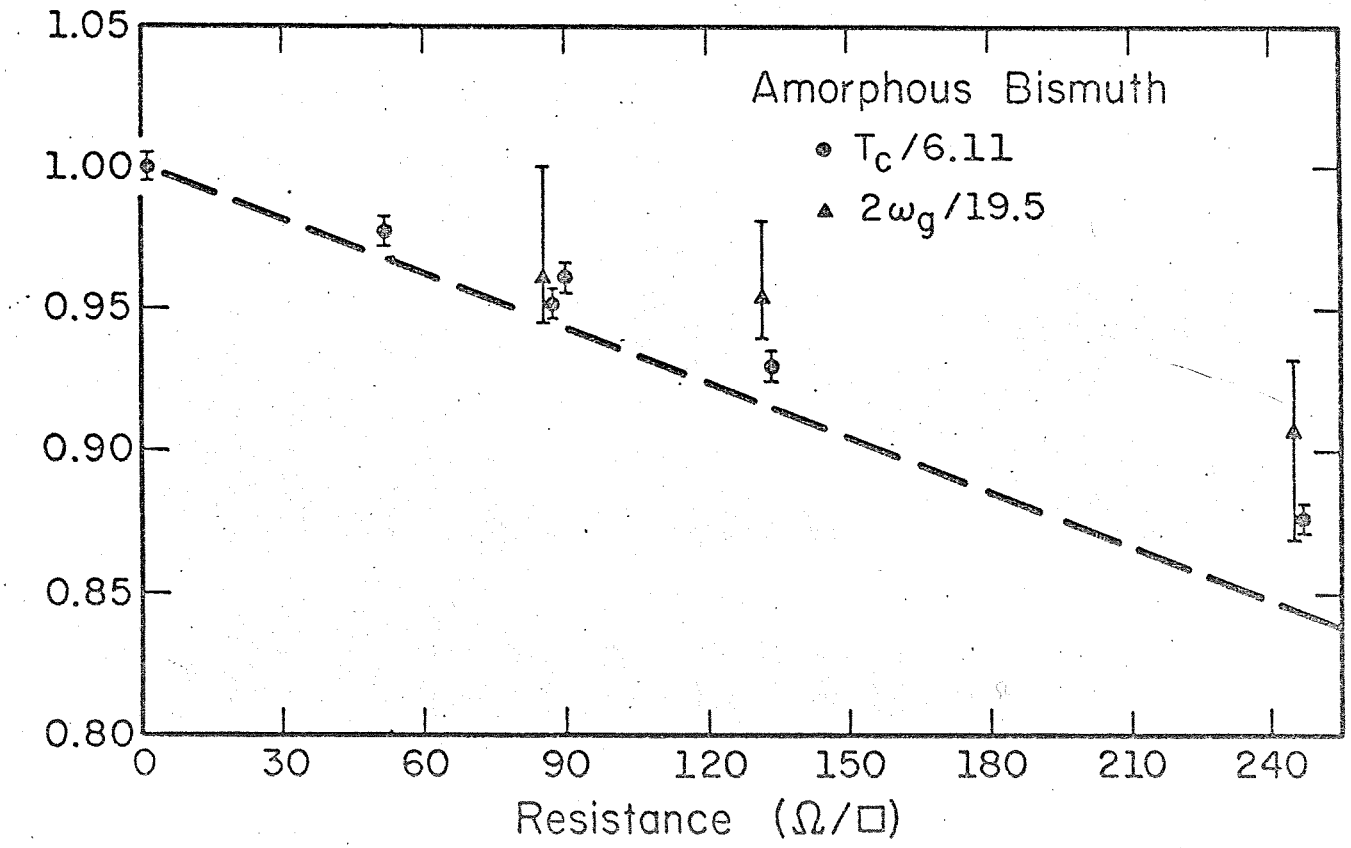
Amorphous Bismuth
$T_c/6.11$
$2\omega_g/19.5$
1.05
1.00
0.95
0.90
0.85
0.80
0
30
60
90
120
150
180
210
240
Resistance ($\Omega/\square$)

abrupt increase in resistance with increasing temperature. Not only did the transitions for these thin films occur at a higher temperature than for the thick ones but also it was not abrupt but gradual. As the gallium films behaved similarly more discussion of this behavior will be given with the data on annealed gallium films.

Amorphous Gallium Films

In Figures 20 through 22 are shown the far infrared data for three amorphous gallium samples and Table 3 gives the remaining results. For one of the three samples, Ga-1, good agreement with theory was obtained solely by scaling the frequency in the theoretical curve. In the cases of Ga-2 and Ga-3, the films were visibly thinner in a band parallel to and overlapping one of the electrodes, but outside the region through which the far infrared passed. Thus the far infrared results are characteristic of the thicker portion. The transition temperature should be characteristic of that portion also as the thinner region should have already been normal at the transition of the thicker area, introducing only a shift in the zero of the ac resistance measurement. The dc resistance, however, would be expected to characterize the entire film, and thus not agree with the far infrared resistance. The agreement between the far infrared data for films Ga-2 and Ga-3 was therefore obtained by adjusting the far infrared resistance until a best fit was achieved. The effect of this change from the dc resistance is primarily to change the theoretical peak height, although it does also shift the theoretical position of the peak slightly.

Figure 20. Data and theory for Ga-1.

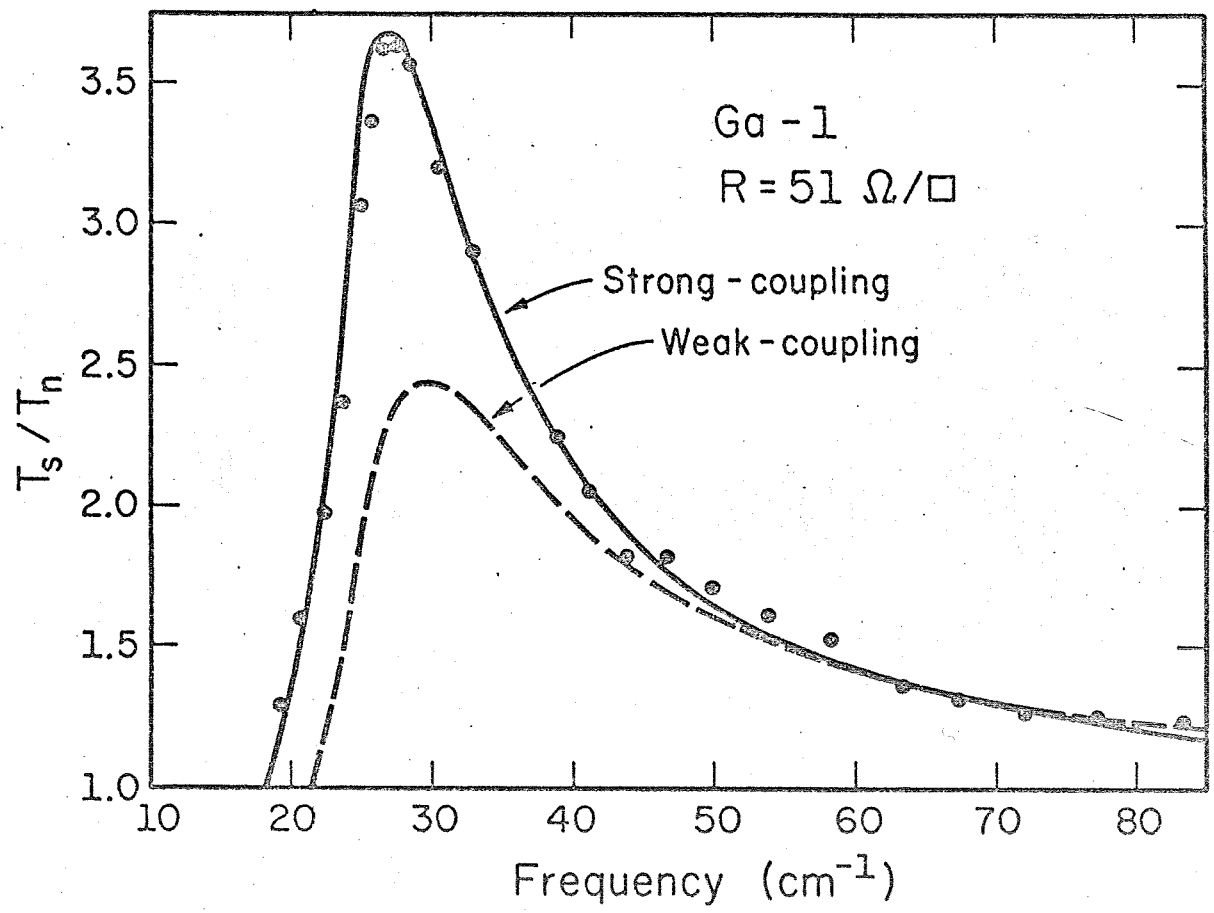
Ga - 1
R = 51 Ω/□
Strong - coupling
Weak - coupling
T_s / T_n
3.5
3.0
2.5
2.0
1.5
1.0
10
20
30
40
50
60
70
80
Frequency (cm^{-1})

Figure 21. Data and theory for Ga-2.

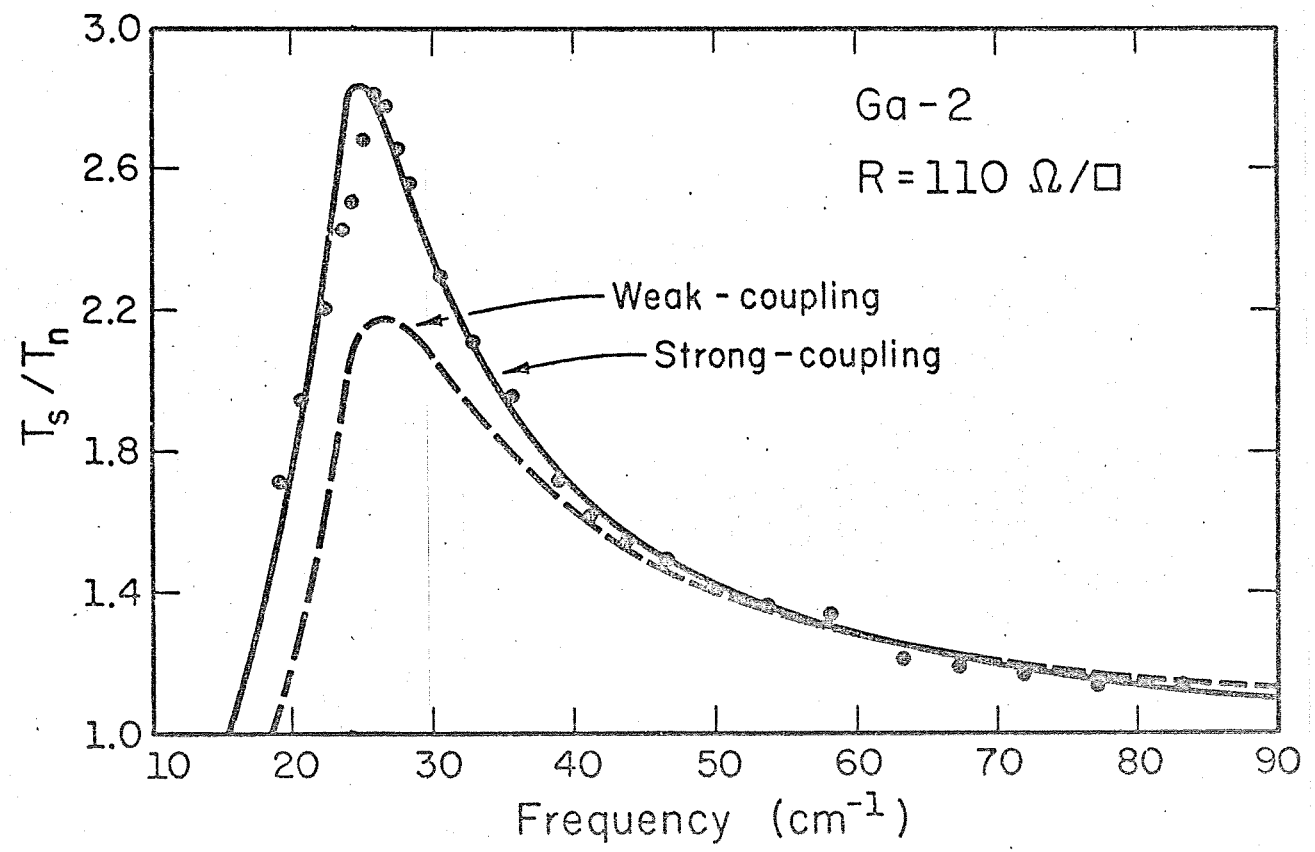
Ga-2
R = 110 Ω/□
Weak - coupling
Strong - coupling
T_s/T_n
3.0
2.6
2.2
1.8
1.4
1.0
10
20
30
40
50
60
70
80
90
Frequency (cm^{-1})

Figure 22. Data and theory for Ga-3.

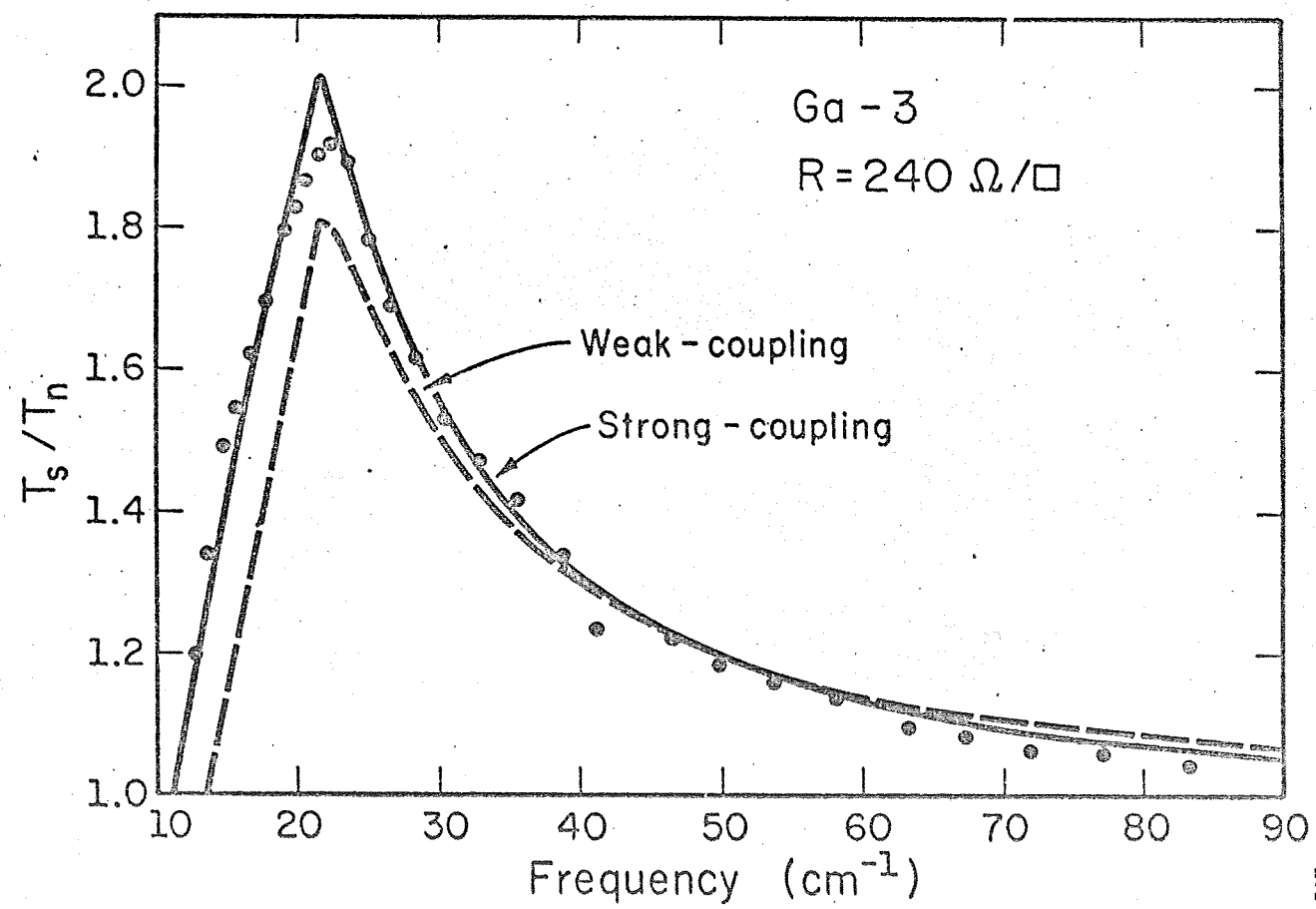
Ga - 3
R = 240 Ω/□
Weak - coupling
Strong - coupling
T_s/T_n
2.0
1.8
1.6
1.4
1.2
1.0
10
20
30
40
50
60
70
80
90
Frequency (cm^{-1})

For the far infrared data the agreement with the theory is not as good as that for bismuth. The major discrepancy is a difference in slope between the data and theory in the region below the gap. It is not known whether the source of the variance is experimental or theoretical, although in defense of the experimental techniques the excellent agreement of theory with the bismuth data should be offered: the same techniques were used with both kinds of films.

In Figure 23, $2\omega_g$ and T_c, normalized to the thick film tunneling results of Wühl, Briscoe, and Jackson,[84] are plotted as a function of resistance for each film. As in the case of bismuth a decrease in both of these quantities with increasing resistance is apparent. Again the dashed line shows the result of Naugle and Glover, this time for gallium, and again the line falls below most of this data. As for bismuth this is in accord with Naugle and Glover's comment that for gallium also, T_c is depressed less than the linear relation for films thinner than 150 Å.

Variation in the T_c's reported in the literature for thick gallium films are greater than those for bismuth. These values are summarized in Table 4.

Annealed Gallium Films

Far infrared data were taken for films Ga-1 and Ga-2 after they were annealed. These data are shown in Figures 24 through 26 along with the strong-coupling theory for gallium films in the β-phase. The MB result is shown also.

Figure 23. $2\omega_g$ and T_c versus resistance for amorphous gallium films.

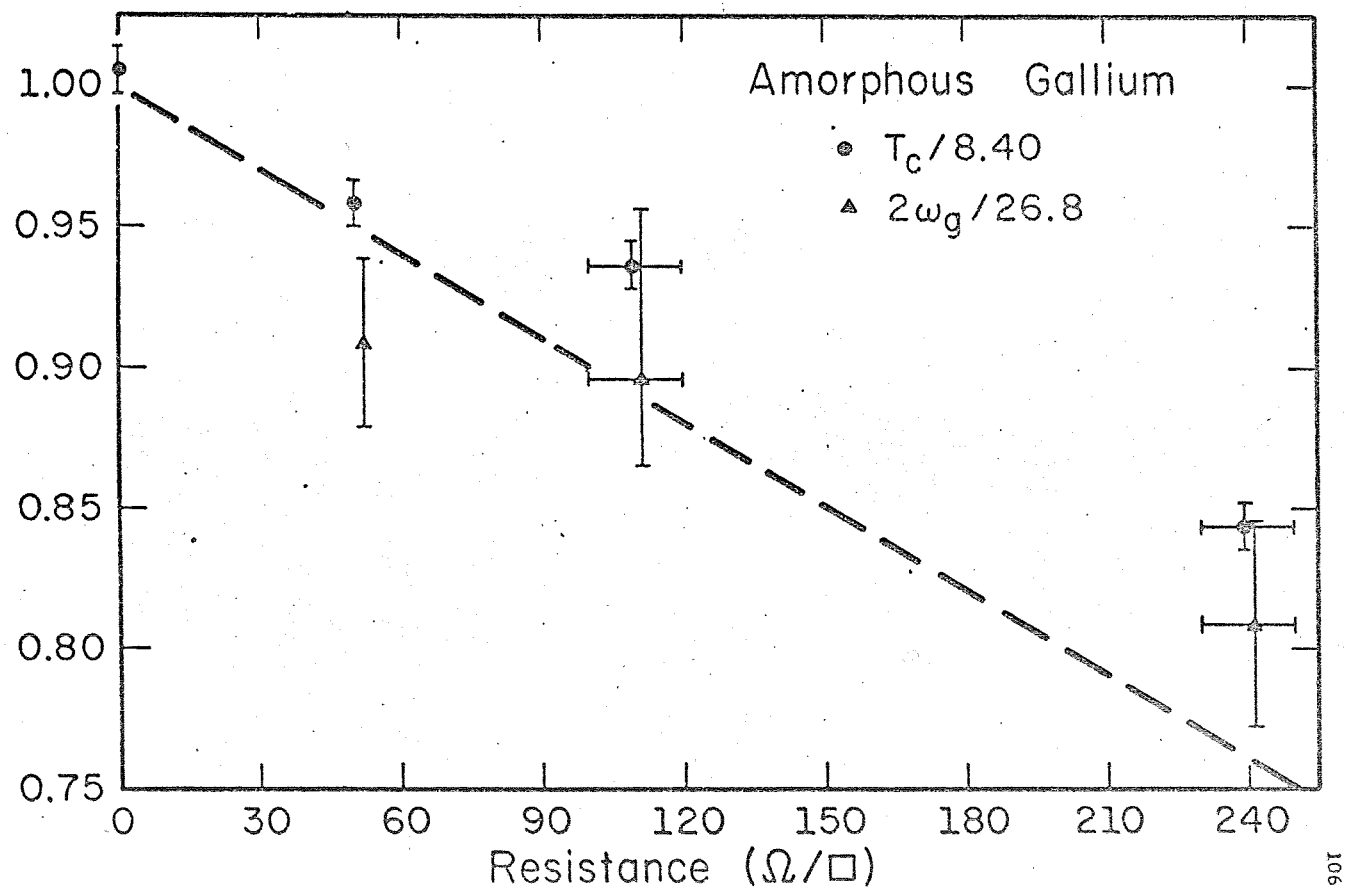
Amorphous Gallium
$T_c/8.40$
$2\omega_g/26.8$
1.00
0.95
0.90
0.85
0.80
0.75
0
30
60
90
120
150
180
210
240
Resistance ($\Omega/\square$)

Figure 24. Data and theory for Ga-1 annealed at 77 K.

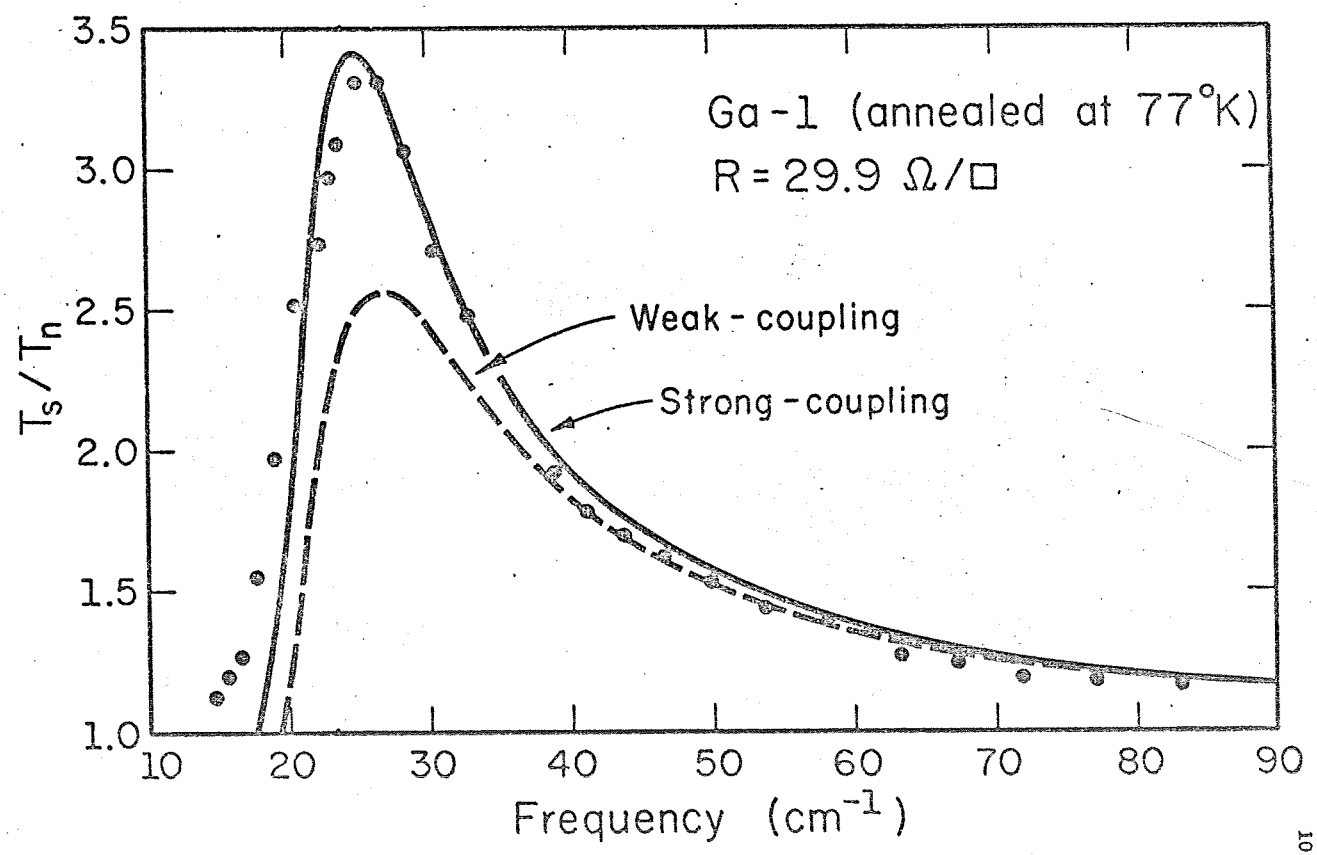
Ga-1 (annealed at 77°K)
R = 29.9 Ω/□
Weak - coupling
Strong - coupling
T_s/T_n
3.5
3.0
2.5
2.0
1.5
1.0
10
20
30
40
50
60
70
80
90
Frequency (cm^{-1})

Figure 25. Data and theory for Ga-1 annealed at 200 K.

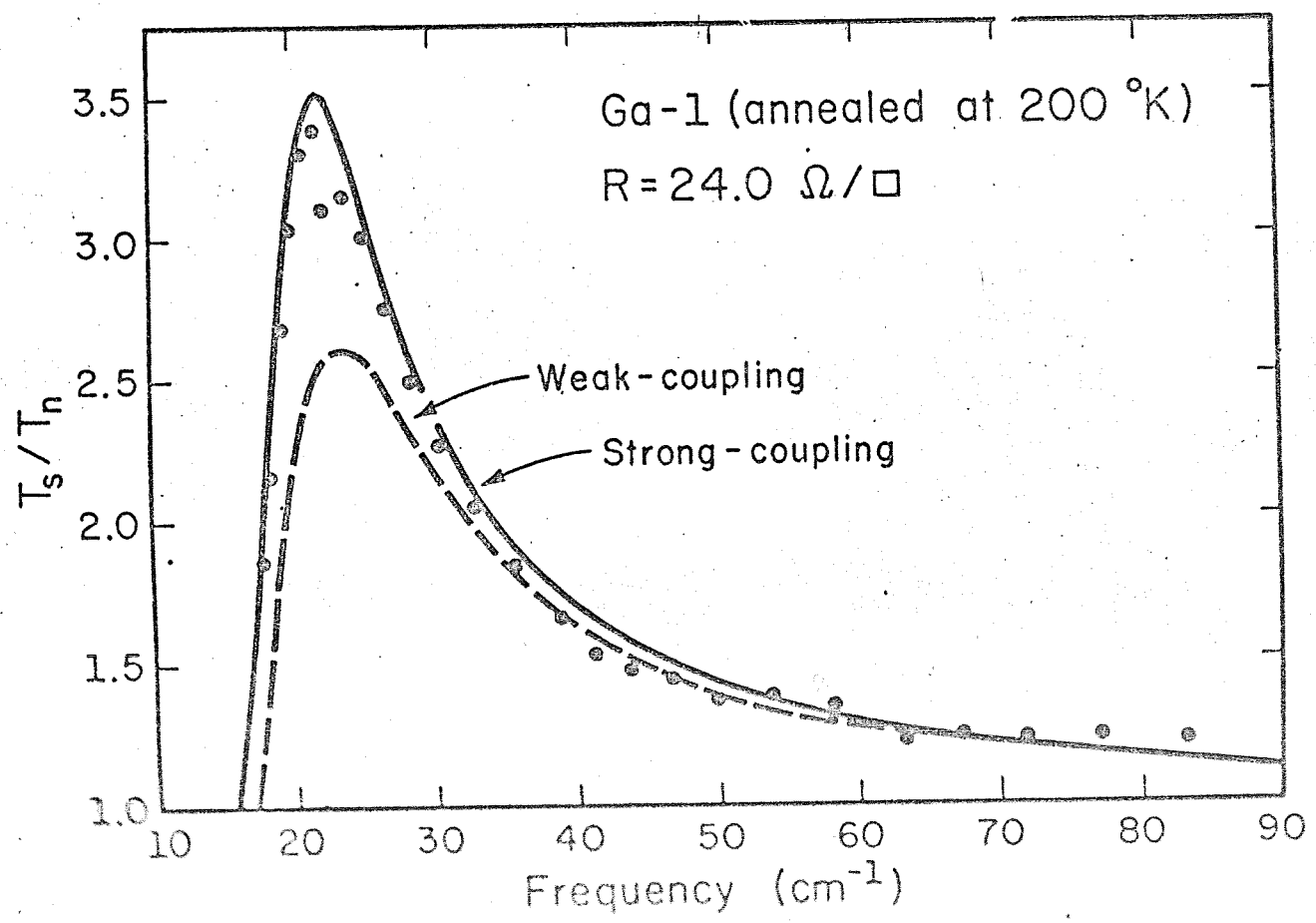
Ga-1 (annealed at 200 °K)
R = 24.0 Ω/□
Weak-coupling
Strong-coupling
T_s/T_n
3.5
3.0
2.5
2.0
1.5
1.0
10
20
30
40
50
60
70
80
90
Frequency (cm^{-1})

Figure 26. Data and theory for Ga-2 annealed at 77 K.

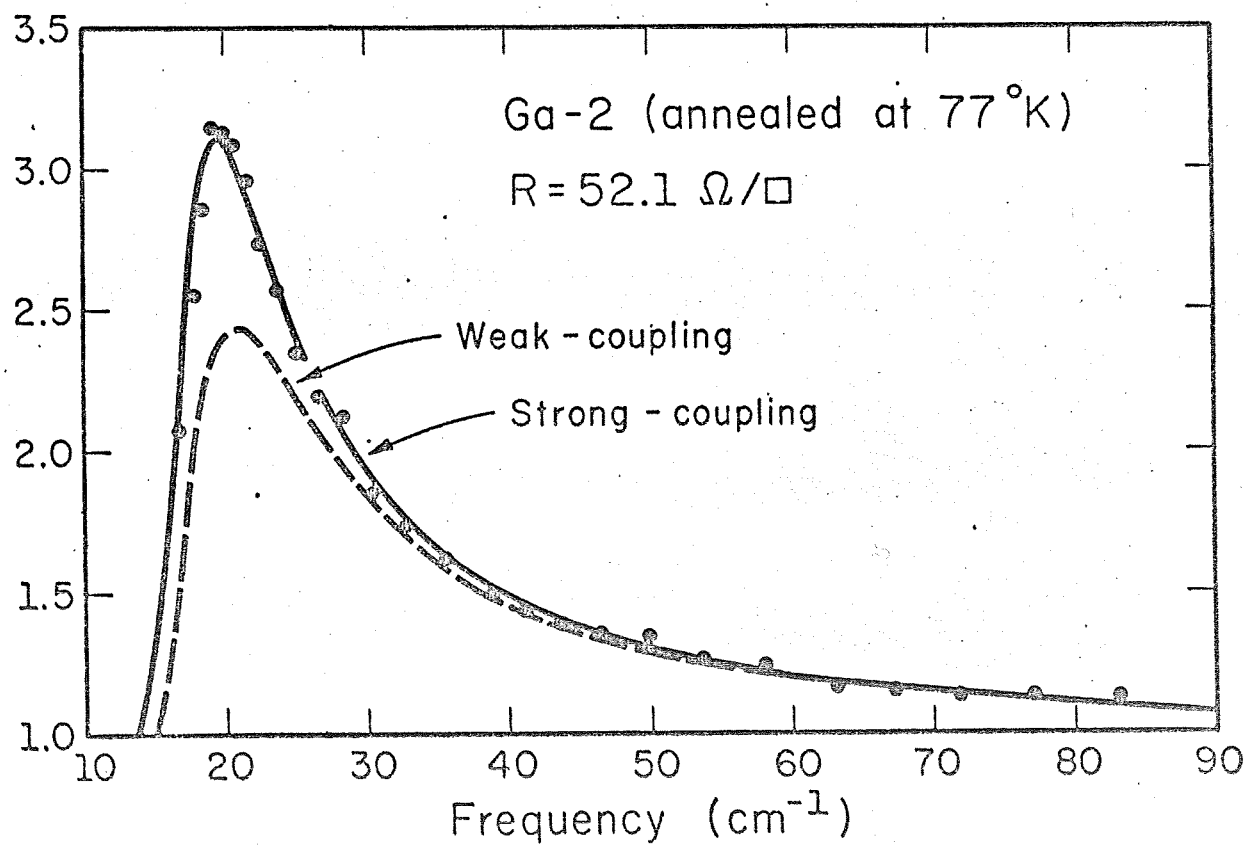
Ga-2 (annealed at 77°K)
R = 52.1 Ω/□
Weak - coupling
Strong - coupling
3.5
3.0
2.5
2.0
1.5
1.0
10
20
30
40
50
60
70
80
90
Frequency (cm^{-1})

The data shown in Figure 25 were treated in a special way. The normalized normal state transmission $\overline{T}_n$ was assumed to be constant. Using the heater T_s/T_n was measured as accurately as possible at one frequency. Then $\overline{T}_s$ was scaled by the same factor at each frequency so that the scaled data coincided with the measurement of T_s/T_n. This produced a transmission ratio which had a magnitude of about 1.4 at the highest frequencies for which data were taken. That is, there was poor agreement with theory at the higher frequencies. The poor agreement depended on a single measurement. Furthermore, because of the very low resistance of the film, the intensity of radiation passing through the film and arriving at the detector was low, producing a low signal-to-noise ratio. Thus the measurement of T_s/T_n was deemed anomalous and the values of $\overline{T}_s$ were scaled by an arbitrary factor chosen to produce good agreement between experiment and theory at frequencies between 40 and 90 cm^{-1}.

Measurements of film resistance as a function of temperature showed that these annealed films had annealing temperatures rather different from those usually reported for thicker films. According to previous reports, amorphous gallium should go into a crystalline phase, called the β-phase, at about 15 K. For our thinner films, however, as can be seen in Table 3, this change occurred above 30 K. Furthermore annealing overnight at 77 K did not produce a film with a T_c as low as 6.2 K to 6.3 K, that reported for thick films in the β-phase. In fact, the resistance of Ga-1 continued to decrease as the temperature was raised to 200 K. Only

then did the resistance begin to increase slightly. When this film was recooled, its transition temperature was 6.55 K, still higher than that quoted for the β-phase in thick films. When Ga-2 was annealed at 77 K its transition temperature fell to 6.31 K. Since it was thinner than Ga-1, it might have been expected to deviate more than Ga-2 from the thick film result, rather than very closely approach it.

Some understanding of these results can be obtained from the work of Sander.[91] He observed that thinner amorphous films anneal at higher temperatures than thicker ones. In fact he used this property so that he could study amorphous films in a liquid hydrogen cooled cryostat. If films were made thicker than 400 Å for bismuth and 1000 Å for gallium, they were already annealed when deposited. In Sander's work measurements were made of the energy released when gallium and bismuth films annealed. He found a heat of transformation for bismuth which was independent of film thickness from the thickest studied, 400 Å, down to 200 Å. For two thinner samples the heat of transformation was smaller by nearly a factor of two. In the case of amorphous gallium the measured heat of transformation was constant for thicknesses down to 320 Å, that of his thinnest sample. An additional property was observed for the thinnest bismuth films. He evaporated a second amorphous bismuth layer over the previously annealed thin bismuth film which had shown a reduced heat of transformation. The heat of transformation per unit volume of the composite film was then

found to be higher than predicted using the constant value previously observed for thicker films and assuming no contribution from the underlying thin film. The excess heat was about equal to the additional heat which would have been given up by the thin film alone had it shown the same heat of transformation as the thicker films. Thus he assumed the thinner "annealed" films had structures only partially transformed into the crystalline phase characteristic of the thicker ones.

It appears therefore that these films are not directly comparable with their thicker counterparts. Nevertheless, the strong-coupling result describes the transmission data moderately well, even though the gap parameter which was used was derived from tunneling data for a much thicker film. No attempt has been made to adjust the infrared resistance from its dc value to improve the agreement. In the case of amorphous Ga-1, no resistance change was necessary; since one might expect the same relative change after the film was annealed, none was made. Changing the resistance of annealed Ga-2 by the same relative amount as in the amorphous case would have made a negligible difference.

DISCUSSION

The measurements have been compared with the theory and with results of other experiments. A few remarks on one comparison deliberately not made and on those which were made are appropriate.

Fluctuations

Recently there has been a great deal of theoretical[92] and experimental[93] interest in the fluctuation pairing of electrons in superconductors at temperatures slightly above their superconducting transitions. Interpretation in these terms of any experimental results which show rounding of the resistive transition in thin films is impeded because it is not possible to be certain that the rounding is due to fluctuations. It might instead be caused by some other unknown effect. Thin films in general are very difficult to accurately characterize. In particular, since the films studied in this work had a necessarily large area for the far infrared measurements, they probably are more inhomogeneous than those used in "fluctuation" measurements. Since conclusions drawn from those experiments are rather tenuous, such conclusions from these experiments would be highly speculative.

Far Infrared Radiation and Strongly-Coupled Superconductors

Quantitative comparison is now possible between far infrared experiments on superconductors and the theory of Nam. The relatively good agreement between experiment and theory, which has been shown by this experiment and that of Palmer and Tinkham, testifies to the great advances in far infrared detectors since the pioneering experiment of Glover and Tinkham.

However, the limitations of far infrared technology are responsible for the present uncertainty as to the existence of the precursor. The theory of Nam predicts no absorption of radiation at frequencies below the gap $2\omega_g$ for $T = 0$. To the extent that the data taken in this work agree with

that theory they exhibit no precursor. Particularly in the case of bismuth that agreement is very good indeed. However, to reduce the maximum possible magnitude of precursor absorption below a few percent of the normal state absorption, a technological advance will be necessary.

Neither have far infrared techniques advanced sufficiently far to enable measurement of the structure predicted by Nam. As has been pointed out, in these experiments it is the shift from the MB result in the quantity A of Equation (16) which is reflected in the peak height of the transmission ratio. The peak height is determined primarily by the far infrared resistance of the film and the quantity A, since σ_1/σ_n and $(\sigma_2/\sigma_n - A)$ do not change appreciably with strong-coupling. It has, therefore, been shown that the dc resistance and A derived from tunneling results, plus scaling of the frequency in the theory to the measured energy gap, lead to moderate agreement with the measured peak height. However, scaling the frequency is disturbing. Before this shift is made structure appears in σ_s/σ_n at frequencies $2\omega_g + \omega_s$, where ω_s represents any of the phonon frequencies at which variations in the phonon density of states occur. Scaling implies that both $2\omega_g$ and ω_s shift downward, which probably is not true.

To the author's knowledge it has not been determined what condition, or combinations of them, leads to the observed decrease of $2\omega_g$ and T_c in these thin films. These conditions might be shifts in the phonon frequencies, substrate effects, boundary effects, fluctuation effects, and so on. Until such an understanding is obtained these data cannot be analyzed in a completely satisfactory manner. The good agreement shown in this experiment indicates that whatever the effect is, scaling is an approximately correct way to deal with the comparison between theory and these data.

To increase the understanding of this problem, two approaches are possible. First, theorists might take upon themselves the exceedingly difficult problem of calculating how such films behave. A rigorous comparison with the data would then be possible. Considering the technological limitations on the accuracy of the present data, it would probably provide good agreement.

However, in this field the existing theory predicts details which are unmeasurable with present technology. The burden therefore seems to fall on the experimenter. He must produce much more accurate data which would not only give a precise determination of A, but also provide details of the structure in σ_s/σ_n. Before such measurements can be made, far infrared technology must be advanced. The best detectors available today are apparently already close to the quantum mechanical limits of performance.[94] The most immediate problem which must be solved is the lack of an intense source of far infrared radiation.

As a beginning, recent reports suggest that a new source may be near.[95,96,97]

LIST OF REFERENCES

1. C. J. Gorter, Rev. Mod. Phys. 36, 3 (1964). This is not the original reference, but it does give an interesting and accessible account of the very early work.

2. D. H. Douglass, Jr. and L. M. Falicov, Progress in Low Temperature Physics, edited by C. J. Gorter (North-Holland, Amsterdam, 1964), Vol. IV, Ch. III. This includes a brief history of the early ideas about the energy gap.

3. B. B. Goodman, Proc. Roy. Soc. (London) A66, 217 (1953).

4. A. Brown, M. Zemansky, and H. A. Boorse, Phys. Rev. 92, 52 (1953).

5. J. Bardeen, Phys. Rev. 97, 1724 (1955).

6. J. Bardeen, L. N. Cooper, and J. R. Schrieffer, Phys. Rev. 108, 1175 (1957).

7. R. Glover and M. Tinkham, Phys. Rev. 108, 243 (1957).

8. W. S. Boyle and K. F. Rodgers, Jr., J. Opt. Soc. Am. 49, 66 (1959).

9. D. M. Ginsberg and M. Tinkham, Phys. Rev. 118, 990 (1960).

10. P. L. Richards and M. Tinkham, Phys. Rev. 119, 575 (1960).

11. D. C. Mattis and J. Bardeen, Phys. Rev. 111, 412 (1958).

12. M. A. Biondi and M. P. Garfunkel, Phys. Rev. Letters 2, 143 (1959).

13. P. B. Miller, Phys. Rev. 118, 928 (1960).

14. I. Gievar and K. Megerle, Phys. Rev. 122, 1101 (1961).

15. J. D. Leslie and D. M. Ginsberg, Phys. Rev. 133, A362 (1964).

16. P. W. Anderson, J. Phys. Chem. Solids 11, 26 (1959).

17. F. J. Low, J. Opt. Soc. Am. 51, 1300 (1961).

18. R. G. Wheeler and J. C. Hill, J. Opt. Soc. Am. 56, 657 (1966).

19. R. L. Cappelletti, D. M. Ginsberg, and J. K. Hulm, Phys. Rev. 158, 340 (1967).

20. P. L. Richards, Eighth European Congress on Molecular Spectroscopy, Copenhagen, 1967 (Butterworth, London, 1965), pp. 535-42.

21. L. H. Palmer and M. Tinkham, Phys. Rev. 165, 588 (1968).

22. S. B. Nam, Phys. Rev. 156, 470 (1967); Phys. Rev. 156, 487 (1967). The second paper contains the result of an incorrect numerical calculation of the conductivity for lead. The error was corrected by Nam and the correct result supplied by private communication.

23. S. L. Norman and D. H. Douglass, Jr., Phys. Rev. Letters 17, 875 (1966).

24. S. L. Norman and D. H. Douglass, Jr., Phys. Rev. Letters 18, 339 (1967).

25. S. L. Norman and D. H. Douglass, Jr., Phys. Rev. 167, 393 (1968).

26. M. Tinkham, Superconductivity (Gordon and Breach, New York, 1962).

27. M. Tinkham, in Optical Properties and Electronic Structure of Metals and Alloys, edited by F. Abeles (North-Holland, Amsterdam, 1966).

28. D. M. Ginsberg and L. C. Hebel, in Superconductivity, edited by R. Parks (Marcel Dekker, New York, 1969), Ch. 4.

29. W. Buckel and R. Hilsch, Z. Phys. 138, 109 (1954).

30. B. G. Lazarev, E. E. Semenenko, and A. I. Sudovtsov, Zh. Eksperim. i Teor. Fiz. 40, 105 (1961) [English transl.: Soviet Phys.--JETP 13, 75 (1961)].

31. W. Buckel, in Structure and Properties of Thin Films (John Wiley, New York, 1959), pp. 53-6.

32. W. L. McMillan, Phys. Rev. 167, 331 (1968).

33. J. W. Garland, K. H. Benneman, and F. M. Mueller, Phys. Rev. Letters 21, 1315 (1968).

34. T. T. Chen, J. T. Chen, J. D. Leslie, and H. J. T. Smith, Phys. Rev. Letters 22, 526 (1969).

35. D. G. Naugle and R. E. Glover, Phys. Letters 28A, 611 (1969).

36. J. S. Shier and D. M. Ginsberg, Phys. Rev. 147, 384 (1966).

37. Optically polished quartz was obtained from Valpey Crystal, 1200 Highland Avenue, Holliston, Mass. The potassium bromide filter was obtained from Harshaw Chemical Co., 1945 E. 97th St., Cleveland, Ohio.

38. Sold in U. S. by James G. Biddle Co., Township Line and Jolly Roads, Plymouth Meeting, Pa.

39. J. S. Shier, Ph.D. Thesis, University of Illinois (1966).

40. Radiation Research Corp.; now available from Andonian Associates, Inc., 26 Thayer Rd., Waltham, Mass. 02154.

41. Cryocal, Inc., 1371 Avenue "E", Riviera Beach, Fla. 33404.

42. R. E. Harris, R. L. Cappelletti, and D. M. Ginsberg, Appl. Opt. 5, 1083 (1966).

43. R. L. Cappelletti, Thesis, University of Illinois (1966).

44. J. D. Leslie, Thesis, University of Illinois (1963).

45. Kewanee Scientific Equipment, Adrian, Michigan.

46. Linde Molecular Sieve, type 4A, Union Carbide Corp., Linde Div., 4511 Harlem Rd., Buffalo, N. Y. 14226.

47. Monsanto Corp., 800 N. Lindbergh Blvd., St. Louis 66, Mo.

48. The resistivity of these samples had been previously measured. See E. A. Davis and W. Dale Compton, Phys. Rev. 140, A2183 (1965).

49. Eagle-Pitcher Co., Quapaw, Okla. These samples were grown to specification.

50. Alscobond Y-725 epoxy, Alloy Supply Co., Rochester, N. Y.

51. Nextel Brand Velvet Coating (Black), 3M Reflective Products Division, 2501 Hudson Road, St. Paul, Minn. 55119.

52. Emerson and Cuming, Inc., Canton, Mass.

53. Princeton Applied Research Corp., P. O. Box 565, Princeton, N. J. 08540.

54. L. H. Palmer, Thesis, University of California (1966).

55. No. 9834 Electronic DC Null Detector, Leeds & Northrup Co., 4901 Stenton Avenue, Philadelphia 44, Pa.

56. Model 7.5-2M, ABC Regulated DC Power Supply, Kepco, Inc., 131-38 Sanford Avenue, Flushing 52, N. Y.

57. D. M. Ginsberg, Thesis, University of California (1959).

58. C. Blake, C. E. Chase, and E. Maxwell, Rev. Sci. Instru. 23, 213 (1952).

59. C. Blake and C. E. Chase, Rev. Sci. Instru. 34, 984 (1963).

60. John Ernest Smith, Jr., Thesis, University of Illinois (1967).

61. Type K-3, No. 7553-5, Universal Potentiometer, Leeds and Northrup Co., 4901 Stenton Avenue, Philadelphia 44, Pa.

62. 1000 ohm No. 4035-B DC Resistance Standard, Leeds and Northrup Co., 4901 Stenton Avenue, Philadelphia 44, Pa.

63. S. Tolansky, Multiple-Beam Interferometry of Surfaces and Thin Films (Oxford University Press, London, 1949).

64. A. E. Jacobs, Thesis, University of Illinois (1968).

65. R. G. Chambers, Proc. Roy. Soc. 65, 458 (1952).

66. G. E. H. Reuter and E. H. Sondheimer, Proc. Roy. Soc. (London) A195, 336 (1948).

67. A. A. Abrikosov, L. P. Gor'kov, and I. M. Khlatnikov, Zh. Eksperim. i Teor. Fiz. 35, 265 (1958) [English transl.: Soviet Phys.--JETP 8, 182 (1958)].

68. J. Bardeen and D. Pines, Phys. Rev. 99, 1140 (1955).

69. A. B. Migdal, Zh. Eksperim. i Teor. Fiz. 34, 1438 (1958) [English transl.: Soviet Phys.--JETP 7, 996 (1958)].

70. G. M. Eliashberg, Zh. Eksperim. i Teor. Fiz. 38, 966 (1960) [English transl.: Soviet Phys.--JETP 11, 696 (1960)].

71. Y. Nambu, Phys. Rev. 117, 648 (1960).

72. D. J. Scalapino, J. R. Schrieffer, and J. W. Wilkins, Phys. Rev. 148, 263 (1966); J. R. Schrieffer, D. J. Scalapino, and J. W. Wilkins, Phys. Rev. Letters 10, 336 (1963).

73. F. Stern, in Solid State Physics, edited by F. Seitz and D. Turnbull (Academic Press, New York, 1963), Vol. 15.

74. K. Kozima, W. Suëtaka, and P. N. Schatz, J. Opt. Soc. Am. 56, 181 (1966). The possibility and limitations of this approach were pointed out by D. M. Ginsberg.

75. R. A. Ferrell and R. E. Glover, III, Phys. Rev. 109, 1398 (1958); M. Tinkham and R. A. Ferrell, Phys. Rev. Letters 2, 331 (1959).

76. J. Bardeen and J. R. Schrieffer, in Progress in Low Temperature Physics, edited by C. J. Gorter (North-Holland, Amsterdam, 1961), Vol. III, Ch. VI, p. 230.

77. R. E. Harris, Technical Report, University of Illinois, Department of Physics (1969).

78. J. R. Waldram, Advan. Phys. 13, 1 (1964).

79. D. M. Ginsberg, Phys. Rev. 151, 241 (1966).

80. This approach was suggested by D. M. Ginsberg.

81. W. Shaw and J. C. Swihart, Phys. Rev. Letters 20, 1000 (1968).

82. W. L. McMillan and J. M. Rowell, Phys. Rev. Letters 14, 102 (1965).

83. J. T. Chen, T. T. Chen, J. D. Leslie, and H. J. T. Smith, Phys. Letters 25A, 679 (1967); Can. J. Phys., to be published; see also Ref. 34.

84. H. Wühl, J. E. Jackson, and C. V. Briscoe, Phys. Rev. Letters 20, 1496 (1968).

85. After the calculations were completed more results for $\Delta(\omega)$ became available: for amorphous gallium by Chen et al, see Ref. 83; final results for amorphous gallium by Wühl, Jackson, and Briscoe, see Ref. 84. The latter authors also stated that the values of $\Delta(\omega)$ for β-gallium are not of high precision.

86. This procedure was suggested by D. M. Ginsberg and its validity verified by L. P. Kadanoff.

87. G. Rickayzen, Theory of Superconductivity (Interscience, New York, 1965), p. 337.

88. This possibility was suggested by D. M. Ginsberg.

89. N. V. Zavaritskii, Zh. Eksperim. i Teor. Fiz.--Psi'ma Redakt. 5, 434 (1967) [English transl.: JETP Letters 5, 352 (1967)].

90. G. v. Minnegerode and J. Rothenberg, Z. Physik 213, 397 (1968).

91. W. Sander, Z. Physik 147, 361 (1957).

92. L. G. Aslamazov and A. I. Larkin, Phys. Letters 26A, 238 (1968); L. P. Kadanoff and G. Laramore, Phys. Rev. 175, 579 (1968); S. Marčelja, Phys. Letters 28A, 180 (1968).

93. R. E. Glover, Phys. Letters 25A, 542 (1967); M. Strongin, O. F. Kammerer, J. Crow, R. S. Thompson, and H. L. Fine, Phys. Rev. Letters 20, 922 (1968); D. C. Naugle and R. E. Glover, Phys. Letters 28A, 110 (1968); S. Marčelja, W. E. Masker, and R. D. Parks, Phys. Rev. Letters 22, 124 (1969); L. R. Testardi, W. A. Reed, P. C. Hohenberg, W. A. Haemmerle, and G. F. Bennert, to be published.

94. H. D. Drew and A. J. Sievers, to be published.

95. D. W. Faries, K. A. Gehring, P. L. Richards, and Y. R. Shen, Phys. Rev. 180, 363 (1969).

96. W. D. Gregory, L. Leopold, D. Repici, and J. Bostock, Phys. Letters 29A, 13 (1969).

97. H. A. Gebbie, N. W. B. Stone, and F. D. Findlay, Nature 202, 685 (1964).

APPENDIX

THE NORMAL STATE DATA

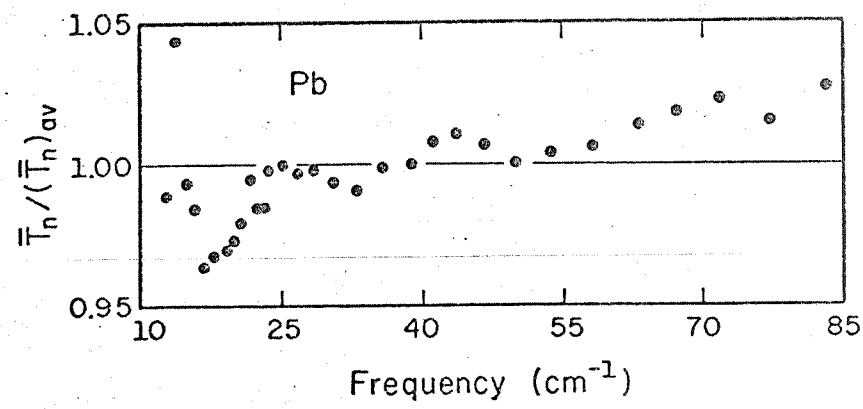

Figure 27. Normal state data for lead film.

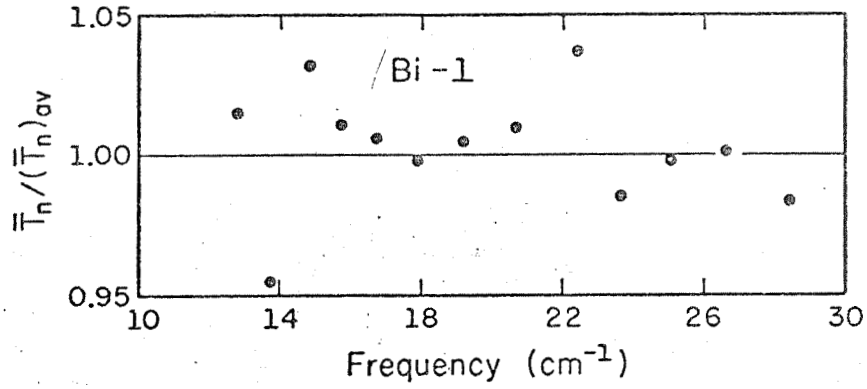

Figure 28. Normal state data for Bi-1.

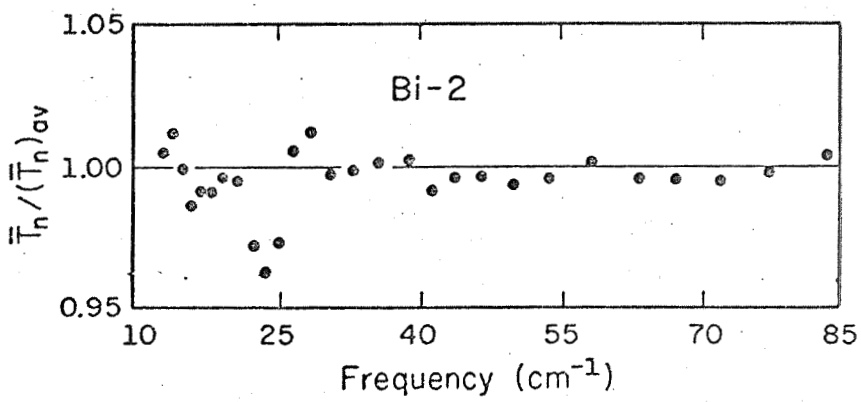

Figure 29. Normal state data for Bi-2.

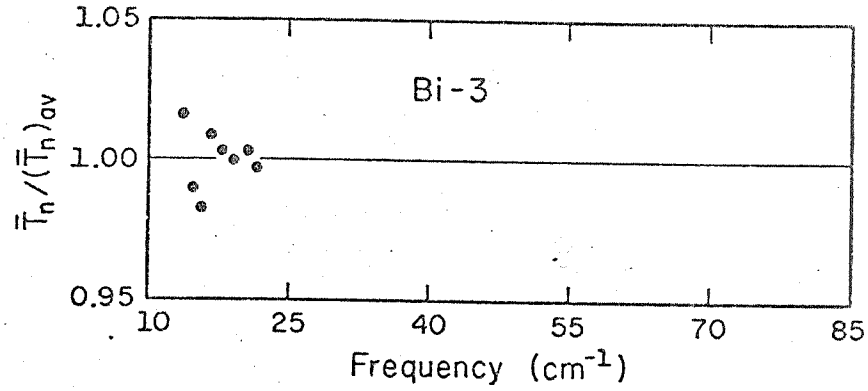

Figure 30. Normal state data for Bi-3.

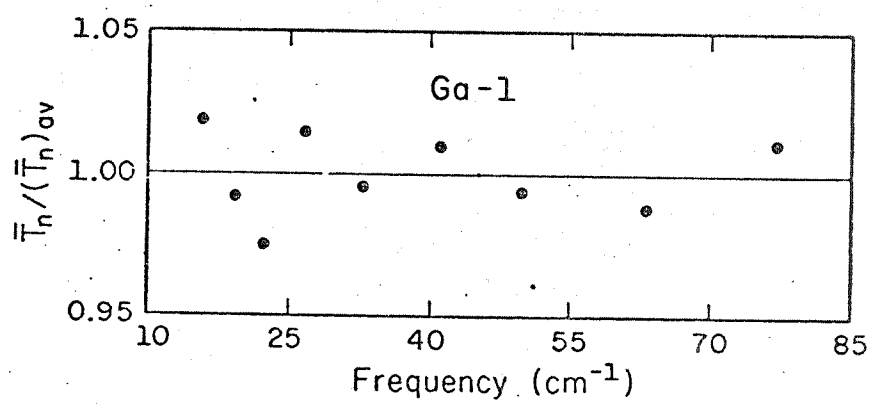

Figure 31. Normal state data for Ga-1.

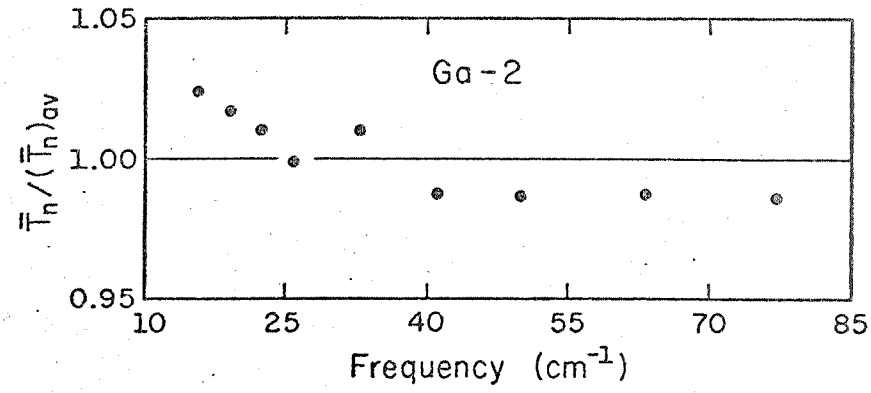

Figure 32. Normal state data for Ga-2.

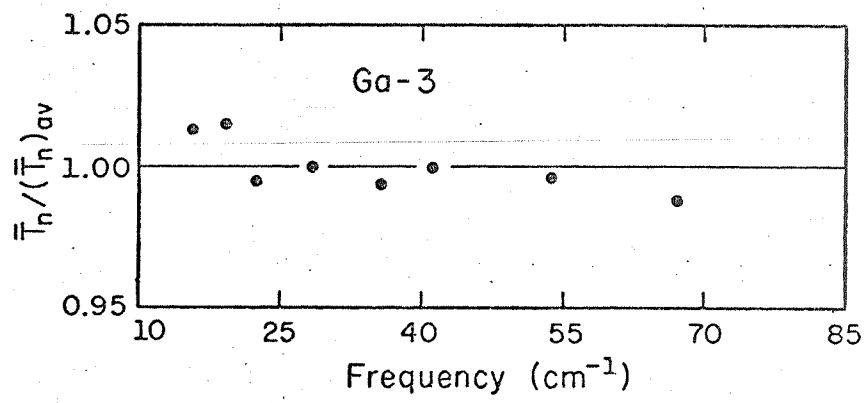

Figure 33. Normal state data for Ga-3.

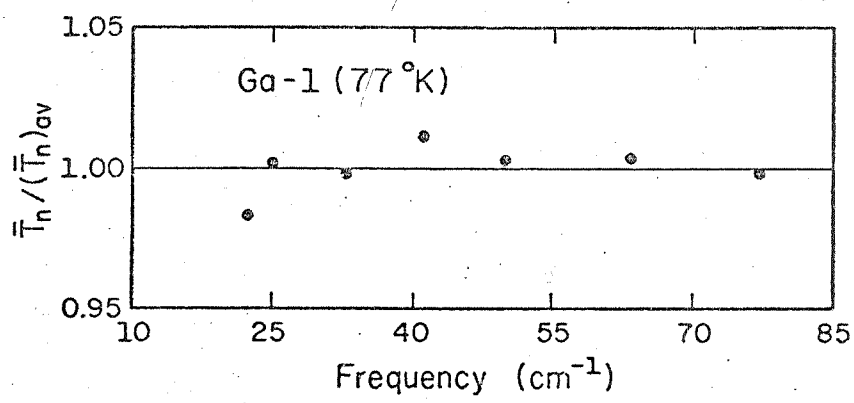

Figure 34. Normal state data for Ga-1 annealed at 77 K.

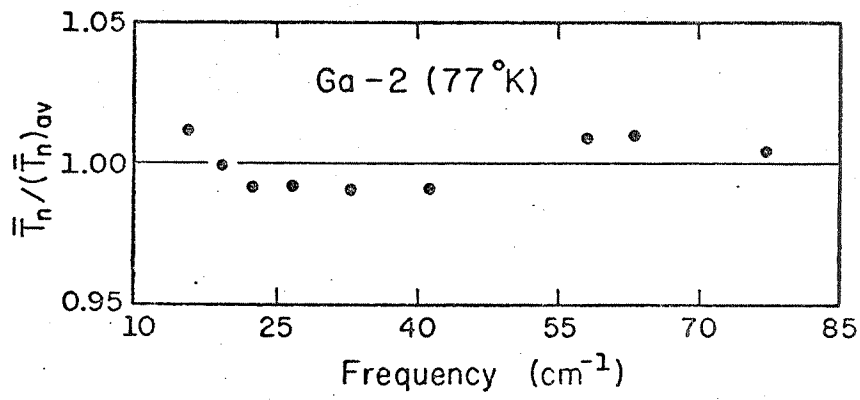

Figure 35. Normal state data for Ga-2 annealed at 77 K.

VITA

Richard Elgin Harris was born in Kansas City, Missouri, on May 28, 1941. He attended public schools in North Kansas City, Missouri, and Springville and Hamburg, New York. He received his undergraduate education from the University of Rochester, receiving in 1963 the degree Bachelor of Science in Physics with High Honors. Since September, 1963, he has been a student at the University of Illinois. He received the degree Master of Science in Physics in 1965. Beginning in September, 1964, he held a National Aeronautics and Space Administration Fellowship for three years. During the academic years beginning in 1963, 1967, and 1968, he held a research assistantship in the Department of Physics.

He is a member of Phi Beta Kappa and the American Physical Society.